The Migdal jump in the nucleon momentum distribution in nuclear matter is determined by the spin–isospin response function

É. E. Sapershteĭn and S. V. Tolokonnikov
Kurchatov Institute Russian Science Center, 123182 Moscow, Russia

(Submitted 21 August 1998)
Pis'ma Zh. Éksp. Teor. Fiz. **68**, No. 7, 529–534 (10 October 1998)

The renormalization factor Z of the single-particle Green's function in nuclear matter, equal to the jump in the nucleon momentum distribution (''Migdal jump''), is expressed in terms of the nuclear response function, using approximations that are realistic for nuclear physics. It is shown that the spin–isospin channel makes the dominant contribution to Z. © *1998 American Institute of Physics.*
[S0021-3640(98)00119-4]

PACS numbers: 21.65.+f

The jump in the momentum distribution $n(p)$ of Fermi particles, the so-called Migdal jump,[1] equals the renormalization factor Z of the single-particle Green's function $G(p,\varepsilon)$, i.e., the residue of G at the quasiparticle pole:

$$Z=(1-(\partial\Sigma/\partial\varepsilon)_0)^{-1}, \tag{1}$$

where $\Sigma(p,\varepsilon)$ is the mass operator: $G(p,\varepsilon)=(\varepsilon+\mu-\varepsilon_p^0-\Sigma(p,\varepsilon))^{-1}$, μ is the chemical potential, and $\varepsilon_p^0=p^2/2m$ (m is the bare nucleon mass). The index 0 in the derivative signifies that the derivative is evaluated at the Fermi surface, i.e., at $\varepsilon=0$ and $p=p_F$.

In condensed-matter theory, Z appears in most observables through the effective interaction of quasiparticles $\mathcal{F}=Z^2\Gamma^\omega$, where Γ^ω is the Landau amplitude.[2] In atomic nuclei the coordinate-dependent factor $Z(\mathbf{r})$ also enters implicitly in the amplitude $\mathcal{F}$ (Ref. 3). But, in addition, $Z(\mathbf{r})$ directly determines the single-particle spectroscopic factors and a number of other important observable quantities. The quantity $(\partial\Sigma/\partial\varepsilon)_0$ is a sum of contributions of approximately equal size, one of which is due to low-lying surface oscillations and can be calculated quite reliably in the self-consistent theory of finite Fermi systems (TFFS).[4,5] The other contribution is a characteristic of nuclear matter and is determined in the self-consistent TFFS by an independent phenomenological parameter. The value in nuclear matter, $(\partial\Sigma/\partial\varepsilon)_0=-0.25$, corresponding to $Z=0.8$, is in good agreement with a large collection of experimental facts, and we shall treat it as an ''experimental'' value.

In the present letter the dispersion relation[3] which relates the real and imaginary parts of Σ is used to calculate Z. In the standard assumptions used in nuclear physics $\mathrm{Im}\Sigma$ can be expressed in terms of the nuclear response function. We shall show that the spin–isospin channel makes the dominant contribution to $\mathrm{Im}\Sigma$. The properties of this

 © 1998 American Institute of Physics

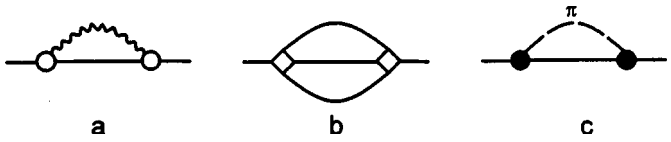

FIG. 1. The simplest diagrams for Σ'. Solid line — nucleon Green's function G; wavy line — zero-sound D function. Open circle — zero-sound creation vertex. Diamond — NN potential V, dashed line — pion D function; filled circle — πNN vertex.

channel are determined by the zeroth harmonic g_0' of the spin–isospin component of $\mathcal{F}$ (''Migdal constant'') as well as by the tensor amplitudes $\mathcal{F}_\pi$ and $\mathcal{F}_\rho$ of the medium-modified single-pion and ρ-meson exchange.[6,7]

From the dispersion relation for Σ it follows that

$$\left(\frac{\partial\Sigma(p,\varepsilon)}{\partial\varepsilon}\right)_0=\frac{1}{\pi}\left\{\int_0^\infty d\varepsilon\frac{\mathrm{Im}\Sigma(p_F,\varepsilon)}{\varepsilon^2}-\int_0^\infty d\varepsilon\frac{\mathrm{Im}\Sigma(p_F,-\varepsilon)}{\varepsilon^2}\right\}. \tag{2}$$

The spin and isospin indices in Eq. (2), as well as in most subsequent formulas, are dropped for brevity. Relation (2) guarantees the required sign $(\partial\Sigma/\partial\varepsilon)_0<0$, which follows from the inequality $Z<1$. Indeed, for positive values of ε the negativity of $\mathrm{Im}\Sigma(p_F,\varepsilon)$ follows from causality. For negative ε the sign of $\mathrm{Im}\Sigma$ changes,[2] so that both terms in Eq. (2) are negative.

Figure 1 shows the simplest diagrams for Σ, the cuts of which determine $\mathrm{Im}\Sigma$. The Hartree–Fock terms in Σ, which do not change the imaginary part, are dropped. Evidently, different physical mechanisms enter in $\mathrm{Im}\Sigma$ additively and with the same sign. For this reason, Eq. (2) has the form of a ''sum rule.''

For the time being we shall confine our attention to the nucleon degrees of freedom only. Then there exists an exact relation[2] which expresses Σ' (Σ minus the Hartree–Fock terms) in terms of the vertex part Γ, the NN potential V, and the Green's function of noninteracting particles and holes, $K_0=GG$:

$$\Sigma'=VGK_0\Gamma. \tag{3}$$

The symbolic multiplication in Eq. (3) signifies integration over intermediate momenta and energies as well as summation over the spin and isospin variables. A formal renormalization of (3) to reduce the problem to quasiparticles is hardly possible. It can be done approximately, using the smallness of $1-Z$, which is a measure of the difference between particles and quasiparticles. Then, when calculating Z from Eqs. (2) and (3) in the first approximation this difference can be neglected on the right-hand side of Eq. (3), and the equation can be written in terms of quasiparticles. In so doing, there arises a quasiparticle interaction amplitude $\mathcal{F}(\mathbf{p},\mathbf{p}',\mathbf{k},\omega)$, which for $k=0$ and $\omega=0$ becomes the Landau amplitude.

More general is the relation for the imaginary part of the quasiparticle mass operator $\mathrm{Im}\Sigma_q=Z\mathrm{Im}\Sigma$:

$$\mathrm{Im}\Sigma_q=\mathcal{F}^*\,\mathrm{Im}G\,\mathrm{Im}K\mathcal{F}, \tag{4}$$

where now G is the quasiparticle Green's function and K is the Green's function of interacting quasiparticles and quasiholes. Indeed, in the first approximation, neglecting the quasiparticle damping on the right-hand side of Eq. (3), the relation (4) can be obtained from Eq. (3). In this case the amplitude $\mathcal{F}$ is real. In the next approximation, the computed $\mathrm{Im}\Sigma_q$ can be substituted for G and K on the right-hand side of Eq. (4). Here the amplitude $\mathcal{F}$ also becomes complex. In this letter we confine our attention to the simplest approximation.

We shall employ for the amplitude $\mathcal{F}$ the approximation adopted in TFFS:[6,7]

$$\mathcal{F}=\mathcal{F}_0+\mathcal{F}_\pi(k,\omega)(\boldsymbol{\sigma}_1\cdot\mathbf{n})(\boldsymbol{\sigma}_2\cdot\mathbf{n})+\mathcal{F}_\rho(k,\omega)([\boldsymbol{\sigma}_1\times\mathbf{n}]\cdot[\boldsymbol{\sigma}_2\times\mathbf{n}]), \tag{5}$$

where $\mathbf{n}$ is a unit vector in the direction of $\mathbf{k}$. We shall confine ourselves to the zeroth harmonics of the central part of $\mathcal{F}_0$:

$$\mathcal{F}_0=C_0[f_0+f_0'\boldsymbol{\tau}_1\cdot\boldsymbol{\tau}_2+(g_0+g_0'\boldsymbol{\tau}_1\cdot\boldsymbol{\tau}_2)\boldsymbol{\sigma}_1\cdot\boldsymbol{\sigma}_2], \tag{6}$$

where the normalization factor C_0 is the reciprocal of the density of states at the Fermi surface: $C_0=(dn/d\varepsilon_F)^{-1}=300\ \mathrm{MeV}\cdot\mathrm{fm}^3$. We employ for $\mathcal{F}_\pi$ and $\mathcal{F}_\rho$ the standard expressions used in the TFFS,[6,7] taking into account the form factors $\Gamma_{\pi NN}$ and $\Gamma_{\rho NN}$, respectively. As a rule, we shall use for $\Gamma_{\pi NN}$ the monopole ansatz,[6] which takes into account the departure of the pion from the mass shell, with the cutoff parameter Λ_π. The data on Λ_π are contradictory: values ranging from 300 MeV up to 1.2 GeV are used in the literature (see the discussion in the review[6]). In the present calculations we employed as the base value the optimal value for describing the effect European Muon Collaboration (EMC) effect,[6] $\Lambda_\pi=620$ MeV, and we investigated the sensitivity of the results to the value of this parameter.

Since in the present problem $\omega\ll m_\rho$, where m_ρ is the mass of the ρ meson, the static limit of the monopolar form factor was used for $\Gamma_{\rho NN}$. Here $\Lambda_\rho=1$ GeV was taken as the base value of the cutoff parameter.

Confining ourselves to the zeroth harmonics of the amplitude $\mathcal{F}_0$, we integrate in Eq. (4) over the momenta $\mathbf{p}_1$ and $\mathbf{p}_2$ and express the answer in terms of the response function:

$$\chi(\mathbf{k},\omega)=\int\frac{d^3p_1}{(2\pi)^3}\,\frac{d^3p_2}{(2\pi)^3}\,K(\mathbf{p_1},\mathbf{p_2},\mathbf{k},\omega). \tag{7}$$

The analogous integral of K_0 is, to within a factor, the well-known Lindhard function[2] $\phi_0=-C_0\chi_0$. We introduce by analogy the dimensionless response function $\Phi=-C_0\chi$. The form of Eq. (6) dictates an analogous spin–isospin structure of Φ with components Φ^{ST}, where the spin S and the isospin T of a particle with a hole are 0 or 1. The equations for Φ^{ST} decouple:

$$\Phi^{ST}=\phi_0-2\phi_0 f_0^{ST}\Phi^{ST}, \tag{8}$$

where $f_0^{00}=f_0$, $f_0^{01}=f_0'$, $f_0^{10}=g_0$, and $f_0^{11}=g_0'$. It is easy to see that the imaginary part of Σ_q is a sum

$$\mathrm{Im}\Sigma_q=\sum_{ST}\mathrm{Im}\Sigma_q^{ST}, \tag{9}$$

where for $\varepsilon>0$

$$\mathrm{Im}\Sigma_q^{ST}(p,\varepsilon)=(2S+1)(2T+1)C_0 \int_0^\infty \frac{d\omega}{2\pi}\int \frac{d^3k}{(2\pi)^3}(f_0^{ST})^2 \times \mathrm{Im}G(\varepsilon-\omega,\mathbf{p}-\mathbf{k})\mathrm{Im}\Phi^{ST}(k,\omega). \quad (10)$$

For $\varepsilon<0$ the substitution $\omega\to-\omega$ must be made in the arguments of the functions in the integrands.

Let us recall the values of the zeroth harmonics of $\mathcal{F}$. For f_0 the density dependence[3] with strongly different values of the inner $f_0^{\mathrm{in}}\simeq 0$ and outer $f_0^{\mathrm{ex}}\simeq -3$ amplitudes is important.[4] Only f_0^{in} enters in the calculation of Z. The enormous value of f_0^{ex} leads to a large surface contribution to $Z(r)$, which in the self-consistent TFFS can be calculated separately. Next, we take $(f_0')^{\mathrm{in}}=0.5$–0.6 (Ref. 8) as well as $g_0=0.05\pm 0.10$ and $g_0'=1.1\pm 0.10$ (Ref. 9).

On this basis, it follows from Eq. (10) that the isoscalar terms $\mathrm{Im}\Sigma_q^{00}$ and $\mathrm{Im}\Sigma_q^{10}$ can be neglected. Only the isovector terms are important, and the quantity $\mathrm{Im}\Sigma_q^{11}$ must be severalfold greater than $\mathrm{Im}\Sigma_q^{01}$.

Expression (10) also contains the contribution $\mathrm{Im}\Sigma_{q(s)}$ of zero sound, a characteristic solution of the homogeneous equation corresponding to Eq. (8) that exists for $f_0^{ST}>0$ in the region where $\mathrm{Im}\phi_0=0$. But it is more convenient to calculate the imaginary part of the diagram 1a directly. This contribution is very small — the corresponding term $(\partial\Sigma_s/\partial\varepsilon)_0^{11}=-0.01$ — and the terms with other ST are negligibly small. The main contribution to Eq. (10) comes from the region of the particle–hole continuum where $\mathrm{Im}\phi_0\neq 0$. We shall first calculate $\mathrm{Im}\Sigma_{q(c)}^{11}$ without taking $\mathcal{F}_\pi$ and $\mathcal{F}_\rho$. into account. The integral in Eq. (10) with $g_0'=\mathrm{const}$ diverges. The dependence of g' on the momentum transfer is known from an analysis of precise data on the elastic magnetic scattering of electrons by odd nuclei:[7]

$$g'(k)=\frac{g_0'}{1+r_0^2k^2}, \quad (11)$$

where $r_0=0.4$ fm. The k dependence of g' makes the integral convergent, but the result is too large in absolute magnitude: $(\partial\Sigma/\partial\varepsilon)_0^{11}=-0.49$. When $\mathcal{F}_\pi$ and $\mathcal{F}_\rho$ are taken into account, the single spin–isospin mode splits into two modes, longitudinal and transverse, with two effective amplitudes:

$$g'_{l(tr)}(k,\omega)=g_0'(k)+\mathcal{F}_{\pi(\rho)}(k,\omega)/C_0. \quad (12)$$

Next, we write $\mathrm{Im}\Sigma_{q(c)}^{11}=\mathrm{Im}\Sigma_{q(c)}^{l}+\mathrm{Im}\Sigma_{q(c)}^{tr}$, where each term is determined by an integral of the form (10) with the factor $2S+1=3$ replaced by 1 for the longitudinal mode and 2 (the number of degenerate transverse modes) for the transverse mode (Fig. 2). For the main parameter set we find $(\partial\Sigma_c/\partial\varepsilon)_0^{l}=-0.016$ and $(\partial\Sigma_c/\partial\varepsilon)_0^{11}=-0.210$, which in sum give $(\partial\Sigma_c/\partial\varepsilon)_0^{11}=-0.226$. Such predominance of the transverse over the longitudinal channel is due mainly (aside from the kinematic factor 2) to the play in the parameters. Thus, the longitudinal contribution depends strongly on Λ_π: It equals -0.080 for $\Lambda_\pi=400$ MeV and -0.267 for $\Lambda_\pi=1200$ MeV. For $\Lambda_\pi=600$–700 MeV it has a minimum, due to strong cancellation of the two terms in Eq. (12). The transverse contribution

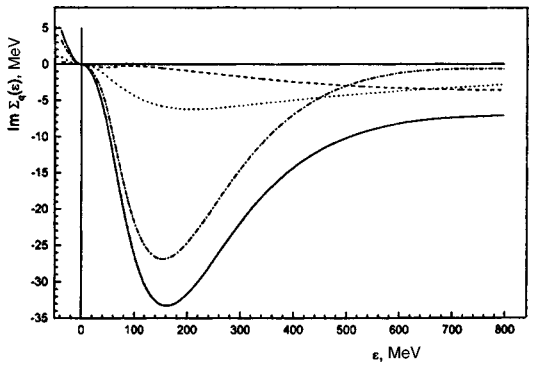

FIG. 2. $\mathrm{Im}\Sigma_q(\varepsilon)$. The dashed and dot–dash lines show the contribution of the longitudinal and transverse modes, respectively, of spin–isospin channel. The dotted line corresponds to the scalar-isoscalar channel. Solid line — sum of partial contributions.

is almost independent of Λ_ρ. The calculation of $\mathrm{Im}\Sigma^{01}_{q(c)}$ in the 01 channel is similar (Fig. 2) and gives $(\partial\Sigma_c/\partial\varepsilon)^{01}_0 = -0.056 - -0.075$ for $(f'_0)^{\mathrm{in}} = 0.5-0.6$, i.e., it is of the order of 20–30% of $(\partial\Sigma/\partial\varepsilon)_0$. Thus the nucleon degrees of freedom exhaust and even somewhat exceed the sum rule (2). Since the pion mode should make some contribution, this signifies that this calculation needs to be improved. The most obvious point, which can cause the integral (10) to decrease, is taking account of the dependence of g' on ω, for example, in a form similar to Eq. (11).

Let us briefly examine the pion contribution to $(\partial\Sigma/\partial\varepsilon)_0$. The corresponding skeleton diagram is displayed in Fig. 1c. Since an analogous diagram also exists for a free nucleon, only the medium-induced change in the diagram should of interest to us. For purposes of estimation, we shall examine the term associated with the change δG in the nucleon Green's function in nuclear matter. This change is produced by two factors: the existence of Fermi filling and the change in the single-particle spectrum. The first term reduces to an integral which is cut off by the Fermi factor and essentially independent of the form factor. It is very small: $(\partial\Sigma^{(1)}_\pi/\partial\varepsilon)_0 = -0.014$. The second term, $\delta\Sigma^{(2)}_\pi(p,\varepsilon)$, due to the change in the nucleon spectrum, depends on the form factor, and for this reason its calculation is more problematic. It is pointless to use $\Gamma_{\pi NN}(k,\omega)$ in the same form[7] as above, since now the pion is on the mass shell, where this expression takes on the value 1. In this situation, it is necessary to take into account the dependence of the vertex πNN on the variables controlling the departure of the nucleon from the mass shell; this dependence is poorly understood. To estimate the pion contribution to $(\partial\Sigma_\pi/\partial\varepsilon)_0$, we shall employ a very simple modification of this form factor, ensuring that the integral of interest converges. The result depends on the parameter Λ_π and equals $(\partial\Sigma^{(2)}_\pi/\partial\varepsilon)_0 = -0.022$ at $\Lambda_\pi = 620$ MeV. A detailed analysis if required in order to calculate the other terms in $(\partial\Sigma_\pi/\partial\varepsilon)_0$. This will be done separately, but the estimates presented already show that the pion contribution is appreciably less than the nucleon contribution.

We shall list the main assumptions made in the present calculation. In the first place, the quasiparticle damping and, accordingly, $\mathrm{Im}\mathcal{F}$ were neglected. The other important approximation is the assumption that $\mathcal{F}$ is independent of the frequency ω. Moreover, the

contribution of the high harmonics of $\mathcal{F}$ was not studied (however, estimates show this contribution to be very small). The slight breakdown in the sum rule for $(\partial\Sigma/\partial\varepsilon)_0$ is somewhat exceeded is an indicator that the computational scheme needs to be improved. We think that a more accurate theory will confirm the main results of this letter: The renormalization factor Z of the Green's function in nuclear matter can be calculated in terms of the nuclear response function and is determined mainly by the spin–isospin mode.

We thank A. B. Kaĭdalov, L. A. Kondratyuk, and V. A. Khodel' for helpful discussions. This work was supported in part by Grant 98-02-16979 from the Russian Fund for Fundamental Research.

[1] A. B. Migdal, Zh. Éksp. Teor. Fiz. **32**, 399 (1957).
[2] E. M. Lifshitz and L. P. Pitaevskiĭ, *Statistical Physics*, Part 2, Pergamon Press, New York [Russian original, Nauka, Moscow, 1978].
[3] A. B. Migdal, *Theory of Finite Fermi Systems and Applications to Atomic Nuclei*, Benjamin, Reading, Mass., 1977 [cited Russian original, 2nd ed., Nauka, Moscow, 1983].
[4] V. A. Khodel and E. E. Saperstein, Phys. Rep. **92**, 183 (1982).
[5] V. A. Khodel, E. E. Saperstein, and V. A. Zverev, Nucl. Phys. A **465**, 397 (1987).
[6] A. B. Migdal, E. E. Saperstein, M. A. Troitsky, and D. M. Voskresensky, Phys. Rep. **192**, 179 (1990).
[7] A. P. Platonov, É. E. Sapershteĭn, S. V. Tolokonnikov, and S. A. Fayans, Yad. Fiz. **58**, 612 (1995) [Phys. At. Nucl. **58**, 556 (1995)].
[8] S. A. Fayans and D. Zawischa, Phys. Lett. B **363**, 12 (1995).
[9] I. N. Borzov, S. V. Tolokonnikov, and S. A. Fayans, Yad. Fiz. **40**, 1151 (1984) [Sov. J. Nucl. Phys. **40**, 732 (1984)].

Translated by M. E. Alferieff

Energy dependence of ratios of multiplicities and their slopes for gluon and quark jets

I. M. Dremin
Lebedev Physical Institute, Russian Academy of Sciences, 117924 Moscow, Russia

(Submitted 24 August 1998)
Pis'ma Zh. Éksp. Teor. Fiz. **68**, No. 7, 535–538 (10 October 1998)

The difference between the ratio of multiplicities and the ratio of their derivatives with respect to energy for gluon and quark jets is calculated up to next-to-next-to leading order of perturbative QCD. Its nonzero value is uniquely defined by the running property of the QCD coupling constant. It is shown that this difference is rather small compared to values which can be obtained from experimental data. This disagreement can be ascribed either to strong nonperturbative terms or to experimental problems with a scale choice, jet separation, and inadequate assignment of soft particles to jets. © *1998 American Institute of Physics.* [S0021-3640(98)00219-9]

PACS numbers: 13.87.−a, 12.38.Bx

The ratio of multiplicities in gluon and quark jets has been of much debate during recent years. The lowest-order prediction of the perturbative QCD drastically overvalues experimental results for this ratio. Therefore, the higher-order corrections up to the next-to-next-to leading terms of the perturbative QCD have been calculated,[1,2] and the ratio has been written as

$$\frac{\langle n_G\rangle}{\langle n_F\rangle}=r(y)=\frac{C_A}{C_F}(1-r_1\gamma_0(y)-r_2\gamma_0^2(y))+O(\gamma_0^3), \tag{1}$$

the scale of the process being set by $y=\ln Q/Q_0$, where Q is the virtuality of the jet, $Q_0=\text{const}$,

$$\gamma_0=\left(\frac{2C_A\alpha_S}{\pi}\right)^{1/2}, \tag{2}$$

α_S is the running coupling constant, $C_A=3$, $C_F=4/3$ are Casimir operators, and

$$r_1=2\left[h_1+\frac{n_f}{12N_c}\left(1-\frac{2C_F}{N_c}\right)\right]-\frac{3}{4}, \tag{3}$$

$$r_2=\frac{r_1}{6}\left(\frac{25}{8}-\frac{3}{4}\frac{n_f}{N_c}-\frac{C_F}{N_c}\frac{n_f}{N_c}\right)+\frac{7}{8}-h_2-\frac{C_F}{N_c}h_3+\frac{n_f}{12N_c}\frac{C_F}{N_c}h_4, \tag{4}$$

$$h_1=\frac{11}{24},\quad h_2=\frac{67-6\pi^2}{36},\quad h_3=\frac{4\pi^2-15}{24},\quad h_4=\frac{13}{3}. \tag{5}$$

 © 1998 American Institute of Physics

Here, n_f is the number of active flavors, and $N_c=3$ the number of colors. Let us note that only the first term of r_2 was obtained in Ref. 1 by the Feynman graph technique. Other terms come from higher derivatives of the generating functions[2] when the QCD equations for the generating functions are solved by Taylor series expansion. They take into account the energy conservation in three-parton vertices.

Asymptotically, the ratio $r(y)$ (1) tends to a constant $C_A/C_F=9/4$, which shows that the gluon jet bremsstrahlung is stronger than for quark jets. However, the correction terms are still noticeable at presently accessible energies.

The energy dependence of the average multiplicities of gluon and quark jets used to be expressed in terms of the anomalous dimension $\gamma(y)$ as

$$\langle n_G(y)\rangle = Ke^{\int^y \gamma(y')dy'}, \quad \langle n_F(y)\rangle = \langle n_G(y)\rangle / r(y). \tag{6}$$

Then it is easy to get the ratio of their derivatives as

$$\frac{\langle n_G(y)\rangle'}{\langle n_F(y)\rangle'} = r(y)\left(1+\frac{r'(y)}{\gamma(y)r(y)-r'(y)}\right), \tag{7}$$

or for its difference with the ratio of multiplicities one gets

$$D(y)=\frac{\langle n_G(y)\rangle'}{\langle n_F(y)\rangle'}-\frac{\langle n_G(y)\rangle}{\langle n_F(y)\rangle}=\frac{rr'}{\gamma r-r'}. \tag{8}$$

The anomalous dimension in terms of the running coupling constant looks like

$$\gamma=\gamma_0(1-a_1\gamma_0)+O(\gamma_0^3). \tag{9}$$

Here

$$a_1=h_1+\frac{n_f}{12N_c}\left(1-\frac{2C_F}{N_c}\right)-\frac{B}{2}, \quad B=\frac{11N_c-2n_f}{24N_c}. \tag{10}$$

The higher-order terms have been omitted in our treatment. Taking into account that

$$\gamma_0'=-h_1\gamma_0^3+O(\gamma_0^5), \tag{11}$$

one estimates that the second term in the denominator of (8) can be neglected and gets finally

$$D(y)\approx\frac{r'(y)}{\gamma(y)}\approx\frac{N_c}{C_F}r_1h_1\gamma_0^2(1+a_1\gamma_0)\left(1+\frac{2r_2\gamma_0}{r_1}\right). \tag{12}$$

Formulas (8) and (12) are the main result of the paper.

It is important to stress that the difference $D(y)$ between the ratios of derivatives and multiplicities directly demonstrates the running property of the QCD coupling constant. It is identically equal to zero for fixed coupling because $r'=0$ in that case. For the running coupling, this difference is always positive and proportional to the value of the coupling constant. Consequently, it tends asymptotically to zero.

The corrections due to the anomalous dimension (9) and due to the multiplicity ratio (1) have been deliberately left as separate factors in brackets in (12) to show their relative

importance. One easily notices that the last correction in $D(y)$ is stronger than in the ratio (1) itself because r' in the numerators of (8) and (12) acquires factors of n upon differentiation of the subsequent terms of γ_0^n in (1).

Asymptotically the terms in brackets tend to 1 since $\gamma_0 \to 0$, but at present energies ($\gamma_0 \approx 0.45-0.5$ at Z^0) the corrections are rather large. In the energy range near Z^0, the factor in front of the brackets in (12) is about 0.05–0.06. The anomalous dimension correction in the first bracket enlarges the value of D by about 15%. More important is the expression in the second bracket. With values of r_1 and r_2 given by (3) and (4) and inserted in (12), one estimates it as about 3.2, i.e., the linear in γ_0 term (NNLO correction) contributes more than 1 (MLLA term), and one must therefore evaluate the next terms. If we were to accept this expression anyway, we would estimate D as

$$D \approx 0.16-0.20. \tag{13}$$

Thus the predicted value of D is comparatively small.

Let us note that the first term from (4) only as calculated first in Ref. 1 contributes to the second bracket a value of about 0.25, and the corresponding contribution to D is approximately 0.06–0.08.

We have considered the one-scale problem without imposing any limitations on the transverse momentum but considering the jet evolution with energy in the total phase space. In experiment, more-severe restrictions are often imposed by the specifics of the installation or some special criteria. In particular, one can consider jet evolution as a function of some internal scale (e.g., similar to the jet transverse momentum) at a given energy (usually chosen at the Z^0 peak because of the better statistics). Such a procedure has been exploited in Refs. 3 and 4. It was claimed that the proportionality of the two scales favors comparison of theoretical predictions with experimental data on the evolution of the above ratios. The scale chosen in Ref. 4 was

$$\kappa = E_{\text{jet}} \sin \frac{\theta}{2}, \tag{14}$$

where E_{jet} is the energy of the jet and θ is the angle with respect to the closest jet. In Ref. 3 a similar scale of the geometric mean of such scales of the gluon jet with respect to the two quark jets in three-jet events has been used. From the data presented in Ref. 4 one can estimate that the difference $D(\kappa)$ ranges approximately from 0.95 at $\kappa = 7$ GeV to 0.7 at $\kappa = 28$ GeV. These values are much larger than predicted above.

However, both the theoretical and experimental approaches to the problem should be further analyzed. The large correction in Eq. (12) implies that next terms of the perturbation expansion can be important in the ratio of derivatives. They are enlarged in (12), as discussed above, and support earlier conclusions (see, e.g., Ref. 5) that subleading effects are quantitatively important at experimentally accessible energies. Our experience tells us also that power corrections due to conservation laws related to recoil effects can become important as well.[6]

Experimental procedures raise even more questions. There exists a scale dependence in the final result if one compares the data of Ref. 3 with the data of Ref. 4. The problem of the scale choice has recently been discussed in Ref. 7. Besides, it has been shown[7] that

different algorithms for jet selection and ascribing soft particles to a jet lead to somewhat different conclusions concerning the jet multiplicities and their slopes. Further study is necessary.

Another problem raised by the procedure used in Ref. 4 is the role of nonperturbative effects in the average multiplicities of gluon and quark jets. It has been claimed[4] that the hadronization of quark jets leads to some constant (assumed as an ansatz!) excess over gluon jets, equal to about two or three particles. It partially compensates the perturbative QCD excess of the gluon jet multiplicities. This constant term in the energy dependence of multiplicities has been ascribed to a possible nonperturbative contribution. Unfortunately, this statement can hardly be tested against any reliable theoretical treatment. These terms do not contribute to the derivatives of the multiplicities but drastically diminish the multiplicity ratio, thus increasing their difference $D(y)$.

At the same time, the theoretical estimate (13) seems quite reasonable qualitatively if one accepts the value of about 2.1 given for the ratio of derivatives in Ref. 4 and the theoretically predicted[5] value of about 1.84 for the ratio of multiplicities, in comparison with the experimental result ~ 1.6 claimed in Ref. 8.

In conclusion, we have evaluated the difference between the ratio of the slopes of the average multiplicities and the ratio of multiplicities in gluon and quark jets in the next-to-next-to leading approximation of the perturbative QCD and compared it to some experimental data.

This work was supported in part by the Russian Fund for Fundamental Research (Grant # 96-02-16347) and by INTAS.

[1] J. B. Gaffney and A. H. Mueller, Nucl. Phys. B **250**, 109 (1985).
[2] I. M. Dremin and V. A. Nechitailo, Mod. Phys. Lett. A **9**, 1471 (1994).
[3] ALEPH Collaboration, R. Barate *et al.*, Z. Phys. C **76**, 191 (1997).
[4] DELPHI Collaboration, P. Abreu *et al.*, Z. Phys. C **70**, 179 (1996); *Proceedings of HEP'97 Conference*, Jerusalem, Israel, Aug. 19–26, 1997, to be published by World Scientific, Singapore; *Proceedings of ICHEP'98*, Vancouver, Canada, July 22–29, 1998 to be published by World Scientific, Singapore; preprint DELPHI 98-78 CONF 146, June 1998.
[5] I. M. Dremin, Phys. Usp. **37**, 715 (1994).
[6] S. Lupia, *Proceedings of the ''Correlations and Fluctuations'' Conference*, Matrahaza, Hungary, June 1998, to be published by World Scientific, Singapore.
[7] P. Eden, preprint LU TP 98-11, May 1998; http://xxx.lanl.gov/abs/hep-ph/9805228.
[8] OPAL Collaboration, G. Alexander *et al.*, Phys. Lett. B **388**, 659 (1996).

Published in English in the original Russian journal. Edited by Steve Torstveit.

Polarization of quadrupolar nuclei

F. S. Dzheparov and Yu. F. Kiselev
Institute of Theoretical and Experimental Physics, 117259 Moscow, Russia

(Submitted 1 September 1998)
Pis'ma Zh. Éksp. Teor. Fiz. **68**, No. 7, 539–543 (10 October 1998)

A method of obtaining high polarization and pure spin states of impurity nuclei with a moderately strong quadrupole interaction in solid diamagnetic hosts whose nuclei have spin 1/2, a large g factor (like ^{1}H and ^{19}F), and a high degree of polarization is proposed. The method employs cross-relaxation transitions of the impurity nuclei with the host spins (with adiabatic variation of the external magnetic field) and simple radio-frequency pulses that invert the host nuclei or give rise to two-spin resonance of the host and impurity nuclei. © *1998 American Institute of Physics.* [S0021-3640(98)00319-3]

PACS numbers: 76.60.Gv, 21.10.Hw

1. The standard methods of obtaining high nuclear polarization were developed mainly for protons and other spin-1/2 nuclei and are ineffective for quadrupolar nuclei.[1,2] The most powerful modern setups give dynamic proton polarization $p_p \approx 0.9$ in samples of volume $V \sim 10^3$ cm^3, but the polarization of ^{2}H nuclei that has been achieved is appreciably smaller, $p_d \approx 0.5$, and for ^{14}N it is only $p_I \sim 0.1$.[3,4] The comparatively large value of p_d is due to the weak quadrupole interaction, which increases sharply with increasing nuclear charge. Using an adiabatic rapid passage, a large value $p_I \approx 0.4$ has been obtained for the cross-relaxation transfer of high proton polarization to ^{14}N nuclei.[3,4] It is shown in this letter that by combining these methods with the pulsed proton polarization reversal one can achieve even higher degrees of polarization, $p_I \approx p_p$, for impurity nuclei, and the impurity nuclei can be put into pure spin states. While giving a somewhat weaker effect, the method can be used for nuclei of the main isotopes of many substances, such as ^{14}N in ammonia and ^{139}La in LaF_3. The experimental implementation of this suggestion can have extensive applications in high-energy nuclear physics, in neutron physical investigations of P- and T-odd effects, and in hyperfine interactions physics.

2. We shall consider first the very simple case of identical impurity nuclei with a g factor much smaller than that of the nuclei of the main isotope (for definiteness protons, $g_I = \epsilon g_p$, $\epsilon \ll 1$), spin $I = 1$, low density, and axisymmetric quadrupole interaction oriented along the z axis, which is arranged parallel to the external static magnetic field $\mathcal{H}_0$. The Hamiltonian

$$H_I = H_Q - \omega_I I_z, \quad H_Q = \beta_Q \left(I_z^2 - \frac{1}{3} I(I+1) \right), \quad \beta_Q = 3\omega_Q \tag{1}$$

(where ω_I and ω_Q are the Larmor and quadrupole frequencies, respectively) determines the principal approximation for the corresponding spin states when dipole–dipole interactions are neglected, and

 © 1998 American Institute of Physics

$$H_I|m\rangle = E_m|m\rangle, \quad E_m = \beta_Q\left[m^2 - \frac{1}{3}I(I+1)\right] - m\omega_I, \quad I_z|m\rangle = m|m\rangle. \tag{2}$$

All nuclear spin–lattice relaxation times are assumed to be quite long and are not discussed below.

Let the proton subsystem be put into a state (by the method of dynamic cooling, for example) with high polarization p_p in a high static field $\mathcal{H}_0$, and let its density matrix be

$$\rho_p = \exp(\beta(F - \omega_p S_z)), \quad p_p = \langle S_j^z\rangle / S_j = \tanh\frac{\beta\omega_p}{2}, \quad 1 - |p_p| \ll 1. \tag{3}$$

Here β is the reciprocal of the temperature, $S_j = 1/2$ is the spin of the jth proton, $S_z = \Sigma S_j^z$ is the projection of the total spin of the protons along the external field, ω_p is the Larmor frequency of the protons, and F is the corresponding free energy.

We shall consider the case $\omega_p > 0$, $\omega_I > 0$, and $\beta_Q > 0$. Let

$$\omega_{\min} = \omega_{1,0} = E_1 - E_0 = \beta_Q - \omega_I, \quad \omega_{\max} = \omega_{-1,0} = E_{-1} - E_0 = \beta_Q + \omega_I. \tag{4}$$

Let us decrease the field $\mathcal{H}_0$ adiabatically right down to the point where ω_p and $\omega_{\max}$ cross. Cross-relaxation of protons with spin states I, coupled with the frequency $\omega_{\max}$, occurs near crossing. It is caused by dipole–dipole interactions and correspondingly its rate is of the order of (see, for example, Ref. 5)

$$W_c(\Delta) = \epsilon^2 \overline{g}(\Delta)/T_{2p}, \tag{5}$$

where T_{2p} is the phase (transverse) relaxation time of the protons, $\Delta = \omega_p - \omega_{\max}$, and

$$\overline{g}(\Delta) = g_c(\Delta)/g_c(0), \quad g_c(\Delta) = \int d\omega g_I(\Delta - \omega) g_p(\omega) \approx g_p(\Delta). \tag{6}$$

Here we took account of the fact that the homogeneous Larmor resonance line $g_I(\omega)$ of the impurity nucleus is much narrower (by the factor ϵ^2) than the proton resonance line $g_p(\omega)$. The variation of the field must be adiabatically rapid, i.e., all important processes must be completed before the spin–lattice relaxation appears, but the width $\Delta_c \sim 1/T_{2p}$ of the cross-relaxation line must be traversed in a time much longer than $1/W_c(0)$. The latter condition can be expressed as

$$\dot{\omega}_p \ll \epsilon^2 / T_{2p}^2. \tag{7}$$

After adiabatic crossing of the frequencies, the quasipolarization $p^I_{0,-1} = (\rho^I_{0,0} - \rho^I_{-1,-1})/(\rho^I_{0,0} + \rho^I_{-1,-1})$ of the spin-I states participating in the cross relaxation becomes equal to the proton polarization, which in similar notation can be written as $p_p = p^p_{1/2,-1/2}$. Here, in accordance with the convention adopted for the signs of ω_p and β_Q, the first state in the difference determining $p^I_{0,-1}$ is the state corresponding to the lower energy. Ultimately, after the crossing one has $p^I_{0,-1} \approx p_p$, $\rho^I_{-1,-1} \approx 0$. In this analysis we neglected the influence of the second transition (between the states $|1\rangle$ and $|0\rangle$), since according to modern ideas[6,7] this rate is exponentially small in the parameter ΔT_{2p}, and $\Delta \approx 2\omega_I$.

As the field decreases further, the crossing $\omega_{\min} = \omega_p$ will occur, as a result of which $\rho^I_{1,1}$ will vanish and only the population of the state $|0\rangle$ will be significantly different from zero:

$$\rho^I_{m,n} \approx \delta_{m,n}\delta_{m,0}, \quad \rho^I \approx |0\rangle\langle 0|. \tag{8}$$

Such pure states are themselves of interest in many physical applications. To obtain high polarization, however, we shall start to increase the field $\mathcal{H}_0$. A secondary crossing of the frequencies ω_p and $\omega_{\min}$ will not change ρ^I, and at $\omega_p = \beta_Q$ we invert the direction of the proton polarization by applying a resonant π pulse to the system. At exact equality $\omega_p = \beta_Q$ this pulse will likewise have a small (to the extent ϵ is small) effect on the I spin also, and to suppress it virtually completely it is sufficient to take $\omega_p = \beta_Q + \Delta_r$, where $|\Delta_r| \sim \epsilon\beta_Q$. Next, as $\mathcal{H}_0$ increases at the frequency crossing $\omega_p = \omega_{\max}$ the quasipolarization $p^I_{0,-1}$ becomes equal to the new value of the proton polarization, opposite to the initial value, and ultimately the impurity nuclei will be in the state

$$\rho^I \approx |-1\rangle\langle -1|, \tag{9}$$

which corresponds to maximum polarization of the I spins relative to the z axis.

3. We shall now extend this analysis to the case of arbitrary integral spin I. The matrix elements of the dipole–dipole $I-S$ interaction allow only transitions with m and S_z changing by 1 or 0. For this reason, for adiabatic variation of $\mathcal{H}_0$ cross relaxation will occur when $\omega_p = |\omega_{m,m-1}|$. For our choice of the signs, the frequencies of transitions with $\Delta m = 1$ fall into the following order: $\omega_{-m-1,-m} > \omega_{m+1,m} > \omega_{-m,-m+1} > \omega_{m,m-1}$, $m \geqslant 1$. Correspondingly, as the external field $\mathcal{H}_0$ decreases from an initial value $\mathcal{H}_{0,\text{in}}$ corresponding to $\omega_p > \omega_{\max} = \omega_{-I,-I+1}$, to a value $\mathcal{H}_{0,f}$ for which $\omega_p < \omega_{\min} = \omega_{1,0}$, first the state $\rho^I_{-I,-I}$ empties and its population is transferred to the matrix element $\rho^I_{-I+1,-I+1}$ and then, similarly, the population of $\rho^I_{I,I}$ is transferred to $\rho^I_{I-1,I-1}$, and so on, in order of decreasing transition frequencies. In the field $\mathcal{H}_{0,f}$ one has $\rho^I \approx |0\rangle\langle 0|$, just as for spin $I = 1$. The state with maximum polarization $|p_I| \approx |p_p|$ will be obtained if first $\mathcal{H}_0$ is increased until $\omega_p = \beta_Q$ and then the proton polarization is inverted, after which $\mathcal{H}_0$ is increased adiabatically to the value $\mathcal{H}_{0,\text{out}}$ for which $\omega_p > \omega_{\max}$. The direction of the obtained polarization is determined by the fact that at the end the highest-energy state is populated. At the moment p_p is inverted all states with $m > 0$ are empty, and the first of the subsequent cross relaxations will occur at the frequency $\omega_{-1,0}$. Next, population is transferred in the direction of the states with higher energy and $m < 0$, since only these states are reachable by allowed transitions with $\Delta m = 1$.

4. If the spin I of an impurity nucleus is half-integral, then once again by decreasing the field $\mathcal{H}_0$ so that all cross-relaxation transitions at similar frequency crossings ($\omega_p = |\omega_{m,m-1}|$) would occur, we find that only the two states with $|m| = 1/2$ will remain populated, and $\rho^I_{1/2,1/2} = \Sigma_{m>0}\rho^{I,\text{in}}_{m,m}$, $\rho^I_{-1/2,-1/2} = \Sigma_{m<0}\rho^{I,\text{in}}_{m,m}$, where the index ''in'' refers to the initial state.

If now the polarization of the protons is inverted and an ac field with frequency $\omega = \omega_p - \omega_{-1/2,1/2} = \omega_p - \omega_I$ and amplitude (at the protons) ω_{1p} such that $\omega^2_{1p}/\omega^2_I \ll 1$ is applied, then two-spin resonance transitions with $\Delta m = -\Delta S_z$ will develop in the system, and in a time $T_{\text{res}} \gg (\omega_I/\omega_{1p})^2 T_{2I}$ they will transfer the impurity nuclei to the state $\rho^I = |-1/2\rangle\langle -1/2|$. Then, as the field $\mathcal{H}_0$ increases, the cross-relaxation transitions at the crossings $\omega_p = \omega_{-m,-m+1}$, $m \geqslant 3/2$, transfer the entire population to a state with the highest energy, just as in the case of integral I, engendering a state with maximum polarization along the z axis.

5. The proposed method should be effective in both single crystals and polycrystals and in glasses. Indeed, for arbitrary polar angles θ and ϕ (and, without loss of generality, $\theta \leqslant \pi/2$), which fix the axis **n** of the axisymmetric quadrupole interaction, the Hamiltonian is

$$H_Q = \beta_Q \left((\mathbf{I}\cdot\mathbf{n})^2 - \frac{1}{3} I(I+1) \right). \tag{10}$$

In the present method the spin states of the impurity nuclei in comparatively weak fields, where $\mu = \omega_I/\beta_Q \ll 1$ and ω_I is the Larmor frequency of the impurity, are important. They correspond to the spin Hamiltonian

$$H_I = H_Q - \omega_I I_z = \mathcal{D}(0,\theta,\phi) \left\{ \beta_Q \left[I_z^2 - \frac{1}{3} I(I+1) \right] - \omega_I (I_z \cos\theta + I_x \sin\theta) \right\} \mathcal{D}^+(0,\theta,\phi), \tag{11}$$

where $\mathcal{D}(\alpha,\theta,\phi) = \exp(i\phi I_z)\exp(i\theta I_y)\exp(i\alpha I_z)$ is a rotation operator. To leading order in μ the states and energies of H_I are determined by the Hamiltonian

$$H_I^0 = \mathcal{D}(0,\theta,\phi) \left\{ \beta_Q \left[I_z^2 - \frac{1}{3} I(I+1) \right] - \omega_I I_z \cos\theta \right\} \mathcal{D}^+(0,\theta,\phi), \tag{12}$$

where

$$H_I^0 |m\rangle = E_m |m\rangle, \quad |m\rangle = \mathcal{D}(0,\theta,\phi)|m_z\rangle, \tag{13}$$

$$E_m = \beta_Q \left[m^2 - \frac{1}{3} I(I+1) \right] - m\omega_I \cos\theta, \quad I_z|m_z\rangle = m|m_z\rangle.$$

The distribution of the directions of **n** serves as the main source of inhomogeneous broadening of the NMR line of I spins. This broadening is ordinarily much greater than the width of the proton line, which, once again, is assumed to be homogeneous. Nonetheless, the estimates (5) and (6) for the cross-relaxation rate with ω_p crossing the transition frequencies $\omega_{m,m-1} = E_m - E_{m-1}$ are once again applicable for nuclei in the same quadrupole field.

The energy values (13) differ from those used previously (2) only by the factor $\cos\theta$ multiplying ω_I. For this reason, the entire preceding analysis carries over to the case under study, as long as $\beta_Q \geqslant \omega_I$.

Now, however, to obtain states with maximum polarization along the z axis the field must be increased adiabatically at the end of the process in order to satisfy the condition $\omega_I \geqslant I\beta_Q$. The choice of the highest-energy state as the final state is due to the fact that only this term does not cross other terms of the Hamiltonian (11) as $\mathcal{H}_0$ increases. Such crossings equalize the populations of the colliding terms and decrease the final polarization. Correspondingly, in the case $\omega_Q < 0$ a related strategy culminating in the lowest-energy state of the Hamiltonian (11) must be chosen.

6. The proposed method can be easily extended to an arbitrary relation between the signs of ω_p, ω_Q, and ω_I. For lack of space we do not examine this question here in greater detail.

Our analysis easily extends to the more general situation where $p_p < 1$ and the density of quadrupolar nuclei is not low. Let a structural unit of the material contain N_p

protons and N_I quadrupolar nuclei. As an example, consider the cross-relaxation transition $\omega_p = \omega_{m,m-1}$, $m \geqslant 1$. Let the precrossing proton polarization and the important states of the quadrupolar nuclei be characterized by the numbers p_p, $\rho^I_{m,m}$, and $\rho^I_{m-1,m-1}$. As a result of one elementary cross-relaxation event, the total population of the pair of levels under consideration $Z_m = \rho^I_{m,m} + \rho^I_{m-1,m-1}$, and the quasimoment

$$\tilde{M} = \frac{1}{2}(N_p p_p + N_I Z_m p^I_{m-1,m})$$

of the structural unit are conserved, and on account of the fact that the polarization and quasipolarization become equal, the new values p'_p and $p^{I'}_{m-1,m-1}$ are determined by the relations

$$\tilde{M} = \frac{1}{2}(N_p + N_I Z_m)p'_p, \quad p^{I'}_{m-1,m} = p'_p. \tag{14}$$

We note in conclusion that in the process under consideration the nonadiabatic losses can be calculated analytically (on the basis of the method developed in Ref. 8 for multispin resonances, generalizing an earlier qualitative and numerical analysis performed in Ref. 9).

This work was supported by the Russian Fund for Fundamental Research (Project 96-15-96418) and the MNTTs (Grant No. 608).

[1] V. A. Atsarkin, *Dynamic Polarization of Nuclei in Solid Dielectrics*, Nauka, Moscow, 1980.
[2] A. Abragam and M. Goldman, *Nuclear Magnetism: Order and Disorder*, Clarendon Press, Oxford, 1970 [Russian translation, Vols. 1 and 2, Mir, Moscow, 1984].
[3] Yu. F. Kiselev, Doctoral Dissertation, Joint Institute for Nuclear Research, Dubna, 1998.
[4] B. Adeva, E. Arik, A. Arvidson *et al.* (Spin Muon Collaboration), CERN preprint CERN-PRE/97-66, 1997.
[5] F. S. Dzheparov, Zh. Éksp. Teor. Fiz. **99**, 982 (1991) [Sov. Phys. JETP **72**, 546 (1991)].
[6] V. E. Zobov and A. A. Lundin, Zh. Éksp. Teor. Fiz. **106**, 1097 (1994) [JETP **79**, 595 (1994)].
[7] Yu. G. Abov, A. D. Gul'ko, F. S. Dzheparov *et al.*, Fiz. Élem. Chastits At. Yadra **26**, 1654, (1995) [Phys. Part. Nuclei **26**, 692 (1995)].
[8] V. P. Gurariĭ, F. S. Dzheparov, V. I. Matsaev, and É. B. Fel'dman, ITÉF Preprint No. 42, Institute of High Energy Physics, Moscow, 1987.
[9] M. Goldman, *Spin Temperature and Nuclear Magnetic Resonance in Solids*, Clarendon Press, Oxford, 1970 [cited Russian translation, Mir, Moscow, 1969].

Translated by M. E. Alferieff

New results on efficient crystal extraction of protons from the 70 GeV accelerator at the Institute of High-Energy Physics

A. G. Afonin, V. M. Biryukov, V. A. Gavrilushkin, V. N. Gres',
B. A. Zelenov, V. I. Kotov, V. A. Maisheev, A. V. Minchenko,
V. I. Terekhov, E. F. Troyanov, and Yu. A. Chesnokov[a)]
Institute of High-Energy Physics, Russian Academy of Sciences, 142284 Protvino, Moscow Region, Russia

M. G. Gordeeva, A. S. Denisov, Yu. M. Ivanov, A. A. Petrunin,
V. V. Skorobogatov, and B. A. Chunin
St. Petersburg Institute of Nuclear Physics, Russian Academy of Sciences, St. Petersburg, Russia

(Submitted 2 September 1998)
Pis'ma Zh. Éksp. Teor. Fiz. **68**, No. 7, 544–548 (10 October 1998)

A record-high particle extraction efficiency, exceeding 40%, in agreement with theoretical predictions, is achieved using a short (5 mm long) crystal bent by 1.5 mrad. An extracted beam intensity of $\sim 6\times 10^{11}$ protons per cycle is obtained. This is five to six orders of magnitude higher than previous results. © *1998 American Institute of Physics.* [S0021-3640(98)00419-8]

PACS numbers: 29.27.Ac

Accelerator data on accelerated-beam extraction using bent crystals[1–5] and a theoretical analysis of these data[6] have shown that a large increase in extraction efficiency can be obtained, for example, by using multiple passage of particles through the crystal. The point is that for slow extraction the depth to which particles are kicked into the crystal in the first revolution is small (a fraction of a micron), while the surface layer damaged during working of the crystal can reach depths ranging from several microns to tens of microns.[7] The multiple-pass regime makes it possible to negotiate this channeling-ineffective layer.[8,9] To implement such an extraction regime, short silicon crystals — 7 and 5 mm long — with bending angles of 1.7 and 1.5 mrad, respectively, were used in the accelerator at the Institute of High-Energy Physics. For such parameters, which were chosen on the basis of the calculations performed, the average number $\langle N\rangle$ of passes for the channeled particles through the crystal will be ~ 12, while the average number of passes required for a nuclear interaction of the particles in the crystal is ~ 60.

Bending a short crystal in conformance with a number of conditions associated with the mounting of the crystal in the accelerator presents a definite problem. The first Si (111) crystal was made in the form of a short slab of large height, with dimensions $0.5\times 40\times 7$ mm (thickness, height, length in the direction of the beam). The crystal was bent in the transverse direction using a metal holder containing a 20 mm slit at the center

 © 1998 American Institute of Physics

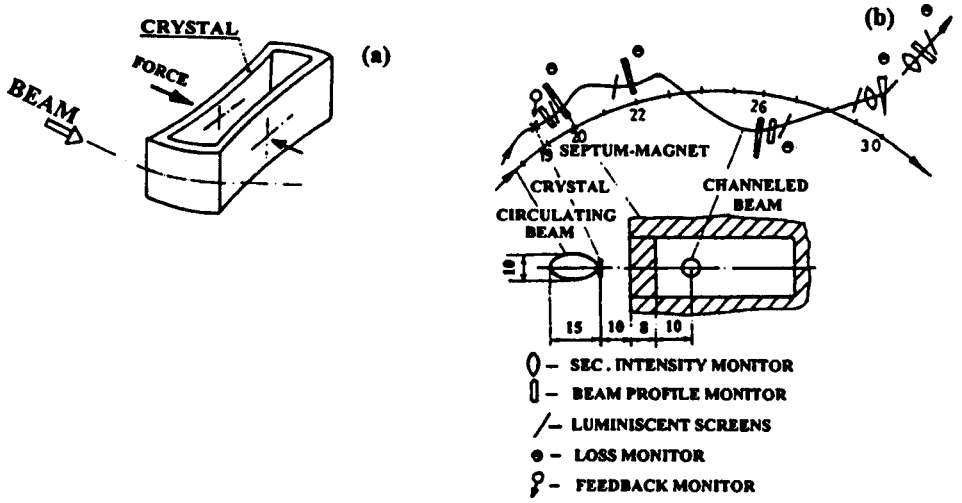

FIG. 1. a) Bent crystal obtained by compressing a monolithic piece of silicon cut in the shape of the letter O. b) Diagram of the experiment (all dimensions are given in mm).

for passing the beam. Despite the presence of bending nonuniformities (twist), encouraging results were obtained with this crystal: an extraction efficiency $\sim 20\%$ and extracted-beam intensity $\sim 1.9\times 10^{11}$ (Ref. 10). To increase the extraction efficiency further, a crystal with no ''twist'' was fabricated at the St. Petersburg Institute of Nuclear Physics in the form of the letter O from a monolithic piece of Si. The crystal is shown schematically in Fig. 1a. The dimensions of the working zone (with Si (110) orientation) of the crystal are $0.6\times 5\times 5$ mm (thickness, height, length in the direction of the beam). The required bending of the crystal by 1.5 mrad was produced by compressing the crystal at the center. The bent part was 3 mm long, and the straight ends were each 1 mm long.

In what follows we shall examine the results obtained with this crystal.

The crystal extraction scheme for a proton beam is displayed in Fig. 1b. In planning the experiment, we proceeded from the fact that small crystal bending angles are insufficient for direct beam extraction from an accelerator. For this reason, we decided to test a crystal in the existing slow-extraction scheme as the first element. The crystal was placed in the rectilinear segment *19* of the accelerator in front of the OM-20 septum magnet of the slow extraction system. The OM-20 barrier is 8 mm thick (see Fig. 1b). The crystal was placed 60–65 mm from the equilibrium orbit. The precision of the horizontal and angular displacements of the crystal was 0.1 mm and 13 μrad, respectively. The accelerated beam was steered onto the crystal using a local slowly increasing bump. The shape of the bump was chosen so that the circulating beam passed at a sufficient distance from the OM-20 magnet. The relative positions of the circulating and channeled beams with respect to the OM-20 magnet are shown in Fig. 1b.

The channeling regime and the characteristics of the extracted beam depend strongly on the parameters of the accelerated beam, which were measured in the horizontal plane at the location of the crystal. The emittance E of the accelerated beam and its angular divergence $X'_{\max}$ are determined by the expressions

$$E=\pi X^2_{\max}/\beta, \quad X^1_{\max}=X_{\max}(1+\alpha^2)^{1/2}/\beta,$$

where α and β are structure functions of the accelerator and $X_{\max}$ is the maximum dimension of the beam. The structure functions are known, and at the location of the crystal in the horizontal plane have the values $\alpha=1.87$ and $\beta=25$ m. Thus the entire process of measuring the parameters of the accelerated beam reduces to finding $X_{\max}$. In our case $X_{\max}\sim 7.2$ mm. For this value of $X_{\max}$, as follows from the formulas presented above, the beam emittance in the horizontal plane is 2 mm·mrad and its angular divergence at the location of the crystal is ~ 0.6 mrad. The beam emittance obtained similarly in the vertical plane does not exceed the beam emittance in the horizontal plane.

A complex diagnostics system, which included a television observation system, loss monitors, profilometers, and intensity meters, was used to control the deflection of the beam into the OM-20 aperture and guidance of the beam along the extraction path.[11] The arrangement of the diagnostics apparatus along the extraction channel is indicated in Fig. 1b. All diagnostics devices were first tested in the fast-extraction regime and calibrated using current transformers. According to the calibration results, the absolute measurement error did not exceed 2% in the intensity range of interest to us.[12] The background conditions were periodically measured with and without the crystal at the working location. According the measurements, the background level, together with the instrument noise, did not exceed 3% of the useful signal. The fraction of the beam steered onto the crystal was determined by the difference of the measurements of the circulating-beam intensity, performed with the current transformers before and after extraction, with a systematic error of $\sim 1\%$ (see Fig. 3 below). With all these factors taken into account, the total systematic measurement error was $\sim 4\%$. The extraction efficiency (ratio of the intensity of the extracted beam to the intensity steered onto the crystal) was estimated in each work cycle of the accelerator. For each experimental point, a statistical sample was accumulated over several hundreds of cycles. A feedback monitor based on a photomultiplier with a scintillator was used to obtain uniform steering of the beam onto the crystal. The feedback monitor was placed at the level of the orbit near the OM-20 magnet. The total frequency band of the feedback system was ~ 10 kHz.

The intensity of the accelerated beam was varied during the experiment from 1×10^{12} to 2.4×10^{12} protons per cycle. The intensity dumped onto the crystal was varied in the course of the experiment from 16 to 92%. An image of the crystal-deflected beam in front of the OM-20 magnet is shown in Fig. 2. The temporal characteristics of the extraction process are presented in Fig. 3 (information about the intensities of the circulating beam 1 and the extracted beam 2 was displayed on a storage oscilloscope). The duration of extraction in the feedback regime varied from 0.6 to 1.3 s. The flat top of the magnetic cycle of the IHEP accelerator has a duration of 2 s, while the complete accelerator cycle is 9.6 s.

The so-called orientational curve — the dependence of the intensity of the extracted beam on the angular orientation of the crystal — serves as direct proof of the fact that the extracted beam is channeled. In Fig. 4a it is compared with computer simulation results[10] with extraction of 23% of the circulating beam. As one can see from the figure, the experimental data agree well with the calculations. The maximum total efficiency, i.e., the efficiency over the extraction time, reaches 42% in this case. As the fraction of the beam steered onto the crystal increases, the total efficiency decreases as a result of drift

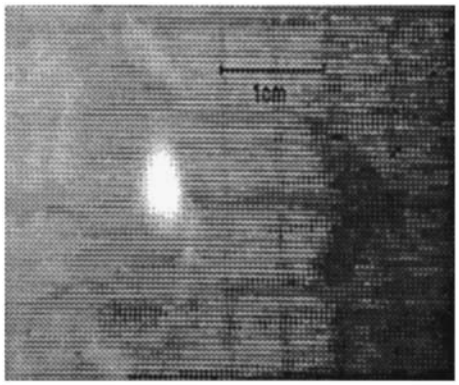

FIG. 2. Image of the deflected beam in front of the OM-20 magnet.

of the angle of incidence of the particles on the crystal (up to 0.3 mrad with the entire accelerated beam steered onto the crystal), which calculations confirm (see Fig. 4b). This phenomenon is due to the fact that the beam was steered onto the crystal in a radial direction with an inclined phase ellipse. For the same reason, the extraction efficiency changed during the extraction cycle (see Fig. 3), especially when a large fraction of the accelerated beam was steered onto the crystal. It is interesting that the peak efficiency was the same — 47%, irrespective of the fraction of the beam that was taken off.

The maximum intensity of the crystal-extracted beam with 2.2×10^{12} protons steered onto the crystal in a cycle was 6×10^{11} protons per cycle, which is five to six orders of magnitude higher than previous results.[1–5] The crystal worked in a strained state for several days, heating up to an estimated several hundreds of degrees. The extracted beam was shaped, by means of a magnetooptic channel, to the target of the experimental setup,

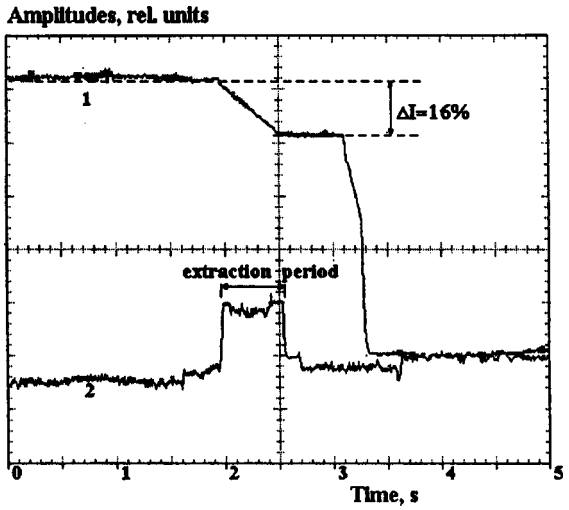

FIG. 3. Time dependence of the circulating (1) and extracted (2) proton beam intensities.

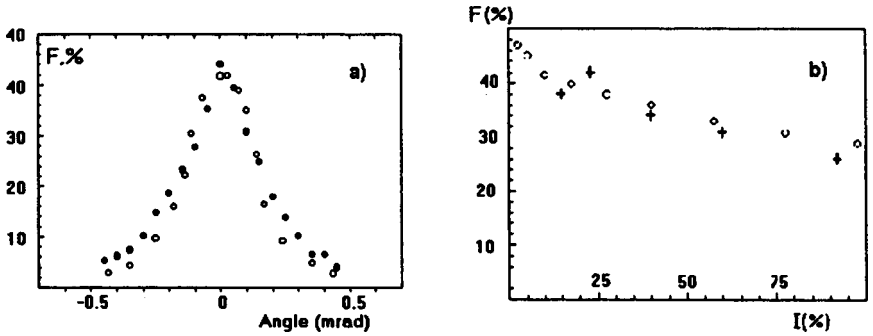

FIG. 4. a) Extraction efficiency as a function of the crystal orientation angle (○ — experiment, ● — computer simulation). b) Extraction efficiency as a function of the beam fraction incident on the crystal (+ — experiment, ○ — computer simulation).

where its dimensions at half maximum were 4×4 mm. It was also shown that the crystal can operate at the same time with one internal target without appreciable degradation of the extraction parameters.

Very good reproducibility was observed throughout the entire experiment. We intend to continue investigations in this direction to determine the limiting possibilities of multiple-revolution extraction.

In closing, we wish to express our deep appreciation to A. A. Logunov and N. E. Tyurin for supporting this work. The work was supported by the Russian Fund for Fundamental Research, Grant 98-02-16941.

[a)]e-mail: chesnokov@MX.IHEP.SU

[1] H. Akbari, X. Altuna, S. Bardin *et al.*, Phys. Lett. B **313**, 491 (1993).
[2] C. T. Murphy, R. A. Carrigan Jr., D. Chen *et al.*, Nucl. Instrum. Methods Phys. Res. B **119**, 231 (1996).
[3] G. Arduini, K. Elsener, G. Fidecaro *et al.*, *Proceedings of the Particle Accelerator Conference PAC-97*, Vancouver, 1997.
[4] A. A. Asseev, M. D. Bavizhev, A. N. Vasiliev *et al.*, Nucl. Instrum. Methods Phys. Res. A **309** (1991).
[5] V. M. Biryukov, V. N. Chepegin, Yu. A. Chesnokov *et al.*, *Proceedings of the Particle Accelerator Conference PAC-97*, Vancouver, 1997.
[6] V. M. Biryukov and C. T. Murphy, Fermilab TM-2026, Batavia (1997).
[7] V. M. Biryukov, Yu. A. Chesnokov and V. I. Kotov, *Crystal Channeling and its Application at High Energy Accelerators*, Springer, Berlin, 1997.
[8] V. M. Biryukov, Nucl. Instrum. Methods Phys. Res. B **53**, 202 (1991).
[9] A. M. Taratin, S. A. Vorobiev, M. D. Bavizhev *et al.*, Nucl. Instrum. Methods Phys. Res. B **58**, 103 (1991).
[10] A. G. Afonin, V. M. Biryukov, V. A. Gavrilushkin *et al.*, JETP Lett. **67**, 781 (1998).
[11] A. G. Afonin, V. N. Gorlov, V. V. Gotsev *et al.*, *Proceedings of the 15th Conference on Charged-Particle Accelerators* [in Russian], Protvino, 1996, p. 286.
[12] A. G. Afonin, V. N. Gres, and V. I. Terekhov, ''Wide range extracted beam intensity measurement at the IHEP,'' contributed to ERAC, Stockholm, 1998.

Translated by M. E. Alferieff

Experimental study of the decay $\phi \to \eta\gamma$ in multiphoton final state

M. N. Achasov, S. E. Baru, A. V. Berdyugin, A. V. Bozhenok, A. D. Bukin, D. A. Bukin, S. V. Burdin, T. V. Dimova, S. I. Dolinsky, V. P. Druzhinin, M. S. Dubrovin, I. A. Gaponenko, V. B. Golubev, V. N. Ivanchenko[a)], A. A. Korol, S. V. Koshuba, I. N. Nesterenko, E. V. Pakhtusova, A. A. Polunin, E. E. Pyata, A. A. Salnikov, S. I. Serednyakov, V. V. Shary, Yu. M. Shatunov, V. A. Sidorov, Z. K. Silagadze, and Yu. S. Velikzhanin

Budker Institute of Nuclear Physics, 630090 Novosibirsk, Russia

(Submitted 2 September 1998)
Pis'ma Zh. Éksp. Teor. Fiz. **68**, No. 7, 549–551 (10 October 1998)

The $\phi(1020) \to \eta\gamma \to 3\pi^0\gamma$ decay is studied in the SND experiment at the VEPP-2M e^+e^- collider. The measurements give a branching ratio $B(\phi \to \eta\gamma) = (1.246 \pm 0.025 \pm 0.057)\%$. © *1998 American Institute of Physics.* [S0021-3640(98)00519-2]

PACS numbers: 13.25.Jx, 13.40.Hq

The $\phi \to \eta\gamma$ decay is a classical magnetic dipole transition from the ϕ to the η meson and has been studied in many experiments.[1] In this work we describe the measurement of the $\phi \to \eta\gamma$ branching ratio in the SND experiment at the VEPP-2M e^+e^- collider in Novosibirsk. The spherical nonmagnetic detector SND[2] was designed for the experimental study of e^+e^--annihilation at a center-of-mass energy of about 1 GeV. Its main part is a three-layer electromagnetic calorimeter consisting of 1630 NaI(Tl) crystals.[3,4] The experiment was performed at VEPP-2M in 1996.[5] It consisted of 6 successive runs at 14 different beam energies in the region $2E_0 = (980-1050)$ MeV, covering the peak and close vicinity of the ϕ resonance. The total integrated luminosity was equal to 3.7 pb^{-1}, which corresponds to 7.6×10^6 ϕ mesons produced. The luminosity was determined using events of the two-quantum annihilation process.

The following reaction was studied:

$$e^+e^- \to \phi \to \eta\gamma \to 3\pi^0\gamma \to 7\gamma.$$

Events were selected in which 6–8 photons were emitted at angles of more than 27° degrees with respect to the beam and no charged particles were emitted. Standard SND cuts[5] on energy–momentum balance in an event were used. As a result of such selection the cosmic background is excluded and the main background process $e^+e^- \to \phi \to K_S K_L \to \pi^0\pi^0 K_L$ is suppressed. It is seen from Fig. 1, which shows the spectrum of the recoil mass $m_{\text{rec}\gamma}$ of the most energetic photon in an event, that the peak at the mass of the η meson dominates. For final selection of $\eta\gamma$ events a soft cut 400 MeV $< m_{\text{rec}\gamma} <$ 620 MeV was used. The $\phi \to K_S K_L$ background contribution is about 1%,

 © 1998 American Institute of Physics

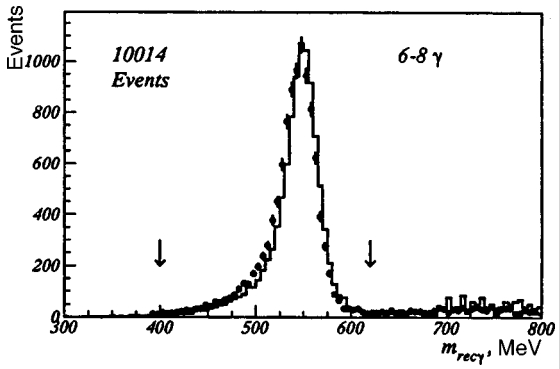

FIG. 1. Points — data, histogram — simulation.

which was evaluated using the number of events from the $m_{\mathrm{rec}\gamma}$ interval from 620 to 840 MeV. It worth noting that number and spectrum of $K_S K_L$ events are in good agreement with a Monte Carlo simulation.

The number of events thus selected at each energy point for each run allows one to determine the visible cross section σ_{vis}, which was fitted for each of 6 runs separately according to following expression:

$$\sigma_{\mathrm{vis}}(s)=\sigma_0\beta(s)\varepsilon\sqrt{\frac{1-m_\eta^2/s}{1-m_\eta^2/m_\phi^2}}\left|\frac{\Gamma_\phi m_\phi}{m_\phi^2-s-im_\phi\Gamma_\phi(s)}+A\right|^2, \qquad s=4E^2,$$

where E is the beam energy, σ_0 is the cross section at the ϕ-meson pole (a free parameter of the fit), $\beta(s)$ is a radiative correction which was calculated according to Ref. 6, ε is the detection efficiency, and A is an interference term. In the fit procedure the beam energy spread (300 keV) and the instability of average beam energy (100 keV) were taken into account. The shifts in the beam energy scale for each run were determined using the decay mode $\phi\to K_S K_L$ (Ref. 5).

The results of the fit are shown in Table I. The detection efficiency is individual for each run because of small differences in the trigger settings and in the number of broken or noisy calorimeter channels. The quantity A describes the interference between the ϕ meson and tails of ρ, ω resonances and with a possible anomaly contribution.[7] The results shown in Table I were obtained for $A=0$. If the fit is performed with A as a free

TABLE I. The results of the study of $\phi\to\eta\gamma$ decay for 6 independent runs.

Experiment	Events	$N_\phi\times10^{-6}$	ε,%	σ_0,nb	χ^2/n_D
PHI9601	1064	0.867	32.15	16.14 ± 0.59	11/8
PHI9602	1465	1.143	32.12	16.79 ± 0.53	13/8
PHI9603	2171	1.721	31.69	16.85 ± 0.45	16/10
PHI9604	1258	1.025	31.33	16.05 ± 0.57	16/11
PHI9605	2286	1.607	32.05	17.92 ± 0.56	16/11
PHI9606	1770	1.227	31.73	18.30 ± 0.66	5/9

parameter the result coincides with the previous assumption. If A is calculated according to Ref. 7, then the results are practically the same. If the standard vector dominance model is used as in the analysis of previous experiments,[8] then the value of σ_0 decreases by only 1.5%. We include the aforementioned model uncertainty in the systematic error.

Averaging the data from Table I, one can find

$$\sigma_0 = (16.95 \pm 0.34 \pm 0.59) \text{ nb},$$

where the first error is the statistical and the second the systematic. Because the results in Table I exhibit some difference, the scale factor for these measurements was calculated according to PDG recommendations. It was found to be 1.5 and was taken into account in the reported statistical error. The systematic error was estimated to be 3.5%. It is mainly determined by the the systematic uncertainty in normalization (3%), the background subtraction error (1%), the error of estimation of the detection efficiency (0.5%), and the error in the value of the interference term (1.5%).

Using the following expression:

$$\sigma_0 = \frac{12\pi B(\phi \to \eta\gamma) B(\phi \to e^+e^-) B(\eta \to 3\pi^0)}{m_\phi^2}$$

and PDG data[1] one can find the value of the branching ratio

$$B(\phi \to \eta\gamma) = (1.246 \pm 0.025 \pm 0.057)\%,$$

where first error is the statistical and the second the systematic. The given values include the systematic errors in σ_0 and in the PDG data for $B(\phi \to e^+e^-)$ (2.7%) and $B(\eta \to 3\pi^0)$ (1.2%).

The result is in agreement with the average PDG value $(1.26 \pm 0.06)\%$ and with each previous experiment.[1] At the moment it is the most accurate single measurement of $B(\phi \to \eta\gamma)$ based on 10^4 selected events. The precision can be improved by lowering the systematic error. Note that the limiting factors for this measurement are the accuracy of normalization and the accuracy of the $\phi \to e^+e^-$ branching ratio.

The work is partially supported by the RFBR (Grants #96-02-19192, #96-15-96327) and STP ''Integration'' (Grant #274).

[a)]e-mail: V.N. Ivanchenko@inp.nsk.su

[1] C. Caso *et al.* (Particle Data Group), Eur. Phys. J. C **3**, 1 (1998).
[2] V. M. Aulchenko *et al.*, in *Proceedings of the Second Workshop on Physics and Detectors for DAΦNE*, Frascati, Italy, April 4–7, 1995, p. 605–613.
[3] A. D. Bukin *et al.*, Yad. Fiz. **56**(11), 75 (1993) [Phys. At. Nucl. **56**, 1494 (1993)].
[4] M. N. Achasov *et al.*, Nucl. Instrum. Methods Phys. Res. A **401**, 179 (1997).
[5] M. N. Achasov *et al.*, Budker INP-97-78, Sep 1997; http://xxx.lanl.gov/abs/hep-ex/9710017; in *Proceedings of HADRON97*, Upton, N.Y., August 24–30, 1997, p. 26.
[6] E. A. Kurav and V. S. Fadin, Yad. Fiz. **41**, 733 (1985) [Sov. J. Nucl. Phys. **41**, 466 (1985)].
[7] M. Benayoun, S. I. Eidelman, and V. N. Ivanchenko, Z. Phys. C **72**, 221 (1996).
[8] S. I. Dolinsky *et al.*, Phys. Rep. **202**, 99 (1991).

Published in English in the original Russian journal. Edited by Steve Torstveit.

Overlapping identical resonances and double radiative interference effects in recombination of heavy multicharged ions

A. V. Nefiodov[a)]
Theory Department, St. Petersburg Nuclear Physics Institute, 188350 Gatchina, St. Petersburg, Russia

D. L. Moores
Department of Physics and Astronomy, University College London, Gower Street, London WC1E 6BT, UK

L. N. Labzowsky
Theory Department, St. Petersburg State University, 198904 St. Petersburg, Petrodvorets, Russia

(Submitted 1 June 1998; resubmitted 24 August 1998)
Pis'ma Zh. Éksp. Teor. Fiz. **68**, No. 7, 552–556 (10 October 1998)

The purely QED effect of double radiative interference in the recombination of electrons with heavy multicharged ions is discussed. Numerical calculations of the corresponding cross sections in the vicinities of the $KL_{12}M_{12}$ and $KM_{12}M_{12}$ dielectronic recombination resonances of heliumlike uranium are reported. The possibility of near-future experimental observation of the effect with the Super-EBIT facility is suggested. © *1998 American Institute of Physics.* [S0021-3640(98)00619-7]

PACS numbers: 34.80.Lx, 32.30.Rj

Overlapping resonances have been thoroughly investigated in nuclear and particle physics. The most interesting case is the overlap of identical resonances, that is, resonances with identical quantum numbers, when the interference terms survive not only in the differential but also in the total cross section of processes after integration over angles. As a consequence, these terms lead to some special interference effects, e.g., quantum beats, which are well known in neutral K-mesons[1] and the ^{8}Be nucleus.[2,3]

In atomic physics, a similar situation was investigated theoretically[4] and observed experimentally[5] in the decay of coherently excited $2s$ and $2p$ states of the hydrogen atom in an external electric field. The electric field mixes even- and odd-parity states so that the resulting combinations have identical quantum numbers. Though the excited levels do not overlap in this case due to the repulsion in the electric field, they are close enough to be excited coherently and to give the interference effect. Overlap of resonances may arise, in principle, if an external magnetic field is also added.[6]

Unlike the case of neutral atoms, where the radiative overlap of identical resonances is very rare, it can easily take place in the spectra of highly charged heavy ions, in

 © 1998 American Institute of Physics

particular in heliumlike uranium. The magnitude of these effects can be estimated qualitatively from the magnitude of the radiative broadening compared to the energy interval between the levels of a multiplet with identical parity and total angular momentum quantum numbers. If there are no special exclusions, the interference effect turns out to be of order $(\alpha Z)^3$ (Ref. 7), that is, about Z times as large as the effect of nonresonant levels on the line shape.[8] From this estimate, one can see that the overlap in the spectra of multicharged heavy ions arises because the radiative shifts and widths become comparable with the electron–electron interaction corrections at very high Z values. It means also that this phenomenon can only be described within QED theory, where all the radiative corrections are treated in a consistent manner. We use here the same technique as in Refs. 7 and 9–15, based on an S-matrix or Green's function approach.

The theory of radiative decay of overlapping identical levels in multicharged ions has been developed in Refs. 9–12. The process of recombination of an electron with a hydrogenlike heavy ion provides one possible practical way of preparing the situation under investigation.[14–16] The total cross section of the recombination process generally includes resonant dielectronic-recombination (DR) and nonresonant radiative-recombination (RR) cross sections, and terms which describe the interference between DR and RR channels. Interference terms due to radiative overlap of identical DR resonances will also be present, but their corresponding effects usually turn out to be masked by DR–RR interference.[14–16] The latter has been investigated in the vicinity of the *KLL* resonances theoretically[14–20] and recently observed experimentally.[21]

It should be noted that in contrast with direct cross-section measurements, the technique of recording the photon energy and electron beam energy for every observed event, which was developed in Refs. 21 and 22, allows for separation of different x-ray transitions from the dielectronic capture resonances. This way of doing the experiment provides a good means for observing the double radiative interference effects first discussed in Ref. 7. By these effects we mean the radiative interference in the recombination process on groups of mutually overlapping identical, e.g., doubly excited, levels. Such situations can give the largest radiative interference effect, since not only initial but also final recombined states overlap in this case. Also it seems to be possible to observe the pure radiative interference effects because, in contrast with them, the DR–RR interference terms in the cross section are suppressed by at least a factor of $1/Z$. In lowest-order perturbation theory, the amplitudes of excitation of the group of doubly excited levels in the process of direct radiative capture of an electron by a hydrogenlike ion in the ground state, with emission of only one photon, vanish due to the orthogonality of the wave functions. These amplitudes only contribute to the cross section if one takes into account higher-order graphs, i.e., either in at least two-photon processes or after refinement of the photon emission operator by the corrections of order $1/Z$ to the electron–electron interaction. The RR process manifests itself only as a background in this case. The characteristic x rays emitted by RR can be used to calibrate the total cross sections.[21,22] The combined spectra of a mixture of highly charged uranium ions have been observed in experiment.[21] However, the resonances of the He-like ion are shifted in energy compared to those from other recombined ions. The situation discussed in this letter is quite general and should also apply to other few-electron multicharged heavy ions.

We shall consider the DR process of an electron with a hydrogenlike multicharged ion $A^{(Z-1)+}$ in its ground state, which may be schematically represented as

$$A^{(Z-1)+}(1s_{1/2})+e^-(\varepsilon)\to A^{(Z-2)+}(d)^{**}\to A^{(Z-2)+}(s)^{**}+\gamma(\omega)\to\ldots,$$

where e^- denotes the incident electron with energy ε, and γ is the emitted photon with frequency ω. The labels d and s merely serve to identify two-electron states and do not here refer to any particular value of orbital angular momentum. The d and s states are assumed to be groups of the doubly excited mutually overlapping levels with identical quantum numbers. Then the resonance condition is $\varepsilon+E_{1s_{1/2}}\simeq E_d$ where $E_{1s_{1/2}}$ and E_d are the energies of the hydrogenlike and heliumlike ions, respectively. In addition, only those photons with frequency in the region of $\omega\simeq E_d-E_s$ are supposed to be measured in all directions of emission.

The amplitude of the DR process in the case of radiative channels of decay was obtained in Ref. 7 within the resonance approximation. Then the expression for the cross section can be written as follows (in relativistic units)

$$\sigma_{\rm DR}(\varepsilon)=\frac{\pi^2}{2p^2}\sum_{j,l}\sum_{J,M}\sum_{s}\sum_{d,d'}\frac{W_{dd',s}\langle d_L|\hat{I}|i\rangle\langle d'_L|\hat{I}|i\rangle^*}{(\varepsilon+E_{1s_{1/2}}-\mathcal{E}_d)(\varepsilon+E_{1s_{1/2}}-\mathcal{E}^*_{d'})}. \tag{1}$$

Here $p^2=\varepsilon^2-m^2$, and the initial state $|i\rangle$ of the system (one-electron ion in its ground $1s_{1/2}$ state plus continuum electron) depends on the set of quantum numbers $|1s_{1/2}\varepsilon ljJM\rangle$, where J is the total angular momentum of the system, M is the projection of J, and l,j are the orbital and total angular momenta of the incoming electron. The continuum wave functions are normalized to δ functions in the energy ε. The matrix elements of the operator

$$\hat{I}(r_{12};E_d^{(0)})=\alpha\frac{(1-\alpha_1\cdot\alpha_2)}{2r_{12}}\{\exp(i|\varepsilon_{d_1}-\varepsilon_{1s_{1/2}}|r_{12})+\exp(i|\varepsilon_{d_2}-\varepsilon_{1s_{1/2}}|r_{12})\} \tag{2}$$

describe the excitation process of the states d by radiationless capture, taking into account the retardation effect. In Eq. (2), $r_{12}=|\mathrm{x}_1-\mathrm{x}_2|$, α_i are the Dirac matrices, and the fine-structure constant $\alpha=e^2$. The zero-approximation energy $E_d^{(0)}$ of the two-electron states d is defined by the sum of the corresponding one-electron Sommerfeld energies ε_{d_i}, $i=1,2$. Note that the one-electron energy $E_{1s_{1/2}}$ includes the Lamb shift corrections, while $\varepsilon_{1s_{1/2}}$ does not. By $\mathcal{E}_d=E_d-i\Gamma_d/2$ we denote the complex eigenvalues of the non-Hermitian operator $\hat{\mathcal{H}}=E_d^{(0)}\cdot\hat{1}+V_d(E_d^{(0)})$ acting in the corresponding subspace of the unperturbed d states.[13–15] The quasipotential V_d, defined in the lowest approximation, contains contributions due to all $1/Z$-order corrections. The right $|d_R\rangle$ and left $\langle d_L|$ eigenvectors of $\hat{\mathcal{H}}$ (Refs. 13–15; see also Ref. 9) where only right vectors have been employed) are normalized by the condition $\langle d_L|d'_R\rangle=\delta_{dd'}$. For states with different quantum numbers there is no difference between the left $|d_L\rangle$ and right $|d_R\rangle$ vectors. The nondiagonal partial widths $W_{dd',s}$ for radiative transitions between d and s states are defined by the multipole expansion of the expression

$$W_{dd',s}=2\pi\omega^2\sum_{\mathbf{e}}\int d\Omega\langle s_R|\hat{R}_\gamma|d_R\rangle\langle s_L|\hat{R}_\gamma|d'_R\rangle^*, \tag{3}$$

where $d\Omega$ means integration over the directions of the photon emission, and the operator for the emission of a photon with polarization $\mathbf{e}$ and momentum $\mathbf{k}$ is given by

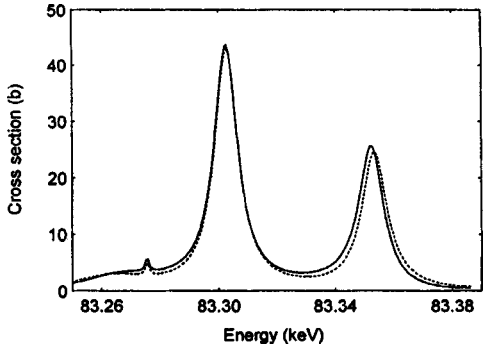

FIG. 1. Total DR cross section for U^{91+} in the vicinity of the $KL_{12}M_{12}$ resonances as a function of the incident electron energy (solid curve). The dashed curve corresponds to the Lorentz terms in the orthogonal basis.

$$\hat{R}_\gamma = e\sum_{n=1}^{2}\frac{(\alpha\cdot e^*)}{2\pi\sqrt{\omega}}e^{-i\mathbf{k}\cdot\mathbf{x}_n}.$$

Note that Eq. (3) differs from the definition given in Ref. 7 and generalizes the corresponding expressions in Refs. 14–16. However, with the present choice of the matrix elements involved in $W_{dd',s}$, our expression for $\sigma_{\rm DR}$ looks similar to the formula for the DR part of the cross section, published in Refs. 14–16. Moreover, definition (3) keeps the Bell–Steinberger equality in its conventional form

$$\sum_s W_{dd',s} = i(\mathcal{E}_d - \mathcal{E}^*_{d'})\langle d'_R|d_R\rangle, \tag{4}$$

but now the final states s may also have identical quantum numbers. Note that, in contrast with Eq. (1), in Eq. (4) the summation over s includes *all* possible low-lying states.

The particular case when $d=d'$ in the sum of Eq. (1) corresponds to the superposition of Lorentz shapes of the DR process. The terms $\sigma_{\rm DR}$ with $d\neq d'$ describe the radiative interference due to overlap between the upper as well as between the lower states, and lead to the asymmetry of the combined shape. It should be noted that the definition of the ''pure'' Lorentz shapes is not unique in different basis sets. This means that even if terms $d\neq d'$ are not taken into account in Eq. (1) the radiative interference turns out to be partially involved in $\sigma_{\rm DR}$ in the biorthogonal basis through the complex mixing coefficients of the identical states. Nevertheless, it is usual to use the orthogonal basis set, and in this case the Lorentz terms do not include the radiative interference. Asymmetry of the shapes can be numerically characterized, for example, by Low's parameter.cite8 We use for this purpose the nonorthogonality integrals $\langle d_R|d'_R\rangle$. In the orthogonal basis for such a parameter one can choose the ratio of the nondiagonal widths to the energy intervals between the overlapping levels.

Numerical calculations of the DR cross sections have been performed using Eq. (1) in the vicinities of the $KL_{12}M_{12}$ and $KM_{12}M_{12}$ resonances of heliumlike uranium. The energies and rates were calculated in the framework of the $1/Z$ expansion. The energies of the levels have the radiative[23–26] (electron self-energy and vacuum polarization) and the exact one-photon electron–electron interaction corrections included. The finite

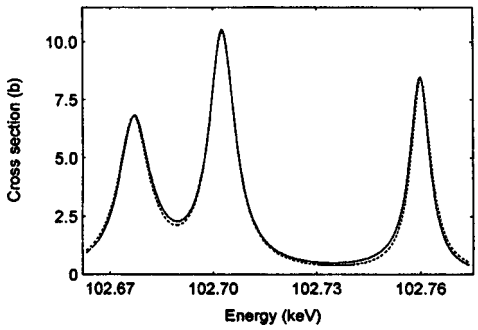

FIG. 2. Total DR cross section for U^{91+} in the vicinity of the $KM_{12}M_{12}$ resonances (solid curve); dashed curve — with no radiative interference included.

nuclear size was taken into account directly in the Dirac wave functions. In the case of the $KL_{12}M_{12}$ DR resonances, there are four pairs of identical levels. As final recombined levels in this case, the doubly excited $[2s^2_{1/2}]_0$, $[2p^2_{1/2}]_0$, and $[2s_{1/2}2p_{1/2}]_{0,1}$ states were chosen. The first pair has the same parity and zero total angular momentum, but the second pair has a different total angular momentum and does not mix. The results of the corresponding DR cross section calculations are shown in Fig. 1. The second example is given by the $KM_{12}M_{12}$ resonances. In this case, there are only two identical upper states, $[3s^2_{1/2}]_0$ and $[3p^2_{1/2}]_0$, and the cross section is resolved with regard to $[2l_{1/2}3l'_{1/2}]_{0,1}$ configurations (see Fig. 2). As can be seen in both examples considered, the interference effects originate from the radiative overlap of the upper and lower groups of doubly excited states with identical quantum numbers. The values of nonorthogonality integrals $|\langle d_R|d'_R\rangle|$ are 0.18 and 0.1 for the $KL_{12}M_{12}$ and $KM_{12}M_{12}$ resonances, respectively. The main error in the calculations is due to the omission of order-$1/Z$ corrections in the evaluation of the radiative widths, which as a consequence are uncertain to about 2–3%. The magnitude of the effect looks large enough to be observable in the experiments. We should note that in Ref. 16 the differential cross section was measured. To observe the effect we discuss, one should measure the total cross section, that is, to detect the photons emitted in all directions. The last problem is not a fundamental one for Super-EBIT experiments. The cross sections obtained may serve as a focus for near-future experimental investigations.

AVN gratefully acknowledges financial support in the form of an Exquota Fellowship from the Royal Society for this study.

[a)]e-mail: anef@thd.pnpi.spb.ru

[1] E. D. Commins and P. H. Bucksbaum, *Weak interactions of leptons and quarks*, Cambridge University Press, Cambridge, 1983.
[2] W. D. Callender and C. P. Browne, Phys. Rev. C **2**, 1 (1970).
[3] A. M. Nathan, G. T. Garvey, P. Paul *et al.*, Phys. Rev. Lett. **35**, 1137 (1975).
[4] T. G. Eck, Phys. Rev. Lett. **31**, 270 (1973).
[5] A. Gaupp, H. J. Andrä, and J. Macek, Phys. Rev. Lett. **32**, 268 (1974).
[6] K. E. Lassila and V. Ruuskanen, Phys. Rev. Lett. **17**, 490 (1966).
[7] L. N. Labzowsky and A. V. Nefiodov, Phys. Rev. A **49**, 236 (1994).

[8] F. Low, Phys. Rev. **88**, 53 (1952).
[9] M. A. Braun, Zh. Éksp. Teor. Fiz. **94**, 145 (1988) [Sov. Phys. JETP **67**, 2039 (1988)].
[10] V. G. Gorshkov, L. N. Labzowsky, and A. A. Sultanaev, Zh. Éksp. Teor. Fiz. **96**, 53 (1989) [Sov. Phys. JETP **69**, 28 (1989)].
[11] V. G. Gorshkov, V. V. Karasiev, L. N. Labzowsky *et al.*, Opt. Spektrosk. **72**, 31 (1992) [Opt. Spectrosc. **72**, 16 (1992)].
[12] V. V. Karasiev, L. N. Labzowsky, A. V. Nefiodov *et al.*, Phys. Scr. **46**, 225 (1992).
[13] V. M. Shabaev, J. Phys. A **24**, 5665 (1991).
[14] V. V. Karasiev, L. N. Labzowsky, A. V. Nefiodov *et al.*, Phys. Lett. A **161**, 453 (1992).
[15] V. M. Shabaev, Phys. Rev. A **50**, 4521 (1994).
[16] A. V. Nefiodov, V. V. Karasiev, and V. A. Yerokhin, Phys. Rev. A **50**, 4975 (1994).
[17] N. R. Badnell and M. S. Pindzola, Phys. Rev. A **45**, 2820 (1992).
[18] M. S. Pindzola, N. R. Badnell, and D. C. Griffin, Phys. Rev. A **46**, 5725 (1992).
[19] M. S. Pindzola, F. J. Robicheaux, N. R. Badnell *et al.*, Phys. Rev. A **52**, 420 (1995).
[20] M. Zimmermann, N. Grün, and W. Scheid, J. Phys. B **30**, 5259 (1997).
[21] D. A. Knapp, P. Beiersdorfer, M. H. Chen *et al.*, Phys. Rev. Lett. **74**, 54 (1995).
[22] D. A. Knapp, R. E. Marrs, M. B. Schneider *et al.*, Phys. Rev. A **47**, 2039 (1993).
[23] G. Soff and P. J. Mohr, Phys. Rev. A **40**, 2174 (1989).
[24] P. J. Mohr and Y.-K. Kim, Phys. Rev. A **45**, 2727 (1992).
[25] P. J. Mohr, Phys. Rev. A **46**, 4421 (1992).
[26] P. J. Mohr and G. Soff, Phys. Rev. Lett. **70**, 158 (1993).

Published in English in the original Russian journal. Edited by Steve Torstveit.

Anomalous transition to turbulence in inert gases

S. A. Novopashin

Institute of Thermal Physics, Siberian Branch of the Russian Academy of Sciences, Novosibirsk State University, 630090 Novosibirsk, Russia

A. Muriel

Center for Fluid Dynamics, University of the Philippines Los Banos College, Laguna, Philippines; Laboratoire de Physique, Ecole Normale Superieure de Lyon, 69364 Lyon Cedex 07, France

(Submitted 14 August 1998)
Pis'ma Zh. Éksp. Teor. Fiz. **68**, No. 7, 557–559 (10 October 1998)

It is found experimentally that the critical Reynolds numbers for the transition to turbulence are different for He, Ar, and Kr flows. © *1998 American Institute of Physics.* [S0021-3640(98)00719-1]

PACS numbers: 47.27.Cn

Numerous experiments show that the Navier–Stokes equation[1]

$$\rho\left(\frac{\partial U}{\partial t}+(U\cdot\nabla)U\right)=-\nabla P+\eta\nabla^2 U+(\zeta+\eta/3)\nabla(\nabla\cdot U) \tag{1}$$

describes laminar fluid flow. For gas flows, the coefficients of viscosity η and ζ are related to the relaxation of the translational and internal degrees of freedom of the molecules.[2] In the study of incompressible fluid flow the last term in Eq. (1) can be dropped. This simplifies the analysis of the flow and makes it possible to introduce a single dimensionless parameter that characterizes the flow — the Reynolds number $\mathrm{Re}=\rho LU/\eta$, where ρ,L, and U are, respectively, the density, the characteristic size, and the characteristic velocity of the flow. A breakdown of stationary flow and transition to turbulence are associated with loss of stability as Reynolds number increases. For compressible flow the last term in Eq. (1) must be retained, which makes it necessary to introduce an additional number, the Mach number $\mathrm{M}=U/c$ (c is the speed of sound) and to study the influence of the bulk viscosity η. Moreover, for compressible flows a heat problem must be solved because of the appearance of temperature fields and heat transfer at the flow boundaries. We note that near a laminar–turbulent transition the second viscosity can influence the flow.[3] For inert gases the second viscosity is strictly zero.[2] In this case the Reynolds and Mach numbers completely characterize the flow. The corrections due to the compressibility of the gas are of the order of M^2. For this reason compressibility effects are ordinarily neglected for flows with Mach numbers less than 0.2 (the errors do not exceed several percent). In accordance with the ideas expounded in Refs. 4 and 5, however, the transition to turbulence can occur in differently even in this case. Our objective in the present work is to compare the critical Reynolds for He, Ar, and Kr flows. A Hagen–Poiseuille flow — flow in a long circular pipe — was chosen for the experiments. This flow is stable with respect to infinitesimal disturbances.[6,7] The

 © 1998 American Institute of Physics

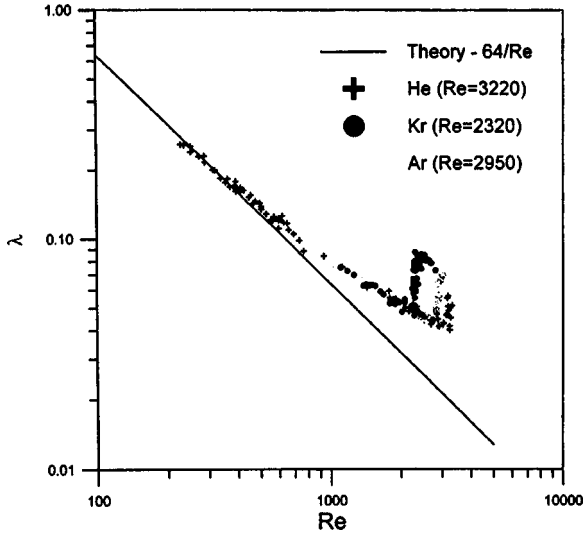

FIG. 1. Drag coefficient versus Reynolds number.

transition to turbulence occurs as a result of finite perturbations or insufficiently smooth boundary conditions at the pipe entrance. In the laminar flow regime the drag coefficient is $\lambda=(\Delta P/L)/(\rho U^2/2d)=64/\mathrm{Re}$.[1] Here $\Delta P/L$ is the average pressure gradient along the pipe, ρ is the gas density, U is the gas flow rate, and d is the pipe diameter. In the turbulent regime the drag coefficient increases sharply, which makes it possible to monitor the critical Reynolds number reliably.

The experiments were performed on the apparatus described in Ref. 3. The measurements were performed with gas flowing out through a glass capillary (300 mm long, 1.3 mm in diameter) from a 0.13 mm^3 hermetically sealed chamber filled with gas at high pressure. The chamber was equipped with systems for evacuating and admitting gas, making it possible to investigate different gases. The pressure drop on the capillary was measured using a membrane-type pressure gauge, giving an accuracy of 0.02 torr. The rate of pressure drop in the chamber makes it possible to determine the gas flow rate (and therefore also the average flow velocity) as a function of the pressure drop on the capillary. In the case of a smooth entrance (the capillary is partially fused at the edges) the transition to turbulence occurred at Reynolds numbers above 10^4. For the experiments, the entrance section of the capillary was sawed off perpendicular to the capillary axis. Under these conditions the transition occurs as a result of perturbations at the entrance. Therefore the transition to turbulence during the flow of different gases occurred under absolutely identical perturbations. The measurement procedure consisted of the following. The chamber was evacuated to pressure 10^{-1} torr and then filled with the experimental gas to a pressure above atmospheric pressure (the maximum pressure obtained for helium — 1.2×10^3 torr). Thermal equilibrium with the surrounding medium and stabilization of the gas flow in the chamber occurred in 30 min. The valve covering the capillary on the outside was opened in 3–4 s. The characteristic pressure drop in this time depends on the gas and the pressure difference. For reference, we note that for argon near the laminar–turbulent transition this drop was $\sim$0.5 torr. The pressure in the chamber

TABLE I.

	He	Ar	Kr
Speed of sound (m/s)	1012	334	222
Kinematic viscosity ν (10^{-6} m^2/s)	114	13.0	7.51
Critical Reynolds number	3220	2950	2320
Mach number	0.22	0.11	0.08
Pressure drop (torr)	300	45	28

decreased as a result of gas efflux and a drop in the temperature of the remaining gas. The gas efflux was neither adiabatic nor isothermal because of heat transfer occurring in the process. After the valve closes, the pressure in the chamber increases as a result of the gas temperature in the chamber being restored to room temperature. The restoration time depends on the gas. For example, for krypton it is about 150 s. The pressure difference in the chamber before start-up and after temperature restoration makes it possible to calculate the gas flow rate. The Reynolds number and the drag coefficient were determined from the parameters of the gas at the capillary entrance. For the initial pressure drop, the flow is turbulent. As pressure decreases to a critical value, the flow becomes laminar. We note that gas efflux in the turbulent regime is accompanied by sound emission, whose intensity drops considerably at the point of the transition to laminar flow.

The drag coefficient as a function of the Reynolds number for He, Ar, and Kr is shown in Fig. 1. The physical characteristics for these gases at 300 K and 750 torr are presented in Table I. The table also shows the critical Reynolds numbers, the Mach numbers, and the pressure drop at the point of the transition.

Figure 1 and Table I show that the critical Reynolds number for krypton is 27% lower than for argon and 38% lower than for helium. The corresponding limit for argon and helium is about 10%. The observed difference of the critical Reynolds numbers looks paradoxical. Indeed, in accordance with the corrections due to compressibility the critical number for helium should differ most strongly from the corresponding values for argon and krypton. The difference between argon and krypton should be much smaller. The solution of this discrepancy could require new hypotheses concerning the nature of the laminar–turbulent transition.

[1] L. D. Landau and E. M. Lifshitz, *Fluid Mechanics*, Pergamon Press, New York, 1987, 2nd edition [Russian original, Nauka, Moscow, 3rd edition, 1986].
[2] E. M. Lifshitz and L. P. Pitaevskiĭ, *Physical Kinetics*, Pergamon Press, Oxford, 1981 [Russian original, Nauka, Moscow, 1979].
[3] O. A. Nerushev and S. A. Novopashin, JETP Lett. **64**, 47 (1996).
[4] A. Muriel and M. Dresden, Physica D **81**, 221 (1995).
[5] A. Muriel and M. Dresden, Physica D **94**, 103 (1996).
[6] J. A. Fox, M. Lesson, and W. V. Bhat, Phys. Fluids **11**, 1 (1968).
[7] H. Salwen, F. W. Cotton, and C. E. Grosch, J. Fluid Mech. **92**, 273 (1980).

Translated by M. E. Alferieff

New experimental data on the possibility of influencing fluctuational particle fluxes in a L-2M stellarator edge plasma

G. M. Batanov, L. V. Kolik, A. E. Petrov, K. A. Sarksyan, N. N. Skvortsova, O. I. Fedyanin, N. K. Kharchev, Yu. V. Khol'nov, and S. V. Shchepetov,
Institute of General Physics, Russian Academy of Sciences, 117942 Moscow, Russia

C. Hidalgo and B. van Milligen
CIEMAT, 28040 Madrid, Spain

(Submitted 20 July 1998; resubmitted 21 August 1998)
Pis'ma Zh. Éksp. Teor. Fiz. **68**, No. 7, 560–565 (10 October 1998)

The results of an experiment show that in the edge plasma of a L-2M stellarator the radial electric field is one of the determining factors influencing the formation of spatial structures and fluctuational particle fluxes. A point where the poloidal velocity of the fluctuations reverses is observed in an experiment with a high neutral-gas flux from the chamber walls. © *1998 American Institute of Physics.*
[S0021-3640(98)00819-6]

PACS numbers: 52.25.Fi, 52.55.Hc, 52.25.Gj

The problem of the effect of fluctuational transport in the edge plasma of toroidal magnetic traps on the global confinement of the plasma is attracting increasing attention.[1] Of special interest are some previously observed structures (see, for example, Refs. 2 and 3) which are characterized by a high degree of correlation between the plasma density fluctuations δn and the floating-potential fluctuations $\delta\phi$. This interest is entirely justified, since it is obvious that the formation of such spatial structures in the edge plasma can lead to intensification of transport processes, specifically, intensification of the local fluctuational radial particle flux $\tilde{\Gamma}$. The fact that the correlated radial structures and intensification of the fluctuational particle flux $\tilde{\Gamma}$ in the edge plasma of a toroidal magnetic trap are related with one another has been indicated in experimental works.[2,4] In these works an increase in the correlation of a solitary unstable magnetohydrodynamic mode in the region of formation of the proposed magnetic island was detected. Intensification of fluctuational particle transport was also observed at the same radius. But the important problem of studying the role of specific plasma parameters, which are not assumed but rather directly measured, in the formation of spatial structures and, in consequence, in the increase of $\tilde{\Gamma}$ has thus far remained beyond the purview of experimenters. This problem was formulated some time ago in the scientific program of experiments on the L-2M stellarator. In the present letter we present the results of the first experiment

 © 1998 American Institute of Physics

performed as part of this program, where it was possible to influence the parameters of the edge plasma by varying the intensity of the neutral-gas flux from the walls of the vacuum chamber.

The L-2M stellarator[5] is an $l=2$ device. The major radius of the torus is $R=100$ cm and the average plasma radius, bounded by the separatrix, is $\langle r_s \rangle = 11.5$ cm. The production and heating of the plasma were performed in the electron cyclotron resonance regime at the second harmonic of the electron gyrofrequency (the magnetic field on the magnetic axis was $B=1.35-1.4$ T) with gyrotron radiation power $P_0 \approx 150$ kW and heating pulse duration up to 10 ms. The measurements were performed in plasma whose average density $\langle n \rangle = (1.3-1.8)\times 10^{13}$ cm^{-3} and central electron temperature $T_e(0)=400-600$ eV. In the edge plasma at radius $r/r_s=0.85-0.9$ (r_s is the radius of the separatrix) one has $n(r)\approx(1-2)\times 10^{12}$ cm^{-3} and $T_e(r)\approx 30$ eV. The relative level of the plasma density fluctuations decreases in the radial direction from the separatrix into the interior of the plasma in the interval from $r/r_s=1$ to $r/r_s=0.75$ from $\delta n/n=0.3-0.4$ to $\delta n/n=0.1-0.2$. Both helium (He) and hydrogen (H_2) were used as the working gas. This made it possible to work in a relatively wide range of neutral gas fluxes from the walls of the vacuum chamber, since hydrogen absorption by the chamber walls (stainless steel) followed by outgassing into the evacuated volume can be much higher than for helium.

The measurements were performed using a probe apparatus consisting of several single cylindrical probes. The single probes were placed in pairs in the poloidal and radial directions at distances from each other $l_s=4-5$ mm. The probe apparatus could be moved in the radial direction toward the center of the plasma by 1.5–3 cm from the separatrix.

The following parameters of the edge plasma were measured using the probe apparatus: the plasma density and its fluctuations δn (in the ion-current saturation regime the ion current on the probe $I_s \sim n$, while $\delta I_s \sim \delta n$); the floating potential ϕ and its fluctuations $\delta\phi$; the radial distribution of the indicated parameters $n(r/r_s)$, $\delta n(r/r_s)$, $\phi(r/r_s)$, and $\delta\phi(r/r_s)$; the electric fields — radial E_r and poloidal E_θ — were determined from these measurements. The fluctuational particle flux $\tilde{\Gamma} \sim (\delta n \cdot \delta E_\theta)/B$ (Ref. 3), where δE_θ is the fluctuation of the poloidal field, was also determined. Besides these parameters, the cross-correlation coefficients of signals from two spatially separated probes in both the poloidal direction $K_{\rm pol}$ and in the radial direction $K_{\rm rad}$ were calculated by a standard method. The formation of correlated spatial structures could be judged from the computed values of $K_{\rm pol}(r/r_s)$ and $K_{\rm rad}(r/r_s)$. Besides the correlation of the fluctuations, the coherence[a)] of the frequency components of the fluctuation signals in real time was determined using spectral analysis with respect to wave packets (wavelet coherence).[6] The wavelet spectra I_ω of the recorded fluctuation signals were also calculated.

Let us now turn to the results of the measurements. Figure 1 shows the radial distributions of the floating potential $\phi(r/r_s)$ for different experimental conditions. Let us consider first the curves *1* and *2*. Curve *1* refers to conditions with a low neutral-gas flux from the walls of the vacuum chamber (we designate these conditions as regime *A*). Curve *2* refers to conditions with a high neutral-gas flux from the walls of the vacuum chamber (we designate these conditions as regime *B*). For each regime the numbers of the pulses whose data were used in our work are presented in the caption to Fig. 1.

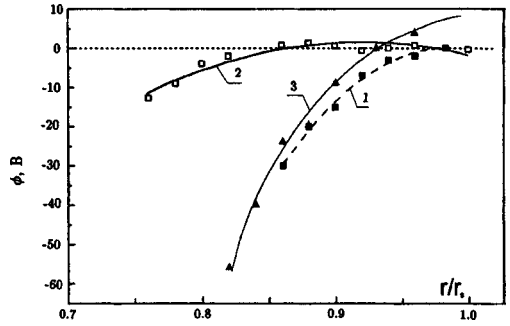

FIG. 1. Radial distribution of the floating potential $\phi(r/r_s)$: Curve *1* — regime *A* (*N* 46786–46805), curve *2* — regime *B* (*N* 47233–47252, *N* 472684–47281)), curve *3* — regime *A* (*N* 45583–45605).

A comparison of the two curves reveals a fundamental difference: In regime *A* the curve *1* turns negative already at the radius $r/r_s=0.98$, and by $r/r_s=0.85$ the absolute value of the floating potential reaches $|\phi|=30$ V, giving a field intensity $E_r\approx 28$ V/cm (taking the radial gradient of T_e into account can only decrease E_r slightly). A different picture is observed in the regime *B*: On curve *2* the point where $\phi(r/r_s)$ turns negative is shifted into the interior of the plasma, to $r/r_s=0.85$, and for $1>r/r_s>0.85$ the radial electric field has values $E_r\approx 1-1.5$ V/cm, i.e., an order of magnitude weaker than in the regime *A*. But now, after the transition point, for $r/r_s<0.85$, a radial electric field $E_r\approx 16$ V/cm is detected over a distance of 6–7 mm. Therefore, in the region of the edge plasma from $r/r_s=0.98$ to $r/r_s=0.85$, where a radial electric field $E_r\approx 28$ V/cm is detected in the regime *A*, in the regime *B* the field is negligibly small and becomes appreciable only for $r/r_s<0.85$. In contrast to a number of experiments on tokamaks (see, for example, Ref. 7), where a reversal of E_r in the edge plasma is observed, under the conditions of the present experiment on L-2M only a transition from a region with low values of E_r to a region with substantially higher values of E_r is explicitly detected.

Small differences are also observed for other plasma parameters accompanying a transition from the regime *A* to the regime *B*. The distributions of the plasma density in the two regimes are similar, but with a radial shift, so that the local values of the density $n(r)$ are tied to regions which are identical with respect to the characteristics of the distribution $\phi(r)$. The relative level $\delta n/n$ of the plasma density fluctuations for regime *B* for $r/r_s\geqslant 0.85$ is somewhat higher (by a factor of 1.3) than for the regime *A* in the same region of the plasma. The differences in the wavelet spectra I_ω for the fluctuation signals δn and $\delta\phi$ between regimes *A* and *B* are negligible.

Figure 2 shows the dependence of the cross-correlation coefficients on r/r_s for regimes *A* and *B*. Figure 2a shows the function $K_{\rm pol}(r/r_s)$ between signals from two probes separated from one another in the poloidal direction; Fig. 2b shows the function $K_{\rm rad}(r/r_s)$ between signals from two probes separated from one another in the radial direction. $K_{\rm pol}$ and $K_{\rm rad}$ were calculated over the averaging time $\Delta t=3$ ms from 54 to 57 ms in real time (the heating pulse was usually switched on at 50 ms). It is clear that one can judge from $K_{\rm pol}$ and $K_{\rm rad}$ whether or not correlated spatial structures with poloidal and radial directionality, respectively, form. Comparing the curves in Figs. 2a and 2b, we see that in both regimes *A* and *B* the radial and poloidal correlation coefficients both

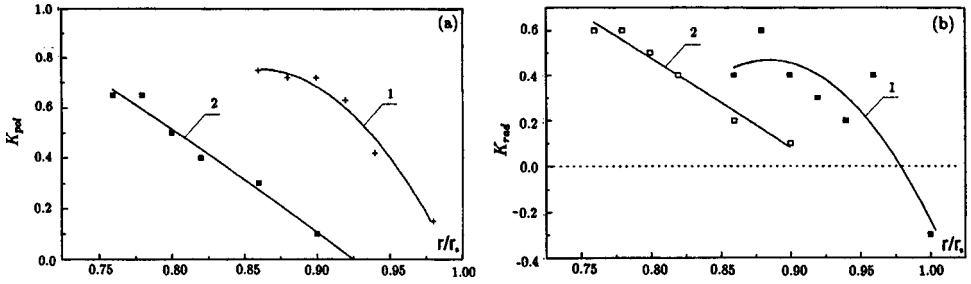

FIG. 2. Radial distribution of the cross-correlation coefficients ($t=54-57$ ms). a) $K_{\text{pol}}(r/r_s)$, curve *1* — regime *A*, curve *2* — regime *B*; b) $K_{\text{rad}}(r/r_s)$, curve *1* — regime *A*, curve *2* — regime *B*.

increase, reaching values $K\approx 0.6-0.8$ in the regions of edge plasma where the radial electric field $E_r\approx 15-30$ V/cm, i.e., after the probes have passed the point where the floating potential ϕ turns negative. As mentioned above, this point is located at $(r/r_s)_{tr}=0.98$ for regime *A* and $(r/r_s)_{tr}=0.85$ for regime *B* (see Fig. 1). Therefore well-correlated poloidal and radial structures form in regions of the edge plasma where $E_r\neq 0$, specifically, under the particular conditions of the present experiment, at $E_r\approx 15-30$ V/cm.

Let us now consider the behavior of $\tilde{\Gamma}$ at a transition from the regime *A* into the regime *B*. We turn to Fig. 3, which displays for both regimes curves of $\tilde{\Gamma}$ (the values of $\tilde{\Gamma}$ are given in relative units) versus the radial position of the probe, i.e., as a function of r/r_s. One can see that for both the regime *A* (curve *1*) and the regime *B* (curve *2*) $\tilde{\Gamma}$ increases by a factor 4–8 in the regions of the edge plasma where the poloidal and radial correlated structures have formed (see Fig. 2) and where an appreciable radial electric field is detected.

In summary, the data presented above make it possible to state the following: First, as the neutral-gas flux from the walls of the vacuum chamber increases, the point of the transition of ϕ to negative values can be moved deeper in the radial direction toward the center of the plasma, and the extent of the part of the edge plasma where the radial electric field $E_r\approx 0$ can thereby be increased; second, well-correlated spatial structures

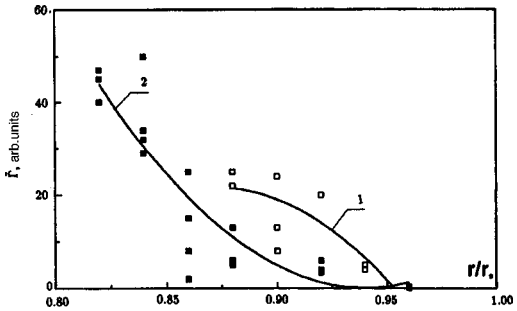

FIG. 3. Radial distribution of the local radial fluctuational particle flux $\tilde{\Gamma}$ ($t=54-57$ ms). Curve *1* — regime *A*, curve *2* — regime *B*.

form in deeper layers of the plasma, which are accordingly located far from the separatrix, at $r/r_s < (r/r_s)_{tr}$, where $E_r \neq 0$; and, third, in these same regions of the edge plasma, as correlated spatial structures form, the local radial fluctuational particle flux $\tilde{\Gamma}$ increases rapidly.

It is obvious that, solely from the data presented above, one cannot reliably identify the radial electric field as a measurable parameter that determines the formation of spatial structures and, ultimately, the intensification of the fluctuational particle flux $\tilde{\Gamma}$, since other measured parameters also vary to some degree. However, in one series of measurements (see Fig. 1, curve *3*, working gas H_2) it was possible to increase the radial electric field to $E_r = 48$ V/cm in the layer of edge plasma from $r/r_s = 0.95$ to $r/r_s = 0.84$, i.e., in the same location as in the case of the regime *A*. The other plasma parameters noted previously remain the same as in regime *A*. For the indicated third regime *A′*, wavelet-coherent spectra of the floating-potential fluctuations were measured in real time in the poloidal and radial directions.

It was found that in this case the coefficient of poloidal coherence increased appreciably to $(K_{\text{coh}})_{\text{pol}} \approx 0.8-1$ (in the frequency range up to 300–400 kHz), while the radial coherence, without which the radial fluctuational flux is small, essentially vanished. This fact in combination with other data shows that in this setup there exists an optimal value of the radial electric field, equal to $E_r \approx 15-30$ V/cm, for which poloidal and radial correlated structures form efficiently and, in consequence, the fluctuational particle flux $\tilde{\Gamma}$ increases.

But the question of why the region with an appreciable radial electric field is displaced in the radial direction accompanying a transition from regime *A* to regime *B* remains open.

Apparently, as the neutral-gas flux from the chamber walls increases, a cooling of the peripheral layer of the plasma column occurs, as a result of which, as the electron temperature T_e decreases, it flattens out in the radial direction and a region with small E_r forms in the edge plasma.

It was also observed that such a change in the parameters of the edge plasma also influences the direction of the poloidal rotational velocity V_θ of the fluctuations. These data were obtained from correlation measurements, specifically, from the sign and magnitude of the correlation time t_{corr} at which a maximum of K_{pol} is observed in the corresponding correlation curves. Figure 4 shows t_{corr} versus r/r_s for the regime *A* (curve *1*) and for the regime *B* (curve *2*). We note immediately that positive values of t_{corr} correspond in our case to the direction of electronic diamagnetic drift, while negative values of t_{corr} correspond to the direction of ionic diamagnetic drift. Comparing curves *1* and *2* it is obvious that in regime *A* the velocity component V_θ is directed in the direction of electronic diamagnetic drift in the entire edge plasma reached by the probes, from $r/r_s = 1$ to $r/r_s = 0.84$, with V_θ increasing in the direction toward the center of the plasma to a value $V_\theta \approx 5 \times 10^5$ cm/s. At the same time, in the regime *B* the velocity V_θ is directed in the direction of ionic diamagnetic drift in the region of the edge plasma from $r/r_s = 1.0$ to $r/r_s = 0.85$, where $E_r \approx 0$. But after the point where the floating potential ϕ turns negative at $r/r_s = (r/r_s)_{tr} = 0.85$, the direction of the poloidal velocity of the fluctuations reverses in the direction of electronic diamagnetic drift. The small values of t_{corr} for $0.85 \leqslant r/r_s \leqslant 0.925$ are interesting (Fig. 4, curve *1*). Such values of t_{corr} could be due

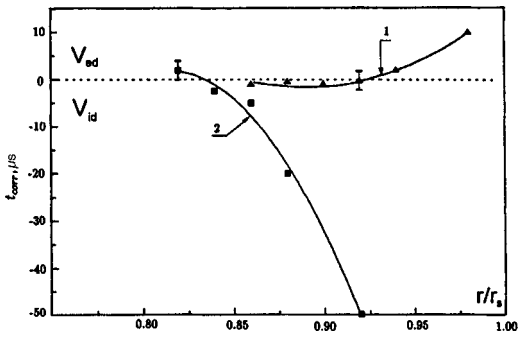

FIG. 4. Correlation time between fluctuation signals of the floating potential versus the radial position of the probes ($t=54-57$ ms).

to rotation of the plasma. However, in the present experiment direct measurements of the rotational velocity of the plasma were not performed.

It is commonly assumed[1] that for a plasma lying outside the last closed magnetic surface the velocity of fluctuations is characteristically oriented in the same direction as the ionic diamagnetic drift velocity (in both tokamaks and stellarators). However, the experiment whose results are reported in the present letter was performed for a magnetic configuration in which the structure of the topologically stable closed magnetic surfaces is bounded by a separatrix ($r/r_s=1$), and it is only outside this that the magnetic field lines emerge onto the vacuum chamber within a period of the helical vacuum field (here the plasma pressure in the region under study is low and is obviously inadequate for destroying the magnetic surfaces). Therefore, by decreasing the temperature of the edge plasma, as a result of a change in the neutral-gas flux from the chamber walls, it is also possible to change the direction of the poloidal velocity of the fluctuations in the plasma near the boundary.

The experimental results presented in this letter make it possible to draw the following conclusions.

1. We have shown that the quasistationary neutral-gas flux from the chamber walls can influence the formation of correlated fluctuation structures.

2. We have measured the optimal value of the radial electric field $E_r \approx 15-30$ V/cm, for which simultaneous formation of poloidal and radial correlated structures occurs and, in consequence, the greatest intensification of the fluctuational particle flux $\tilde{\Gamma}$ occurs.

3. We have detected a point where the poloidal velocity of the fluctuations reverses under conditions with a high neutral-gas flux from the chamber walls was observed far from the plasma boundary.

In closing, we wish to express our deep appreciation to the members of the L-2M Stellarator team who made it possible to perform the experiment. This work was supported by the Russian Fund for Fundamental Research (Project 98-02-18345).

[a)]The concept of coherence refers to the frequency components of the fluctuation signals, while the concept of correlation refers to the signals themselves.

[1] C. Hidalgo, Plasma Phys. Controlled Fusion **37**, A53 (1995).
[2] C. Hidalgo, M. A. Pedrosa, B. van Milligen *et al.*, *Proceedings of the 16th IAEA*, Montreal, 1996, AP1-4.
[3] N. N. Skvortsova, G. M. Batanov, O. I. Fedyanin *et al.*, J. Plasma Fusion Res., J. Plasma Fusion Res. Ser. **1**, 298 (1998).
[4] M. A. Pedrosa, C. Hidalgo, B. van Milligen *et al.*, Plasma Phys. Controlled Fusion **38**, 365-373 (1996).
[5] V. V. Abrakov, D. K. Akulina, E. D. Andrukhina *et al.*, *Proceedings of the 10th International Conference on Stellarators*, EUR-CIEMAT, 1995, p. 30.
[6] B. van Milligen, E. Sanchez, T. Estrada *et al.*, Phys. Plasmas **2**, 3017 (1996).
[7] V. A. Vershkov, V. V. Greva, S. V. Soldatov *et al.*, J. Nucl. Mater. **241–243**, 873 (1997).

Translated by M. E. Alferieff

Nonadiabatic heating of a plasma produced by the ionization of a gas by a short intense laser pulse

N. E. Andreev, M. V. Chegotov, and M. E. Veĭsman
Joint High-Temperature Institute, Russian Academy of Sciences, 127412 Moscow, Russia

T. Auguste, P. D'Oliveira, S. Hulin and P. Monot
Centre d'Etudes de Saclay, Commissariat à l'Energie Atomique, 91191 Gif-Sur-Yvette, France

A. Ya. Faenov, T. A. Pikuz, A. I. Magunov, and I. Yu. Skobelev
All-Russia Scientific-Research Institute of Physicotechnical and Radio Engineering Measurements, 141570 Mendeleevo, Moscow Region, Russia

F. B. Rosmej
Darmstadt Technical University, D-44780 Darmstadt, Germany

M. Yu. Romanovskiĭ
Institute of General Physics, Russian Academy of Sciences, 117942 Moscow, Russia

(Submitted 9 September 1998)
Pis'ma Zh. Éksp. Teor. Fiz. **68**, No. 7, 566–571 (10 October 1998)

A hydrodynamic model of the interaction of a short, intense laser pulse with moderate-density gases is constructed. The model systematically takes into account both tunneling-ionization processes and the relativistic motion of the electrons that are produced by the ionization of the gas in the relativistically strong field of the pulse. X-ray spectroscopy data agree well with the proposed theory. © *1998 American Institute of Physics.* [S0021-3640(98)00919-0]

PACS numbers: 52.50.Jm, 52.40.Nk

1. A great deal of attention is now being devoted to the interaction of short (duration τ_{pul} less than or of the order of 100 fs), intense (peak intensity $I_{\max}$ of the order of or higher than 10^{16} W/cm^2) laser pulses with different gases.[1,2] In many experimental schemes or proposed setups the state of the plasma produced in course of the ionization of a gas by an intense pulse or some time after the pulse leaves plays an important role (see, for example, Refs. 3–7).

One of the most important characteristics of this state is the temperature of the electron gas that is associated with the so-called residual electron energy.[8,9] The main properties of the electron temperature are determined by the mechanism of ionization of neutral atoms or ions. For moderate gas densities (less than or of the order of 10^{20} cm^{-3}) the effective collisional ionization frequency is less than $1/\tau_{\text{pul}}$ and the principal ionization mechanism is ionization by the electromagnetic field of the laser pulse. On account of the high intensity of the laser pulse, the Keldysh parameter γ (Ref. 10) is less than or of the order of 1. In this case the field ionization occurs by the tunneling mechanism. The

 © 1998 American Institute of Physics

ionization probability is described by the well-known ADK formulas, which have been checked in a number of experiments.[11] However, a contradictory picture of the experimental results and theoretical attempts to explain them has now emerged.[3–7] Specifically, direct or indirect measurements of the electron temperature turned out to be at variance with the values of the temperature calculated using the ADK formulas for the ionization of multielectron atoms.

In our opinion, the disagreement between theory and experiment is due to the simplified point of view of the ionization process and its results. When the residual electron energy is treated only as an average energy per electron after the passage of the pulse, in many cases a substantial fraction of the information about the real electron energy distribution is lost.

In the present letter we propose a hydrodynamic description of the interaction of a short, intense laser pulse with moderate-density gases. The description systematically takes account of both the tunneling-ionization processes and the relativistic motion of the electrons that are produced when the gas is ionized in the relativistically strong field of the pulse. The processes leading to the formation of the temperatures of the groups of electrons arising as a result of successive ionization of multielectron atoms are examined. The proposed approach is used to explain the experimental results on the irradiation of nitrogen with particle density of the order of 10^{19} cm^{-3} by a laser pulse with peak intensity 10^{19} W/cm^2 and duration of the order of 70 fs.

2. To describe the dynamics of the ionization and the accumulation of energy by free electrons in the field of a short, intense laser pulse, we shall employ the equations of hydrodynamics obtained from the kinetic equation for the electron momentum distribution function $f(\mathbf{r},\mathbf{p},t)$. At moderate gas densities as well as for sufficiently short laser pulses, the collisions of electrons with heavy particles during a pulse can be neglected.[3–9] Moreover, under the same conditions the ponderomotive forces and the generation of electrostatic fields can be neglected in the description of the accumulation of energy by the electrons that are produced.[8,9] Then, concentrating our attention on the region of maximum intensity of the laser beam, i.e., the spatial region near the beam axis and the plane of maximum focusing, we arrive at the analysis of a local kinetic equation

$$\frac{\partial f}{\partial t}+e\left(\mathbf{E}+\frac{1}{c}\mathbf{v}\times\mathbf{H}\right)\cdot\frac{\partial f}{\partial \mathbf{p}}=\Gamma(\mathbf{r},t)\,\delta(\mathbf{p})+[St]_{e,e}\,. \tag{1}$$

Here $\mathbf{E}(\mathbf{H})$ is the electric (magnetic) field of the laser radiation and $[St]_{e,e}$ is the electron-electron collision integral. The term $\Gamma(\mathbf{r},t)\,\delta(\mathbf{p})$ is the electron source due to tunneling ionization by an intense electromagnetic field. The velocity of the free electron produced in the process of tunneling ionization possesses is close to zero.[12,13] This is why the ionization source in Eq, (1) is proportional to $\delta(\mathbf{p})$.

Premultiplying Eq. (1) by 1, $\mathbf{p}$, and $\epsilon=\sqrt{m^2c^4+p^2c^2}-mc^2$ and integrating the results over the momenta, we obtain, respectively, the equations for the electron density $n_e(\mathbf{r},t)\equiv\int d^3\mathbf{p}f(\mathbf{r},\mathbf{p},t)$, for the average electron momentum $\mathbf{P}_e(\mathbf{r},t)\equiv n_e^{-1}(\mathbf{r},t)\int d^3\mathbf{p}\,\mathbf{p}f(\mathbf{r},\mathbf{p},t)$, and the average electron kinetic energy $\langle\epsilon\rangle(\mathbf{r},t)\equiv n_e^{-1}(\mathbf{r},t)\int d^3\mathbf{p}(\sqrt{m^2c^4+p^2c^2}-mc^2)f(\mathbf{r},\mathbf{p},t)$ ($m(e)$ — electron mass (charge))

$$\frac{\partial n_e}{\partial t}=\Gamma,\quad \frac{\partial \mathbf{P}_e}{\partial t}+\frac{\Gamma}{n_e}\mathbf{P}_e=e\left(\mathbf{E}+\frac{1}{c}\mathbf{V}_e\times\mathbf{H}\right),\quad \frac{\partial\langle\epsilon\rangle}{\partial t}+\frac{\Gamma}{n_e}\langle\epsilon\rangle=e\mathbf{E}\cdot\mathbf{V}_e\,, \tag{2}$$

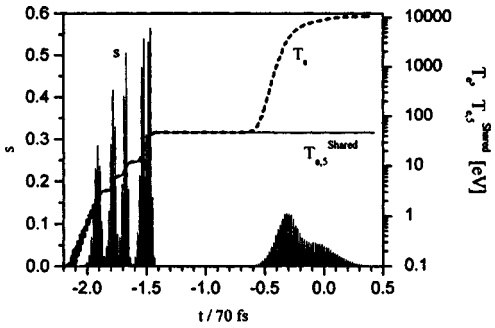

FIG. 1. Time dependence of the normalized electron production rate $s(t)=\Gamma(t)/(\omega n_a)$, $T_e(t)$ (dashed line), and $T_{e,5}^{\text{shared}}(t)$ (continuous line) in (eV). Matter — nitrogen, laser pulse — Gaussian with maximum intensity $I_{\max}=10^{19}$ W/cm^2, duration (FWHM) $\tau_{\text{pul}}=70$ fs, and wavelength $\lambda=0.78$ μm. The time t is in units of τ_{pul}, measured from the peak of the pulse.

where $\mathbf{V}_e(\mathbf{r},t)\equiv n_e(\mathbf{r},t)\int d^3\mathbf{p}\mathbf{v}f(\mathbf{r},\mathbf{p},t)$ is the average velocity of the directed motion of the electrons. The laser field $\mathbf{E}(\mathbf{r},t)$ enters explicitly on the right-hand sides of Eq. (2). For this reason, depending on the intensity of the laser radiation, the electron momentum $\mathbf{P}_e(\mathbf{r},t)$ and the electron kinetic energy $\langle\epsilon\rangle$ can be very substantial during the time that the laser pulse acts.

The width of the momentum distribution function $f(\mathbf{r},\mathbf{p},t)$ can be characterized by the electron temperature $T_e(\mathbf{r},t)$ determined by the relation $T_e(\mathbf{r},t)\equiv 2[\langle\epsilon\rangle(\mathbf{r},t)-\epsilon_d(\mathbf{r},t)]/3$, where $\epsilon_d(\mathbf{r},t)\equiv\sqrt{m^2c^4+\mathbf{P}_e^2(\mathbf{r},t)c^2}-mc^2$ is the kinetic energy of the directed motion of the electrons. Forming the scalar product of Eq. (2) and $\mathbf{V}_e(\mathbf{r},t)$ and subtracting the result from the third equation in Eqs. (2), we obtain an equation for T_e:

$$\frac{\partial T_e}{\partial t}+\frac{\Gamma}{n_e}T_e=\frac{2\Gamma}{3n_e}\frac{mc^2\epsilon_d}{mc^2+\epsilon_d}. \tag{3}$$

In deriving this relation we assumed that the width of the momentum distribution function is comparatively small $\int d^3\mathbf{p}(p_j-P_{e,j})(p_k-P_{e,k})f\ll n_e(m^2c^2+P_e^2)$, $k,j=1,2,3$, so that the standard relativistic relation between the average velocity $\mathbf{V}_e(\mathbf{r},t)$ and average momentum $\mathbf{P}_e(\mathbf{r},t)$ of the directed electron motion holds. We note that in contrast to Eqs. (2), the laser field does not enter explicitly in Eq. (3).

The source Γ, which is the rate of production of free electrons per unit volume, enters in the hydrodynamic equations (2) and (3). To determine Γ it is necessary to calculate the rate of stripping of electrons from all atomic shells: $\Gamma=\Sigma_{k=0}^{Z-1}W_{k+1}N_k$, where W_{k+1} is the probability of tunneling ionization per unit time for an ion with ionization multiplicity k ($k=0$ corresponds to a neutral atom), and N_k is the density of such ions. W_{k+1} is determined by the well-known ADK formula.[11] The temporal evolution of the densities N_k of atoms and ions can be described using the equations of ionization kinetics.[14] The characteristic form of the normalized electron production rate $s(t)=\Gamma(t)/\omega n_a$, where n_a is the initial density of atoms in the gas, is shown in Fig. 1 and is a rapidly oscillating function. The period of the oscillations is one-half the period of the laser field. The envelope of $s(t)$ consists of a sequence of peaks corresponding to the ionization of ions with the corresponding ionization multiplicity. The durations of

these peaks, which can be interpreted as the characteristic ionization times of ions with the corresponding ionization multiplicity, are of the order of several laser periods for sufficiently high intensity of the laser radiation.

The following formal solutions can be written down for the density and temperature of the electrons from Eqs. (2) and (3):

$$n_e(t)=\int_{-\infty}^{t}\Gamma(t')dt', \quad T_e(t)=\frac{2}{3n_e(t)}\int_{-\infty}^{t}\frac{mc^2\epsilon_d(t')}{mc^2+\epsilon_d(t')}\Gamma(t')dt'. \tag{4}$$

The most important consequence of Eqs. (4) is the possibility of neglecting relativistic effects when determining the density and temperature of the electrons under conditions such that the oscillatory velocity of the free-electron motion in the laser field during ionization of the atomic shells is less than the velocity of light, $eE_{\rm ion}/m\omega\leqslant c$. Indeed, $\Gamma(t)$ and therefore the integrand in Eqs. (4) are different from zero only in time intervals corresponding to the ionization of the atomic shells. Therefore, all the way up to the ionization of shells that require relativistic intensities I ($I>10^{18}$ W/cm^2), the electron temperature is determined by Eqs. (4), where ϵ_d is determined by Eqs. (2) in the nonrelativistic limit (compare with Ref. 15).

Figure 1 shows the characteristic time dependence $T_e(t)$, which is of a step form. The appearance of each new step in $T_e(t)$ corresponds to the appearance of a new group of electrons during ionization of an ion with the corresponding ionization multiplicity. In a comparatively rarefied plasma, the ionization time of ions with ionization multiplicity k is short compared with the electron-electron and electron-ion collision times. For this reason, it makes sense to associate to each new group of electrons appearing as a result of ionization of the kth ion its own temperature $T_{e,k}(t)$:

$$T_{e,k}(t)=\frac{2}{3n_{e,k}(t)}\int_{-\infty}^{t}\frac{mc^2\cdot\epsilon_d(t')}{mc^2+\epsilon_d(t')}\Gamma_k(t')dt', \tag{5}$$

where $\Gamma_k(t)\equiv N_k(t)W_{k+1}(t)$, $n_{e,k}(t)\equiv\int_{-\infty}^{t}\Gamma_k(t')dt'$ is the density of the free electrons appearing as a result of ionization of an ion with ionization multiplicity k. We note that for multielectron atoms $T_e(t)$ in Eq. (4) is not, in the general case, the temperature of any of these groups of electrons. It is obvious that the temperature $T_{e,k}(t)$ is physically meaningful during the time interval from the onset of ionization of the kth ion such that electron-electron collisions are not important. Over the time $\tau>\tau_{ee,k}$, where $\tau_{ee,k}$ is the collision time of the electrons in the kth group with electrons which have already been produced, energy exchange between the electrons equalizes the temperatures. According to the law of conservation of energy, if $\tau_{ee,m}<\tau<\tau_{ee,m+1}$, then the temperature of each group of electrons with number $k\leqslant m$ becomes equal to the same value

$$T_{e,m}^{\rm shared}(t)\equiv\sum_{k=0}^{m}n_{e,k}(t)T_{e,k}(t)/\sum_{k=0}^{m}n_{e,k}(t). \tag{6}$$

To estimate $\tau_{ee,k}$ we shall use the well-known formula for the electron-electron collision-free frequency in plasma,[16] giving $\tau_{ee,k}\approx 10^{-14}(10^{19}/kn_a)(T_{e,k})^{3/2}$. Under our experimental conditions, toward the end of the pulse we obtain using Eq. (5): $T_{e,1}=3.3$ eV, $T_{e,2}=9.7$ eV, $T_{e,3}=23.4$ eV, $T_{e,4}=79.5$ eV, $T_{e,5}=120$ eV, $T_{e,6}=38.8$ keV, and $T_{e,7}=43.4$ keV. Correspondingly, the collision times for electrons in the kth group with

previously formed free electrons are: $\tau_{ee,1}\approx 60$ fs, $\tau_{ee,2}\approx 150$ fs, $\tau_{ee,3}\approx 380$ fs, $\tau_{ee,4}\approx 1.8$ ps, $\tau_{ee,5}\approx 2.6$ ps, $\tau_{ee,6}\approx \tau_{ee,7}\approx 13$ ns. According to Eq. (6), it follows hence that by the end of the third picosecond the temperatures of the electrons in the first five groups equalize to ≈ 47 eV. The electrons in the last sixth and seventh groups are so fast that they need 13 ns in order to heat up the first five groups. We underscore that this is why the inaccuracy of the ADK formulas employed with relativistic intensities of the order of 10^{19} W/cm^2 (when ionization of the last two electrons occurs) in no way influences the indicated temperature dynamics of the first five electron groups.

3. The experimental investigations were performed by x-ray spectroscopy on the UNI10 laser setup at the Research Center in Saclay (France). A pulsed nitrogen stream with transverse size 200 μm and N_2 density in the region of interaction with the laser radiation equal to 1.5×10^{19} cm^{-3} was used as the target. A 70 fs laser pulse with energy 70 mJ, focused by an off-axis parabolic mirror, made it possible to obtain a 16 μm in diameter focal spot and thereby a flux density 10^{19} W/cm^2 in the focal plane.

The x-ray radiation of the plasma was detected with a one-dimensional spatial resolution using a spectrograph with a spherically bent mica crystal, installed in the FSSR-1D arrangement.[17] The spectrograph was tuned to the range 18.9–19.6 Å, its spectral resolution was determined by the width of the reflection curve of the crystal and equalled $\lambda/\delta\lambda = 2000$ with 30 μm spatial resolution.

The detected spectral range corresponded to the position of the Rydberg terms of the resonance series $np-1s$ $(n=5-9)$ of the H-like ion N VII. The spectral composition of the plasma radiation is quasicontinuous, containing several wide peaks with a very complicated structure. In previous work[18] we showed that these peaks are not spectral lines of the H-like N VII ion, broadened by the Stark or Doppler mechanisms, but probably they are a collection of transitions in the hollow He-like ion N VI.

Calculations performed using the radiation–collisional kinetic code ''Mariya''[19] with the atomic constants obtained by the Hartree–Fock method with relativistic corrections[20] show (see Fig. 2) that the experimental spectrum can indeed be explained by radiative transitions from Rydberg states $nln'nl'$ $(n,n'=3-8)$ of hollow N VI ions if two conditions are satisfied simultaneously: If the electron temperature of the plasma is sufficiently low (15–30 eV), while its ionization state is a recombination state.

It follows from the foregoing hydrodynamic analysis that this situation is realized when a gas is heated by a femtosecond superintense pulse. Indeed, the ionization of state of plasma in this case is formed at the moment the laser pulse acts and by the end of the pulse the nitrogen atoms are completely ionized, i.e., the ''ionization'' temperature of the plasma is very high. The temperature of a large fraction of the free electrons in the plasma, as follows from our calculations, during the first several picoseconds after the laser pulse ends, i.e., at the moment of maximum plasma luminosity, is $\sim 12-47$ eV. We note that the presence of two groups of hot electrons with $T_e\approx 40$ keV will essentially have no effect on the kinetics of the ions investigated, since their energy is much higher than the characteristic excitation and ionization energies of H- and He-like ions N VII, VI.

4. In summary, the hydrodynamic description, proposed in the present letter, of the interaction of a short intense laser pulse with moderate-density gases, systematically taking account of both ionization processes and the relativistic motion of the electrons

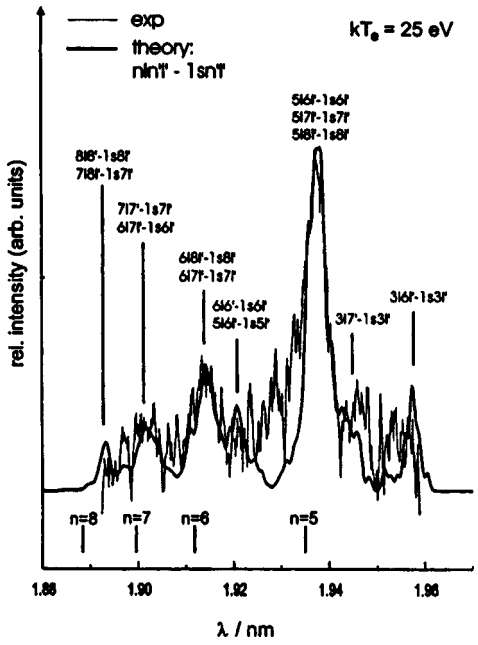

FIG. 2. Comparison of the experimental spectrum with the results of a kinetic calculation.

produced by ionization of the gas in a relativistically strong field of the pulse, makes it possible to describe correctly the x-ray emission spectrum of the plasma. In turn, the agreement of the x-ray spectroscopy data with the results of the proposed hydrodynamic model shows that the model is adequate for describing the interaction of femtosecond laser pulses with a gas.

This work was supported in part by grants 98-02-16263 and 96-02-16111 from the Russian Fund for Fundamental Research.

[1] P. Amendt, D. C. Eder, S. C. Wilks, Phys. Rev. Lett. **66**, 2589 (1991).
[2] Y. Nagata *et al.*, Phys. Rev. Lett. **71**, 3774 (1993).
[3] T. E. Glover *et al.*, Phys. Rev. Lett. **73**, 78 (1994).
[4] Y. Nagata *et al.*, Phys. Rev. A **51**, 1415 (1995).
[5] U. Mohideen *et al.*, Phys. Rev. Lett. **71**, 509 (1993).
[6] 6. W. J. Blyth, *et al.*, Phys. Rev. Lett. **74**, 554 (1995).
[7] G. Pretzler and E. E. Fill, Phys. Rev. E **56**, 2112 (1997).
[8] B. M. Penetrante and J. N. Bardsley, Phys. Rev. A **43**, 3100 (1991).
[9] P. Pulsifer *et al.*, Phys. Rev. A **49**, 3958 (1994).
[10] L. V. Keldysh, Zh. Éksp. Teor. Fiz. **47**, 1945 (1964) [Soy. Phys. JETP **20**, 1307 (1965)].
[11] M. V. Ammosov, N. B. Delone, and V. P. Kraĭnov, Zh. Éksp. Teor. Fiz. **91**, 2008 (1986) [Sov. Phys. JETP **64**, 1191 (1986)]; N. B. Delone and V. P. Kraĭnov, Usp. Fiz. Nauk **168**, 531 (1998).
[12] P. B. Corcum, N. H. Burnett, and F. Brunel, Phys. Rev. Lett. **62**, 1259 (1989).
[13] N. B. Delone and V. P. Krainov, J. Opt. Soc. Am. B **8**, 1207 (1991).
[14] V. P. Kandidov, O. G. Kosareva, and S. A. Shlenov, Kvant. Elektron. (Moscow) **21**, 971 (1994).
[15] N. E. Andreev, M. V. Chegotov, M. E. Veisman *et al.* in *Proceedings of ICONO'98*, Moscow, June 29–July 3, 1998.
[16] N. Krall and A. Trivelpiece, *Principles of Plasma Physics*, Academic Press, New York, 1973 [Russian translation, Mir, Moscow, 1975].

[17] I. Yu. Skobelev, A. Ya. Faenov, B. A. Bryunetkin *et al.*, Zh. Éksp. Teor. Fiz. **108,** 1263 (1995) [JETP **81**, 692 (1995)].
[18] T. Auguste, P. D'Oliveira, S. Hulin, *Proceedings of the XXV European Conference on Laser Interaction with Matter (ECLIM98)*, Formia, Italy, May 4–8, 1998.
[19] F. B. Rosmej, J. Phys. B **30**, L819 (1997).
[20] R. D. Cowan, *Theory of Atomic Structure and Spectra*, University Press, Berkeley, 1981.

Translated by M. E. Alferieff

Nonlinear transport through NS junctions due to imperfect Andreev reflection

G. B. Lesovik
Institute of Solid State Physics, Russian Academy of Sciences, 142432 Chernogolovka, Moscow Region, Russia

G. Blatter
Theoretische Physik, ETH-Hönggerberg, CH-8093, Zürich, Switzerland

(25 August 1998)
Pis'ma Zh. Éksp. Teor. Fiz. **68**, No. 7, 572–577 (10 October 1998)

We investigate a normal-metal–superconductor (point) contact in the limit where the number of conducting channels in the metallic wire is reduced to few channels. As the effective Fermi energy drops below the gap energy, a conducting band with a width twice the Fermi energy is formed. Depending on the mode of operation, the conduction band can be further squeezed, leading to various nonlinear effects in the current–voltage characteristics such as current saturation, a N-shaped negative differential resistance, bistability, and hysteresis. © *1998 American Institute of Physics.* [S0021-3640(98)01019-6]

PACS numbers: 74.80.Fp, 74.25.Fy

Coherent transport phenomena in microstructured normal–superconductor (NS) systems have recently attracted a lot of interest.[1] The transport across an NS boundary is governed by the phenomenon of Andreev reflection:[2] An electron incident from the normal metal on the NS junction with an excitation energy $|\varepsilon|$ below the superconducting gap Δ cannot penetrate into the bulk superconductor (we measure the excitation energy ε of the electron with respect to the chemical potential μ in the superconductor). Nevertheless, subgap transport across the junction is possible via the process of Andreev reflection, where the electron incident on the boundary is accompanied by a (coherently reflected) hole, producing effectively a state with two incoming electrons which convert into a Cooper pair upon entering the superconductor. For an ideal NS boundary, such a process leads to a conductance $G=4e^2/h$ per channel,[3] twice as high as the maximum possible normal one. If the transparency T of the boundary is smaller than unity, the NS linear conductance decreases as T^2 at small $T\ll 1$ (Ref. 3). New effects appear in the finite-bias or finite-temperature conductance when the transmission of electrons and holes differs significantly as a consequence of their different longitudinal kinetic energies.[1,4–6] In this letter we show how Andreev scattering, combined with specific conditions for the propagation of electrons and holes, leads to the formation of a subgap conduction band with a width which strongly depends on the bias voltage, leading to new transport characteristics exhibiting a negative differential resistance, bistability, and hysteresis effects.

To fix ideas, consider a single-channel normal-metal point contact to a bulk super-

 © 1998 American Institute of Physics

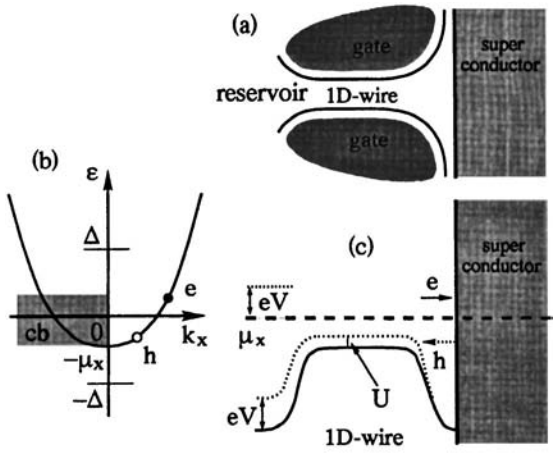

FIG. 1. a) Geometry of the NS point contact with the 1D normal wire adiabatically connected to the normal reservoir on the left and the bulk superconductor on the right; see Ref. 8. b) Dispersion relation in the normal wire. Note the formation of a conducting band (cb) of width $2\mu_x$. c: Energy diagram for the wire sketched in part (a). A change in bias eV induces a shift U in the wire potential, which in turn may lead to a reflection of the backpropagating hole. The electron then is reflected normally from the NS boundary and does not contribute to the current.

conductor (see Fig. 1a). Here we have in mind geometries such as quantum point contacts realized in heterostructures[7,8] or via manipulations with a scanning tunneling microscope.[9] Given the chemical potential μ, we define the longitudinal chemical potential $\mu_x=\mu-\varepsilon_\perp$, where $\varepsilon_\perp$ denotes the transverse energy of quantization in the normal channel. Here, we are interested in situations where the longitudinal kinetic energy $K_{e,h}$ at the Fermi surface is small, such that the condition $\mu_x<\Delta$ is realized. In this case, electrons with excitation energies $\varepsilon=E-\mu=K_e-\mu_x>0$ can propagate through the contact, whereas the corresponding hole state with the same excitation energy can propagate only if its kinetic energy $K_h=\mu_x-\varepsilon$ remains positive, i.e., $\varepsilon<\mu_x$ (in this simplified discussion we assume that the conducting normal channel is long enough to generate transmission probabilities 0 or 1 only).

An electron incident on the superconductor defines the Andreev state (in the normal single-channel region)

$$\Psi_\varepsilon(x)=\begin{pmatrix}1\\0\end{pmatrix}\frac{e^{ik_+x}}{\sqrt{v_+}}+\begin{pmatrix}r_{ee}\\0\end{pmatrix}\frac{e^{-ik_+x}}{\sqrt{v_+}}+\begin{pmatrix}0\\r_{eh}\end{pmatrix}\frac{e^{ik_-x}}{\sqrt{v_-}}, \tag{1}$$

with $k_\pm=\sqrt{2m(\mu_x\pm\varepsilon)}/\hbar$ and $v_\pm=\hbar k_\pm/m$ (the above states are normalized to carry unit particle flux, with a normalization $\langle\Psi_\varepsilon,\Psi_{\varepsilon'}\rangle=2\pi\hbar\,\delta(\varepsilon-\varepsilon')$, implying that $|r_{ee}|^2=1-|r_{eh}|^2$). Following the above discussion, the quenching of the hole state for energies $\varepsilon>\mu_x$, combined with the restriction in the allowed energies for incident electron states $\varepsilon>-\mu_x$, leads to the formation of a conducting band of width $2\mu_x$ (see Fig. 1b and the inset of Fig. 2). Within this band, incident electrons are (nearly) perfectly reflected into holes, whereas electrons with energies above this band ($\varepsilon>\mu_x$) are reflected as electrons and do not carry current (electrons with energies ($\varepsilon<-\mu_x$) do not enter the normal channel at all).

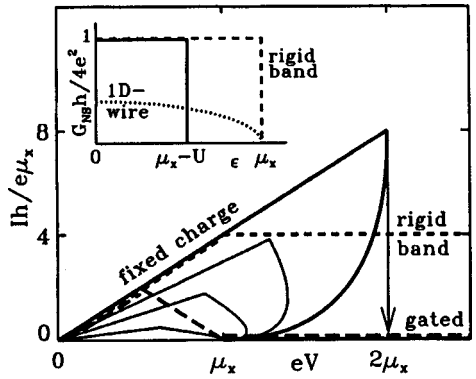

FIG. 2. Current–voltage characteristics of the NS contact. Keeping the band rigid (dashed line), the current saturates when all electrons within the band $2\mu_x$ contribute. In the gated wire (long dashes), the backpropagation of holes is partially inhibited when the voltage increases beyond $\mu_x/2$ and completely quenched beyond $eV=\mu_x$. In the wire with fixed charge (thick solid line) the current switches from the upper to the lower branch, producing a pronounced negative differential resistivity. A finite reflectivity reduces the instability (fixed charge, thin solid lines, $|r_{ee}|^2=0.25$, 0.5, 0.8). Inset: Spectral conductance $G_{\rm NS}$ versus energy ε. For the 1D NS wire the conductance is suppressed due to imperfect Andreev reflection (dotted line). For the adiabatically connected wire of Fig. 1a the Andreev approximation is applicable and $G_{\rm NS}$ reaches is maximal value. The width of the conduction band depends on the wire potential U (solid line: gated/fixed-charge wire; dashed line: rigid band.

In the simplest formulation of the problem we consider a single-channel NS junction. The Andreev states are found by solving the Bogoliubov–de Gennes equations

$$\begin{pmatrix} -\dfrac{\hbar^2\partial_x^2}{2m}-\mu_x & \Delta(x) \\ \Delta^*(x) & \dfrac{\hbar^2\partial_x^2}{2m}+\mu_x \end{pmatrix} \begin{pmatrix} u_\varepsilon(x) \\ v_\varepsilon(x) \end{pmatrix} = \varepsilon \begin{pmatrix} u_\varepsilon(x) \\ v_\varepsilon(x) \end{pmatrix} \tag{2}$$

with the gap function $\Delta(x)=\Delta\Theta(x)$, using the ansatz (1) in the normal region and

$$\Psi_\varepsilon(x)=t_e\begin{pmatrix}1\\ \gamma\end{pmatrix}\frac{e^{(ip-q)x}}{\sqrt{v}}+t_h\begin{pmatrix}1\\ \gamma^*\end{pmatrix}\frac{e^{(-ip-q)x}}{\sqrt{v}} \tag{3}$$

in the superconducting region $x>0$, with $p^2-q^2=2m\mu_x/\hbar^2$, $pq=m\sqrt{\Delta^2-\varepsilon^2}/\hbar^2$, $\gamma=(\varepsilon-i\sqrt{\Delta^2-\varepsilon^2})/\Delta$, and the normalizing velocity $v=\hbar p/m$. Solving for the transmission and reflection coefficients, we obtain the spectral conductance $G_{\rm NS}(|\varepsilon|<\Delta)\approx(8e^2/h)\Theta(\mu_x-|\varepsilon|)\sqrt{\mu_x^2-\varepsilon^2}/\Delta$, valid in the limit $\mu_x\ll\Delta$ (see inset of Fig. 2; note that the Andreev approximation is not valid in the present case). Assuming a rigid band, implying that the applied bias drops at the boundary of the reservoir to the normal lead, the finite conduction band produces a current–voltage (I–V) characteristic $I=\int^{eV}d\varepsilon\, G_{\rm NS}/e$ which saturates at a bias $eV=\mu_x$ (we assume a negative bias $V<0$, hence $eV>0$). This then is the simplest example where the quenching of the backpropagating holes limits the width of the conducting band and entails a nontrivial saturation phenomenon in the transport characteristics of the NS junction. It is in contrast to the normal point contact, where an increasing bias eV opens up the channels (see Refs. 10;

note that a nontrivial structure in the $I-V$ characteristics can occur in a normal point contact as well, though at much higher voltages $eV>\mu$; see Ref. 11).

The above 1D example cannot be trivially applied to a physical situation: strictly speaking, we have neither a superconducting instability nor a normal Fermi liquid in a single-channel 1D system. Let us then discuss the more realistic single-channel NS point contact with a geometry as sketched in Fig. 1a; see also Ref. 7. The 1D normal wire is adiabatically connecting the normal reservoir with the bulk superconductor. The smooth form of the wire guarantees the appropriate matching of the wave functions in the three device segments, reservoir, 1D wire, and bulk superconductor. An imperfect matching leads to a normal reflection of the incident particle at the NS boundary and thus reduces the subgap transport with its interesting new features (below we will discuss the consequences of normal reflection for the device characteristics in more detail). The main properties of this geometry are the following: i) the confining potential of the wire produces a narrow conduction band connecting the reservoir with the NS boundary, ii) the 1D wire is long enough to guarantee a sharp onset of the transmission (but short enough to let us ignore strong interaction effects due to the one-dimensionality), iii) the wide NS contact helps the proper matching of the wave functions, and iv) the large chemical potential in the bulk superconductor allows us to adopt the Andreev approximation. The functioning of this device resembles that of the idealized structure above: whereas in the 1D wire the backpropagation of the hole was limited by the bottom of the conduction band, in the present situation holes reflected from the NS boundary with minimal kinetic energy $\mu_x-\varepsilon<0$ have to tunnel through the effective potential due to the transverse quantization in the wire (see Fig. 1c).

As we can apply the Andreev approximation for the geometry of Fig. 1a, the determination of the conductance is trivial, $G_{\rm NS}(\varepsilon)=(4e^2/h)\Theta(\mu_x-|\varepsilon|)$, and the corresponding $I-V$ characteristics for the rigid band model follows from simple integration (see Fig. 2).

So far, the determination of the current–voltage characteristics has been based on a rigid band model, where the voltage drop in the device occurs at the boundary to the normal reservoir. A more accurate calculation of the transport current $I(V)$ involves a self-consistent determination of the charge $\rho(x)$ and the electric potential $e\varphi(x)$ in the wire, given an applied bias V; see, e.g., Ref. 12. Here we refrain from such a calculation, but rather discuss two interesting limiting cases illustrating the potential features of such a device.

The first case we wish to analyze is the gated wire, where a top gate placed over the wire modifies its potential $e\delta\varphi\equiv U(V,V_g)$. In the simplest case, considered by Brown *et al.*,[11] the gate potential V_g follows the applied bias, $\delta V_g=V$. Assuming further that the wire potential is slaved to the gate, the band bottom in the wire is lifted by $U=eV$, implying that backpropagating holes and low-energy incident electrons are cut off at $|\varepsilon|=\pm(\mu_x-eV)$ rather than $\pm\mu_x$. Within the Andreev approximation the spectral conductance $G_{\rm NS}$ is narrowed down to the interval $|\varepsilon|<\mu_x-eV$ and takes the form

$$G_{\rm NS}(\varepsilon,U(V))=\frac{4e^2}{h}\Theta[(\mu_x-U(V))-|\varepsilon|]. \tag{4}$$

A simple integration produces the $I-V$ characteristics

$$I(V<\Delta/e)=\frac{1}{e}\int_0^{eV} d\varepsilon G_{\rm NS}(\varepsilon,U(V)), \tag{5}$$

exhibiting a negative differential resistance (NDR) regime within the bias interval $\mu_x/2 < eV < \mu_x$ (see Fig. 2): When the applied bias eV is increased up to $\mu_x/2$, additional current-carrying states are occupied, and the transport current I increases. As one goes beyond the value $\mu_x/2$, the rising bottom of the band quenches the back propagation of the holes and fewer states are available, until at $eV=\mu_x$ all current-carrying states are blocked.

The above NDR phenomenon is further accentuated in a device where the charge of the wire rather than its potential is fixed — this is the second limiting case we wish to study here. The contribution to the charge density of an individual channel averaged over the wire cross section is given by

$$\rho(x)=2e\sum_k \{f_v(\varepsilon_k)|u_k(x)|^2+[1-f_v(\varepsilon_k)]|v_k(x)|^2\}, \tag{6}$$

with $f_v(\varepsilon)$ the (bias dependent) distribution function for the Bogoliubov quasiparticles. We evaluate the density in the middle of the wire and allow for a nonzero potential shift U. Using the normalization introduced in (1), we arrive at the form

$$\rho=\frac{e}{\pi\hbar}\int d\varepsilon\left[\frac{1+|r_{ee}|^2}{v_+(\varepsilon)}f_v(\varepsilon)+\frac{|r_{eh}|^2}{v_-(\varepsilon)}[1-f_v(\varepsilon)]\right], \tag{7}$$

with $v_\pm=\sqrt{2(\mu_x-U\pm\varepsilon)/m}$ the velocities of the quasiparticles. For the case of perfect Andreev reflection the above expression simplifies to [we assume an open channel configuration with $0<eV<\mu_x-U$; the occupation numbers are determined by those of the metallic reservoir, $f_{\rm V}(\varepsilon)=\Theta(-\varepsilon+eV)$ at zero temperature]

$$\rho=\frac{e}{\pi\hbar}\sqrt{\frac{m}{2}}\left(\int_{-\mu_x+U}^{eV} d\varepsilon\frac{1}{\sqrt{\mu_x-U+\varepsilon}}+\int_{eV}^{\mu_x-U} d\varepsilon\frac{1}{\sqrt{\mu_x-U-\varepsilon}}\right). \tag{8}$$

Requiring that the charge difference $\delta\rho=\rho(eV,U)-\rho(0,0)$ vanishes at any applied bias V leads to the condition ($k_{{\rm F},x}=\sqrt{2m\mu_x}/\hbar$)

$$\delta\rho=\frac{ek_{{\rm F},x}}{\pi}\left[\sqrt{1-\frac{U-eV}{\mu_x}}+\sqrt{1-\frac{U+eV}{\mu_x}}-2\right]=0,$$

determining the potential shift $U(V)$ in the wire. Solving for U we obtain the result

$$U(V)=-\frac{(eV)^2}{4\mu_x}, \quad 0<eV<\mu_x-U(V). \tag{9}$$

The negative shift in the wire potential seems quite puzzling at first sight, but can be easily understood in terms of the reduced group velocity of the backpropagating holes. A second solution is found for a positive shift $U>\mu_x$, where the Andreev scattering is quenched and all incident electrons are reflected back as electrons ($|r_{ee}|^2=1$). With $\delta\rho=(2ek_{{\rm F},x}/\pi)[\sqrt{1-(U-eV)/\mu_x}-1]=0$ we find the shift

$$U(V)=eV, \quad \mu_x-U(V)<0<eV. \tag{10}$$

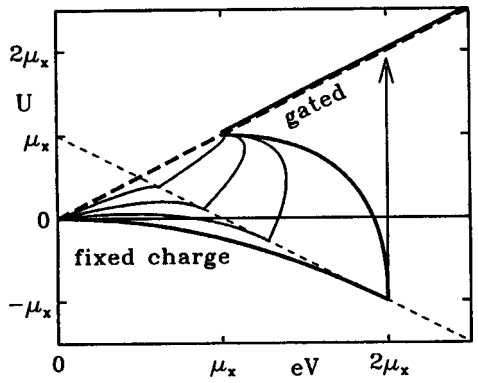

FIG. 3. Potential U within the normal wire versus applied bias for the case of a fixed charge and different values of the reflection coefficient r_{ee}, $r_{ee}=0$ (thick solid line), $|r_{ee}|^2=0.25,\ 0.5,\ 0.8$ (thin solid lines). The lower branch becomes unstable at high applied bias and the internal potential U jumps to the gated value (long dashes), leading to a NDR in the $I-V$ characteristics of the contact.

Finally, a regime with partially quenched Andreev scattering is found in the interval $0<\mu_x-U<eV$, with $U(V)$ determined by the relation $\delta\rho=(ek_{\mathrm{F},x}/\pi)[2\sqrt{1-(U-eV)/\mu_x}-\sqrt{2(1-U/\mu_x)}-2]=0$, and the result

$$U=2eV-5\mu_x+4\sqrt{\mu_x(2\mu_x-eV)}. \tag{11}$$

The internal potential shift U versus applied bias V is shown in Fig. 3 (thick solid line). The three branches of $U(V)$ exhibiting completely open, partially quenched, and entirely quenched hole propagation in the wire arrange to define a typical bistable configuration of the wire within the bias interval $\mu_x<eV<2\mu_x$. The lower branch with the open channel terminates at $eV=2\mu_x$ and the system has to jump to the state where the back-propagation of holes is quenched. Physically, the jump between the two branches corresponds to a rearrangement of the potential drop in the device: At low bias (lower branch) the applied bias drops on the left side of the channel, towards the reservoir. At high bias (upper branch) the potential drops on the superconductor side, producing the gated situation described above. Translating this behavior of the internal device bias U to the $I-V$ characteristics (see Fig. 2), we find a jump from the ''open,'' current-carrying state at low bias to the ''closed,'' gated state at high bias as the applied bias eV grows beyond the band width $2\mu_x$, thereby producing a characteristics with an N-shaped negative differential resistance. At voltages $eV>\Delta$ a finite conductance is restored. Note that the $I-V$ characteristics is not symmetric: for a positive applied bias $V>0$ (eV<0) the conduction band stays open up to the bias $eV=-2\mu_x$, where the wire potential aligns with the potential in the reservoir, $U-\mu_x=eV$; see (9). Increasing the bias further, the current saturates (similarly to the rigid band case) as part of the incoming electrons are excluded from entering the wire.

The above analysis for the case of ideal Andreev reflection at the NS boundary can be easily generalized to take a finite normal reflectivity of the barrier into account. It is convenient to characterize the junction through its normal state properties: Given the reflection coefficient R for electrons entering the 1D wire, the parameter $|r_{ee}|^2$ switches between the values $|r_{ee}|^2=4R/(1+R)^2$ (''open'' channel) and $|r_{ee}|^2=0$ (''closed''

channel) (see Refs. 13,6) we assume that $\partial_\varepsilon R(\varepsilon)\approx 0$ and $\varepsilon \ll \Delta$, allowing us to ignore the energy dependence in $|r_{ee}|^2$). A finite value of R then leads to a smoothing of the potential-bias relation and the current–voltage characteristics see Figs. 2 and 3. As R approaches unity, the fixed-charge characteristic approaches the result for the gated wire.

Above we have concentrated on the single-channel limit, where the nonlinear effects leading to the NDR phenomenon are most pronounced. Going over to a multichannel geometry, our analysis can be carried over to the grazing incidence trajectories[4] with the modification $\mu_x \to \mu_{x,n} = \mu - \varepsilon_{\perp,n}$, where $\varepsilon_{\perp,n} = \hbar^2 K_n^2/2m$ is the transverse energy of the nth channel. The interesting structure obtained in the single-channel case (see Fig. 2) then survives for the states with an effective chemical potential $\mu_{x,n} < \Delta$. The maximum number of channels to be saturated or cut off in this fashion below a bias $eV \sim \Delta$ is of order $\delta n \sim (\Delta/\mu)n$, where $n \gg 1$ is the total number of channels. In a bulk system with a planar NS boundary these states correspond to grazing incidence trajectories with angles $\vartheta < \sqrt{\Delta/\mu}$.

In conclusion, the different propagation conditions for electrons and holes in NS junctions produce a rich variety of phenomena. Both, the zero- and finite-bias anomalies[1] in dirty NS junctions can be understood in such terms.[6] Here, we have shown how the coherent electron–hole transport in a one/few channel system may lead to strong nonlinearities in the device characteristics, resulting in an N-shaped NDR $I-V$ curve in its most extreme variant. In conventional semiconductor devices this kind of instability leads to the formation of domain walls, e.g., the Gunn effect. In the present case, where the transport is nonlocal and coherent, we can expect a device operation more similar to that of a double-barrier resonant-tunneling structure.[14]

We thank A. Fauchère, Ch. Glattli, I. Larkin, and L. Levitov for some stimulating discussions and the Swiss National Foundation for financial support.

[1] B. van Wees and H. Takayanagi, in *Mesoscopic Electron Transport*, edited by L. Son *et al.*, NATO ASI Series, Vol. 345, Kluwer, 1997, p.469, and references therein; C. W. J. Beenakker, in *Mesoscopic Quantum Physics*, edited by E. Akkermans *et al.*, Elsevier, 1995.
[2] A. F. Andreev, Zh. Éksp. Teor. Fiz. **46**, 1823 (1964) [Sov. Phys. JETP **19**, 1228 (1964)].
[3] G. Blonder, M. Tinkham, and T. M. Klapwijk, Phys. Rev. B **25**, 4515 (1982).
[4] Yu. K. Dzhikaev, Zh. Éksp. Teor. Fiz. **68**, 295 (1975) [Sov. Phys. JETP **41**, 144 (1975)].
[5] G. Wendin and V. S. Shumeiko, Phys. Rev. B **53**, R6006 (1996).
[6] G. B. Lesovik, A. L. Fauchére, and G. Blatter, Phys. Rev. B **55**, 3146 (1997).
[7] H. Takayanagi, T. Akazaki, and J. Nitta, Phys. Rev. Lett. **75**, 3533 (1995).
[8] D. A. Wharam *et al.*, J. Phys. C **21**, L209 (1988); B. J. van Wees *et al.*, Phys. Rev. Lett. **60**, 848 (1988).
[9] A. P. Sutton, Curr. Opin. Solid State Mater. Sci. **1**, 827 (1996).
[10] L. I. Glazman and A. V. Khaetskii, Europhys. Lett. **9**, 263 (1989); N. K. Patel *et al.*, J. Phys. C **2**, 7247 (1990).
[11] R. J. Brown *et al.*, J. Phys. C **1**, 6285 (1989).
[12] I. Larkin and J. Davies, Phys. Rev. B **52**, R5535 (1995).
[13] C. W. J. Beenakker, Phys. Rev. B **46**, 12841 (1992).
[14] V. J. Goldman, D. C. Tsui, and J. E. Cunningham, Phys. Rev. Lett. **58**, 1256 (1987).

Published in English in the original Russian journal. Edited by Steve Torstveit.

On the analytical solutions of the Hamiltonian of a Frenkel exciton for the lattice of a regular polyhedral cluster

V. V. Rotkin[a)] and S. F. Kharlapenko
A. F. Ioffe Physicotechnical Institute, Russian Academy of Sciences, 194021 St. Petersburg, Russia

(Submitted 26 August 1998)
Pis'ma Zh. Éksp. Teor. Fiz. **68**, No. 7, 578–582 (10 October 1998)

The Coulomb Hamiltonian of a small-radius exciton on a cluster whose atoms occupy the sites of a group lattice is studied. The spectrum of Frenkel excitons can be obtained analytically for definite modes by the methods of harmonic analysis of the lattice Hamiltonian. The carbon cluster C_{60} with icosahedral symmetry is given as an example. © *1998 American Institute of Physics.* [S0021-3640(98)01119-0]

PACS numbers: 71.35.Aa, 61.46.+w, 61.48.+c

This letter presents a method for calculating the spectrum of small-radius excitons (Frenkel excitons[1]) in atomic clusters whose atoms occupy the sites of a two-dimensional group lattice. The importance of this problem is due to, on the one hand, the latest progress made in the synthesis of different nonmetallic clusters of carbon, silicon, nitrides, and other materials and, on the other hand, the fact that the investigation of the physical properties of these quantum objects requires a theory going beyond the single-electron approximation. Different theoretical estimates made primarily in the Hubbard model, and also various experimental data obtained for the intensively investigated cluster C_{60}, attest to the need to take into account the Coulomb interaction between the electrons of a cluster. The adequate incorporation of this interaction is still an unsolved problem.

Quantum-size effects are manifested in most nonmetallic clusters in that an energy gap exists between the occupied and unoccupied discrete cluster levels and optically allowed transitions occur with excitation of an electron–hole pair, possessing a dipole moment, through the gap. An important manifestation of the Coulomb interaction of the carriers is renormalization of the frequency of such a transition as a result of the binding of carriers into an exciton. We note that the structure of the clusters is such that the carrier motion on a closed curved surface is quasi-two-dimensional.[2] Depending on the ratio of the kinetic energy of the carriers and the Coulomb interaction energy, different theoretical models are used to describe an exciton. If an electron–hole pair is strongly localized on a lattice site (i.e., its kinetic energy is low), a Frenkel exciton is formed,[3] in contrast the more common situation occurring in bulk semiconductor materials, where the Coulomb interaction is strongly weakened by dielectric screening and a large-radius exciton arises[4] (Wannier–Mott exciton). In clusters the kinetic energy of the carriers can

 © 1998 American Institute of Physics

be low because of the low two-dimensional electron density on the surface of the cluster, while the Coulomb energy is fixed, since the distance between the carriers does not exceed the size of the cluster. Thus, the condition for the existence of a *small-radius exciton* can be satisfied. In the present letter we present a method for diagonalizing the Hamiltonian of a Frenkel exciton on a group lattice of various structure of clusters of semiconductor materials. As already mentioned, experimental data exist for fullerene C_{60}, so that this icosahedral carbon cluster will be studied as an illustrative example (see, also Refs. 5 and 6). The final group lattice is defined as a lattice each of whose sites can be obtained from an initial site by a definite rotation from a point group given beforehand.[7] It is natural to assign to the initial site the group identity element e. In the case of C_{60} these rotations carry a truncated icosahedron into itself (details can be found in Refs. 4–6). All sites of the group lattice are equivalent and possess z bonds with nearest neighbors. The number z is determined by the number of group elements formed.

We shall proceed from the condition that the electrons are strongly localized on sites, so that an atom in an excited state remains neutral. We assume the excitation energy to be small compared with the atomic energy. This makes it possible to study transitions only between the nearest levels. We are interested primarily in an optical transition associated with a change in the parity of the electron wave function, specifically, $s \rightarrow p$. The Coulomb interaction of excited atoms is determined in the first nonvanishing order[3] by the dipole–dipole term (we recall that excitation preserves the electrical neutrality of the atom):

$$V=\frac{1}{2}\sum_{g,g'}{}' \frac{1}{r^3(g,g')}[\mathbf{P}_g\cdot\mathbf{P}_{g'}-3(\mathbf{P}_g\cdot\mathbf{e}(g,g'))(\mathbf{P}_{g'}\cdot\mathbf{e}(g,g'))], \tag{1}$$

where $\mathbf{P}_g$ and $\mathbf{P}_{g'}$ are the dipole moments of the sites g and g'; $\mathbf{r}(g,g')$ is the distance between the sites; $\mathbf{e}(g,g')=\mathbf{r}(g,g')/|\mathbf{r}(g,g')|$; and, the prime on the sum means that the summation extends over over $g\neq g'$. In the second-quantized representation the energy can be written in terms of the creation and annihilation operators of dipole excitations on the sites. One should remember that in our case of an excitation from a level s to a level p the electron wave function has three components, while the wave function of the electron–hole excitation, having three mutually perpendicular polarization directions, is a polar vector. As a result of this, the components of the excitation creation and annihilation operators have the form $\mathbf{p}_i^{\dagger}(g)=a_i^{\dagger}(g)d^{\dagger}(g)$, where $a_i^{\dagger}(g)$ and $d^{\dagger}(g)$ are electron and hole creation operators at the site g. The Coulomb part of the Hamiltonian operator has the form

$$\hat{V}=\frac{1}{2}\sum_{g,g'}{}' \frac{1}{r^3(g,g')}\mathbf{p}^{\dagger}(g)\cdot\hat{\tau}(g,g')\cdot\mathbf{p}(g'), \tag{2}$$

where the angular part of the dipole–dipole interaction operator, $\hat{\tau}(g,g')$, depends only on the directions to interacting atoms located at the sites g and g', and it does not depend on the distance between the sites and can be represented by a traceless antisymmetric tensor of rank 2:

$$\tau(g,g')_{ij}=\delta_{ij}-3\mathbf{e}(g,g')_i\mathbf{e}(g,g')_j, \tag{3}$$

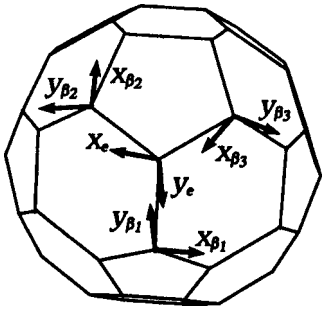

FIG. 1. Diagram showing the construction of local coordinate systems for a C_{60} cluster. The local axes $x(g)$ and $y(g)$ are shown for the base site $g=e$ and three nearest neighbors $g'=\beta_i$. The z axes at each site are directed in a radial direction.

where δ_{ij} is the Kronecker delta. The distance dependence of expression (2) is separated into the cofactor $r^{-3}(g,g')$.

We have already assumed the excitation to be strongly localized. Therefore it is natural to take account of the interaction of nearest neighbors only. It is convenient to characterize the neighboring sites of a chosen site by corresponding rotations from the group of the lattice. We denote the neighbors of the site g as βg, where β is one of z group operators. It follows from the group properties that this set is identical for all sites (in the case of C_{60} there are three rotations $\{C_5, C_5^{-1}, C_2\}$).[8] To investigate the sum (2) it is convenient to switch from the laboratory coordinate system tied to the basis site e defined above to local coordinate systems (LCSs) tied to an arbitrary site. This will make it possible to simplify the expression by separating in the operator τ the part that is invariant under the group rotations. For the specific example of the lattice of the icosahedral C_{60} cluster it is convenient to introduce the LCS as follows[9] (see Fig. 1): Orient the **z** axis from the site radially away from the cluster; orient the **y** axis in a plane passing through the **z** axis and an edge connecting two hexagons; and, define the **x** axis by the product $\mathbf{y}\times\mathbf{z}$. For this choice the transition from the LCS at the site g of the cluster to the LCS at the site g' is evidently given by the rotation $\hat{D}^{(T)}(g'g^{-1})$, which transfers the first site into the second site. We denote the rotation of the laboratory coordinate system in the LCS at the site g as $\hat{D}^{(T)}(g^{-1})$. Then the operator creating a dipole at the site g, given in the LCS tied to it, is given by $\mathbf{p}^{\dagger}_{g_i}=D^{(T)}_{ij}(g^{-1})\mathbf{p}^{\dagger}_j(g)$.

The Coulomb part of the Hamiltonian in the LCS acquires the form (we temporarily drop the indices corresponding to the polarization of the excitation)

$$V=\frac{1}{2}\sum_{g,\beta}\frac{1}{r_\beta^3}\mathbf{p}^{\dagger}_g[\hat{D}^{(T)}(g^{-1})]^{\dagger}\,\hat{\tau}(g,\beta g)\,\hat{D}^{(T)}([\beta g]^{-1})\,\mathbf{p}_{\beta g}=\frac{1}{2}\sum_{g,\beta}\frac{1}{r_\beta^3}\mathbf{p}^{\dagger}_g\hat{\tau}_\beta\mathbf{p}_{\beta g}. \quad (4)$$

For generality we retain the difference in the bond lengths, r_β, for the nearest neighbors. One can see that the operator $\hat{\tau}_\beta$ depends only on the rotation β fixing the pair of neighbors, and it does not depend on the specific position of a pair of sites in the cluster. Therefore expression (4) can be put into the maximally compact form by a harmonic expansion over a group (see below).

The components of the matrix τ_β in explicit form are:

$$\tau_{\beta ij}=[D^{(T)}(\beta^{-1})-3(D^{(T)}(g)\mathbf{e}_{g,\beta_g})\otimes(D^{(T)}(\beta g)\mathbf{e}_{g,\beta_g})]_{ij}$$
$$=D^{(T)}(\beta^{-1})_{ij}-3\frac{(D^{(T)}(e)_{i3}-D^{(T)}(\beta^{-1})_{i3})(D^{(T)}(\beta^{-1})_{3j}-D^{(T)}(e)_{3j})}{|D^{(T)}(e)_{i3}-D^{(T)}(\beta^{-1})_{i3}|^2}, \qquad (5)$$

where $D^{(T)}(e)$ denotes the identity rotation. To find the eigenstates of the Hamiltonian (4) it is necessary to solve a secular equation of order $3N$, where N is the number of atoms in the cluster (for C_{60}, of the order of $3\times 60=180$), which makes it difficult to obtain an analytical solution.

We now use the symmetry properties of the Hamiltonian and switch in Eq. (4) from a sum over lattice sites to a sum over irreducible representations (IRs) of this group. For this we expand the components of the dipole excitation creation operator $\mathbf{p}^\dagger_{g_i}$ over all IRs contained in the regular representation of the group. In what follows, unless indicated explicitly, summation over repeated indices is assumed:

$$\mathbf{p}^\dagger_i(g)=a^\dagger_i(g)d^\dagger(g)=D^{*(\alpha_1)}_{n_1m_1}(g)a^{\dagger(\alpha_1)}_{i;n_1m_1}D^{*(\alpha_2)}_{n_2m_2}(g)d^{\dagger(\alpha_2)}_{n_2m_2}, \qquad (6)$$

where $D^{(\alpha)}_{ij}(g)$ are the Wigner matrices for the IR α and the group element g, and the creation operators on the right-hand side of the equation create an electron (hole) in the symmetry state of the IR α. Switching to the coupled basis for the electron–hole excitation creation operator and transforming the product of Wigner matrices, we obtain

$$\mathbf{p}^\dagger_i(g)=C^{\alpha_1,\alpha_2,\gamma}_{n_1m_1,n_2m_2,k_1,k_2}a^{\dagger(\alpha_1)}_{i;n_1m_1}d^{\dagger(\alpha_2)}_{n_2m_2}D^{*(\gamma)}_{k_1k_2}(g)=D^{*(\gamma)}_{k_1k_2}(g)\mathbf{p}^{\dagger(\gamma)}_{i;k_1k_2}, \qquad (7)$$

where $\mathbf{p}^{\dagger(\gamma)}_{i;k_1k_2}$ is by definition the creation operator of an exciton in the IR γ, while $C^{\alpha,\beta,\gamma}_{n_1m_1,n_2m_2,k_1,k_2}$ are the Clebsch–Gordan coefficients for intercoupling the corresponding representations.[10] Substituting the excitonic creation and annihilation operators (7) into the Coulomb Hamiltonian (4), expanding the rotation operator $\hat{D}^{(\gamma)}(\beta g)$ into a product of the corresponding rotation operators for β and g, and summing over the group lattice using the orthogonality relations for unitary transformations, we obtain the final form of the Coulomb Hamiltonian

$$H_0+V=H_0+\frac{1}{2}\sum_\beta\frac{1}{r^3_\beta}\sum_\gamma\mathbf{p}^{\dagger(\gamma)}_{i;k,n}\tau_{\beta ij}D^{(\gamma)}_{mk}(\beta)\mathbf{p}^{(\gamma)}_{j;m,n}. \qquad (8)$$

One can see that the dipole interaction matrix in this expression is a direct product of the operator $\hat{\tau}_\beta$, which depends only on the group element β fixing the pair of interacting dipoles, and the rotation matrix of this element, given in one of the IRs. Thus, instead of a secular equation of dimension $3N$ we now need to solve a set of identical equations with the dimensions $3n$, where n is the dimension of the corresponding IR, i.e., 3, 9, 12, and 15 for C_{60}. This made it possible to find analytical solutions for some modes of the system.[5,6] An important feature of our method is the possibility of performing a symmetry analysis of the desired two-particle excitations, since the form of the corresponding IR determines uniquely the possibility of constructing a nonzero matrix element between this excited state and the ground (completely symmetric) state of a cluster for any exci-

tation potential. This makes it possible to solve the problem only for the modes of interest to us, for example, for the five dipole-active modes T_{1u} in the case of C_{60} (Ref. 5).

We have presented a method for systematically calculating the spectrum of the Coulomb Hamiltonian given on the lattice of a regular polyhedral cluster, the symmetry group of whose lattice makes it possible to use the method of harmonic analysis of the matrix of the Coulomb interaction and switch from the initial coordinate representation to the space of irreducible representations of the given group lattice. Diagonalization of the Hamiltonian, obtained in the Frenkel exciton approximation, in the space of electron–hole excitations makes it possible to classify the states by symmetry and also gives the spectrum and wave functions of the two-particle modes of a system where the Coulomb energy is much greater than the kinetic energy of the carriers.

We thank E. L. Ivchenko for a discussion which stimulated this work, and I. Yu. Solov'ev for helpful remarks. This work was supported in part by Grant No. 96-02-17926 from the Russian Fund for Fundamental Research and Grant No. 98062 from the program ''Fullerenes and Atomic Clusters.''

[a)]e-mail: rotkin@theory.ioffe.rssi.ru

---

[1] Ya. I. Frenkel, Phys. Rev. **37**, 17 (1931); Phys. Rev. **37**, 1276 (1931)].
[2] V. V. Rotkin and R. A. Suris, Fiz. Tverd. Tela (St. Petersburg) **36**, 3569 (1994) [Phys. Solid State **36**, 1899 (1994)]; V. V. Rotkin and R. A. Suris, Mol. Mater. **5**, 87 (1994).
[3] V. M. Agranovich, *Theory of Excitons* [in Russian], Nauka, Moscow, 1968.
[4] J. M. Ziman, *Principles of the Theory of Solids*, Cambridge University Press, London, 1969, 2nd edition [Russian translation, Mir, Moscow, 1974].
[5] S. F. Harlapenko and S. V. Rotkin, *Proceedings of the Symposium on Recent Advances in the Chemistry and Physics of Fullerenes and Related Materials*, edited by K. M. Kadish and R. S. Ruoff, Pennington, N. J., 1998, PV 98-8, p. 113.
[6] S. F. Harlapenko and S. V. Rotkin, Carbon (accepted) 1998.
[7] M. Rasetti and R. Zecchina, Physica A **199**, 539 (1993).
[8] S. Samuel, Int. J. Mod. Phys. B **7**, 3877 (1993).
[9] R. Friedberg, T. D. Lee, and H. C. Ren, Phys. Rev. B **46**, 14150 (1992).
[10] L. D. Landau and E. M. Lifshitz, *Quantum Mechanics: Non-Relativistic Theory*, 3rd ed., Pergamon Press, Oxford, 1977 [cited Russian original, Nauka, Moscow, 1989].

Translated by M. E. Alferieff

Characteristic features of *d* pairing in bilayer cuprates under conditions of Peierls instability of the normal phase

M. V. Eremin[a)] and I. A. Larionov
Kazan State University, 420008 Kazan, Russia

(Submitted 28 August 1998)
Pis'ma Zh. Éksp. Teor. Fiz. **68**, No. 7, 583–587 (10 October 1998)

A system of self-consistent integral equations for the superconducting gap is formulated and solved taking account of the instability of the normal phase of bilayer cuprates against charge-density waves. The critical parameters are calculated as a function of the wave vector, temperature, and doping index. It is found that the region in which superconductivity coexists with *d*-type charge-density waves depends strongly on the doping index. The effective energy-gap parameter, determined as the interval between the peaks of the density of states, can have a local minimum at temperatures $T<T_c$. © *1998 American Institute of Physics.* [S0021-3640(98)01219-5]

PACS numbers: 74.72.−h, 74.25.Jb

It can now be regarded as an established experimental fact that *d*-type pairing is realized in most layered cuprates, and in addition the determining component of the order parameter of the pseudogap in the normal phase of underdoped samples possesses the same *d*-type symmetry.[1,2] At least this conclusion does not raise any objections for $YBa_2Cu_3O_{7-\delta}$, $Bi_2Sr_2CaCu_2O_{8+\delta}$, and other bilayer cuprates. The question of the nature of the pairing and the origin of the pseudogap in the normal phase is still open. Specifically, it is still not clear whether or not they are interrelated or completely independent. In the present letter we show that the empirical dependences of T_C and the pseudogap closure temperature T^* on the doping index and the dependences of their order parameters on the wave vector can be qualitatively understood in a model of a quasi-two-dimensional metal with strong electronic correlations, in which case the gap in the elementary excitations spectrum is due to anomalous averages of the type $\langle \Psi^{2\sigma}_{\mathbf{k}} \Psi^{2\sigma}_{\mathbf{k}+\mathbf{q}} \rangle$, characteristic for a Peierls instability of the normal phase.

The problem of the existence of superconductivity under conditions of Peierls instability is a classic problem. For ordinary metals it has been discussed in a number of works (see, for example, Refs. 3 and 4), where the anomalous averages were due to the Fröhlich interaction and did not depend on the wave vector. In the present letter the main interaction responsible for the formation of the superconducting state is the short-range superexchange interaction, and the normal phase exhibits strongly non-Fermi-liquid behavior. The spectral weight of the conduction band under study depends nonlinearly on the doping index, and it is already half-filled when the number of holes per unit cell of the

 © 1998 American Institute of Physics

Cu_2O_4 bilayer is 2/7 (Ref. 5) instead of 1, as would have happened in the case of normal metals.

To describe the subsystem of current carriers in bilayer high-T_c superconductors we employ a Hamiltonian of the form

$$\hat{H}=\sum_{l\sigma}\epsilon_p\Psi_l^{\sigma\sigma}+\sum_{lm}t_{lm}^{pp}\Psi_l^{2\sigma}\Psi_m^{\sigma 2}+\sum_{l>m}j_{lm}\left[2(\overline{S_l}\overline{S_m})-\frac{n_l n_m}{2}\right]+\sum_{l>m}g_{lm}\delta_l\delta_m, \qquad (1)$$

where $\Psi_m^{2\sigma}(\Psi_m^{\sigma 2})$ are Hubbard-type operators corresponding to creation (annihilation) of quasiparticles in the bonding singlet-correlated oxygen band,[6] $n_l=\Psi_l^{\uparrow,\uparrow}+\Psi_l^{\downarrow,\downarrow}$; $\delta_l=n_l+2\Psi_l^{2,2}$; and, j_{lm} and g_{lm} are the superexchange and Coulomb interactions parameters. The quasiparticle dispersion relation has the form

$$\epsilon_{\mathbf{k}}=P_{pd}[2t_1(\cos\mathbf{k}_x a+\cos\mathbf{k}_y a)+4t_2\cos\mathbf{k}_x a\cos\mathbf{k}_y a +2t_3(\cos 2\mathbf{k}_x a+\cos 2\mathbf{k}_y a)]-\mu, \qquad (2)$$

where μ is the chemical potential, which under optimal doping, according to photoemission data,[7] lies 10 meV below the saddle peak of the density of states, $P_{pd}=(2+\delta)/4$ is the average value of the anticommutators $\{\Psi_m^{2\sigma},\Psi_m^{\sigma 2}\}$ with tunneling taken into account, δ is the number of current carriers per unit cell in the Cu_2O_4 bilayer, a is the lattice constant, and $t_1=t_1^{(90)}[1+\langle S_iS_j\rangle/P_{pd}^2]$. We take the following parameter set, which is consistent with the Fermi surface and the temperature behavior of the spin susceptibility of the normal phase of $YBa_2Cu_4O_8$: $t_1^{(0)}=70$ meV, $t_2^{(0)}=0$, and $t_3^{(0)}=5$ meV.[8] Following Ref. 9, we give the spin correlation functions of the nearest neighbors phenomenologically as $\langle S_iS_j\rangle=(-0.2\exp(0.6+\delta/2)^{-1}+0.6)/1.8356$, so that the width of the band would approach zero as $\delta\to 0$, which is necessary for a correct description of the insulator–metal transition in these compounds.

In the mean-field approximation the elementary excitations spectrum of the Hamiltonian (1) is determined by the equation

$$\det\begin{vmatrix}\epsilon_{\mathbf{k}}-E & G_{\mathbf{k+Q}} & \Delta_{\mathbf{k}} & U_{\mathbf{k}}\\ G_{\mathbf{k}} & \epsilon_{\mathbf{k+Q}}-E & U_{\mathbf{k+Q}} & \Delta_{\mathbf{k+Q}}\\ \Delta_{\mathbf{k}}^* & U_{\mathbf{k+Q}}^* & -\epsilon_{\mathbf{k}}-E & -G_{\mathbf{k+Q}}^*\\ U_{\mathbf{k}}^*\Delta_{\mathbf{k+Q}}^* & \Delta_{\mathbf{k+Q}}^* & -G_{\mathbf{k}}^* & -\epsilon_{\mathbf{k+Q}}-E\end{vmatrix}=0. \qquad (3)$$

The order parameter of the superconducting transition (ST) is given by the expression

$$\Delta_{\mathbf{k}_1}=\frac{1}{P_{pd}N}\sum_{\mathbf{k}}[2j(\mathbf{k}_1-\mathbf{k})-g(\mathbf{k}_1-\mathbf{k})+P_{pd}^2B(\mathbf{k}_1,\mathbf{k}_1-\mathbf{k})]\langle\Psi_{\mathbf{k}}^{\downarrow 2}\Psi_{-\mathbf{k}}^{\uparrow 2}\rangle, \qquad (4)$$

where $j(\mathbf{q})$, $g(\mathbf{q})$, and $B(\mathbf{k}_1,\mathbf{q})$ are the Fourier transforms of the superexchange, Coulomb, and Fröhlich interactions potentials, respectively. Specifically, $j(\mathbf{q})=j_0(1-6\delta^2)\times(\cos q_x a+\cos q_y a)$, where $j_0=125$ meV for YBaCuO compounds[10] and $g(\mathbf{q})=g_0\exp(-7\delta)(\cos q_x a\cos q_y a)$, where $g_0=315$ meV. Among all possible phonon modes, the bending modes make the most important contribution to pairing. In this case

$$B(\mathbf{k},\mathbf{q}) = 2B_0^2 \hbar\omega_{\mathbf{q}} \frac{1+1/2[\cos(q_x a)+\cos(q_y a)]}{(\hbar\omega_{\mathbf{q}})^2 - (\epsilon_{\mathbf{k}} - \epsilon_{\mathbf{k+q}})^2}$$
$$\times \Theta(\hbar\omega_D - |\epsilon_{\mathbf{k}} - \epsilon_{\mathbf{k+q}}|)\Theta(\hbar\omega_D - |\epsilon_{\mathbf{k}}|), \tag{5}$$

$\hbar\omega_D$ is the Debye frequency of the order of 45 meV, $\Theta(x)$ is the theta function, and $B_0 \approx 35$. In the range of doping indices δ of interest to us, Eq. (4) has a solution of the form $\Delta_{\mathbf{k}} = \Delta_0(\cos k_x a - \cos k_y a)$.

As was pointed out in Ref. 5, the CDW parameter G_k is a sum of two components with a different dependence on the wave vector. The component associated with the short-range potentials

$$G^{\rm ex}_{\mathbf{k}_1} = \frac{1}{P_{pd}N}\sum_{\mathbf{k}} [j(\mathbf{k}_1 - \mathbf{k}) + g(\mathbf{k}_1 - \mathbf{k})]\langle \Psi^{2\uparrow}_{\mathbf{k}} \Psi^{\uparrow 2}_{\mathbf{k+Q}}\rangle, \tag{6}$$

possesses d-type symmetry $G^{\rm ex}_{\mathbf{k}} = iG_0(\cos k_x a - \cos k_y a)$, while the phonon part

$$G^{ph}_{\mathbf{k}_1} = \frac{P_{pd}}{N}\sum_{\mathbf{k}} V_{\mathbf{k},\mathbf{Q}} \langle \Psi^{2\uparrow}_{\mathbf{k+Q}} \Psi^{\uparrow 2}_{\mathbf{k}}\rangle + V_{\mathbf{k}_1,Q} \frac{P_{pd}}{N}\sum_{\mathbf{k}} \langle \Psi^{2\uparrow}_{\mathbf{k+Q}} \Psi^{\uparrow 2}_{\mathbf{k}}\rangle, \tag{7}$$

possesses s-type symmetry. It is relatively small and is neglected below.

The order parameter $U_{\mathbf{k}}$ entering in Eq. (3) is related with thermodynamic average $\langle \Psi^{\downarrow 2}_{\mathbf{k}} \Psi^{\uparrow 2}_{-\mathbf{k}-\mathbf{Q}}\rangle$, which appears naturally in the equations of motion in the presence of superconductivity and Peierls instability. In the general case it is determined by the expression

$$U_{\mathbf{k}_1} = \frac{1}{P_{pd}N}\sum_{\mathbf{k}} [j(\mathbf{k}_1 - \mathbf{k}) + j(\mathbf{k}_1 - \mathbf{k} - \mathbf{Q}) - g(\mathbf{k}_1 - \mathbf{k}) + P^2_{pd} B(\mathbf{k}_1, \mathbf{k}_1 - \mathbf{k})]\langle \Psi^{\downarrow 2}_{\mathbf{k}} \Psi^{\uparrow 2}_{-\mathbf{k}-\mathbf{Q}}\rangle. \tag{8}$$

We investigate below the approximately optimal doping regime, where $Q \approx (\pi,\pi)$. One can see from Eq. (8) that $U_{\mathbf{k}}$ is comparatively small and can possess only s symmetry, since for $\mathbf{Q} = (\pi,\pi)$ the sum $j(\mathbf{k}_1 - \mathbf{k}) + j(\mathbf{k}_1 - \mathbf{k} - \mathbf{Q})$ vanishes. We note that for $U_{\mathbf{k}} = 0$ Eq. (3) leads to the spectrum

$$E_{1,2} = \sqrt{1/2(\epsilon^2_{\mathbf{k}} + \epsilon^2_{\mathbf{k+Q}}) + \Delta_{\mathbf{k}}\Delta^*_{\mathbf{k}} + G_{\mathbf{k}}G^*_{\mathbf{k}} \pm 1/2E^2_{12}}\,, \tag{9}$$

where

$$E^2_{12} = \sqrt{(\epsilon^2_{\mathbf{k}} - \epsilon^2_{\mathbf{k+Q}})^2 + 4G_{\mathbf{k}}G^*_{\mathbf{k}}(\epsilon_{\mathbf{k}} + \epsilon_{\mathbf{k+Q}})^2 + 4\Delta_{\mathbf{k}}\Delta^*_{\mathbf{k}}(G_{\mathbf{k}} + G^*_{\mathbf{k}})^2} \tag{10}$$

and $E_4 = -E_1$ and $E_3 = -E_2$.

In the general case we have the following system of integral equations:

$$\langle \Psi^{\downarrow 2}_{\mathbf{k}} \Psi^{\uparrow 2}_{-\mathbf{k}}\rangle = \frac{P_{pd}\Delta_{\mathbf{k}}}{4}\left[\frac{1}{E_1}\tanh\left(\frac{E_1}{2k_BT}\right) + \frac{1}{E_2}\tanh\left(\frac{E_2}{2k_BT}\right)\right]$$
$$+ \frac{P_{pd}N_{\Delta}}{2E^2_{12}}\left[\frac{1}{E_1}\tanh\left(\frac{E_1}{2k_BT}\right) - \frac{1}{E_2}\tanh\left(\frac{E_2}{2k_BT}\right)\right], \tag{11}$$

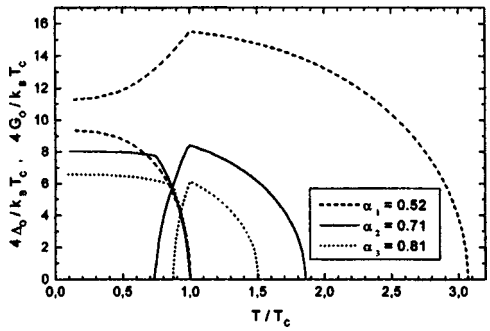

FIG. 1. Computed temperature dependences of the amplitudes of the order parameters Δ_0 and G_0. The curves corresponding to the superconducting gap parameter Δ_0 start at the point $T/T_C=1$. The relative-doping parameter α is defined in the text.

$$\langle \Psi^{2\uparrow}_{\mathbf{k}} \Psi^{\uparrow 2}_{\mathbf{k+Q}} \rangle = \frac{P_{pd} G_{\mathbf{k}}}{4}\left[\frac{1}{E_1}\tanh\left(\frac{E_1}{2k_BT}\right)+\frac{1}{E_2}\tanh\left(\frac{E_2}{2k_BT}\right)\right] + \frac{P_{pd} N_G}{2E_{12}^2}\left[\frac{1}{E_1}\tanh\left(\frac{E_1}{2k_BT}\right)-\frac{1}{E_2}\tanh\left(\frac{E_2}{2k_BT}\right)\right], \tag{12}$$

$$\langle \Psi^{\downarrow 2}_{\mathbf{k}} \Psi^{\uparrow 2}_{-\mathbf{k-Q}} \rangle = \frac{P_{pd} U_{\mathbf{k}}}{4}\left[\frac{1}{E_1}\tanh\left(\frac{E_1}{2k_BT}\right)+\frac{1}{E_2}\tanh\left(\frac{E_2}{2k_BT}\right)\right] + \frac{P_{pd} N_U}{2E_{12}^2}\left[\frac{1}{E_1}\tanh\left(\frac{E_1}{2k_BT}\right)-\frac{1}{E_2}\tanh\left(\frac{E_2}{2k_BT}\right)\right], \tag{13}$$

where

$$\begin{aligned} N_\Delta &= 1/2\Delta_{\mathbf{k}}(\epsilon^2_{\mathbf{k}}-\epsilon^2_{\mathbf{k+Q}})+\Delta_{\mathbf{k}}G^*_{\mathbf{k}}(G_{\mathbf{k}}+G^*_{\mathbf{k}})+U_{\mathbf{k}}(\Delta_{\mathbf{k}}U^*_{\mathbf{k}}-\Delta^*_{\mathbf{k}}U_{\mathbf{k}})+2\epsilon_{\mathbf{k+Q}}G^*_{\mathbf{k}}U_{\mathbf{k}}, \\ N_G &= 1/2G_{\mathbf{k}}(\epsilon_{\mathbf{k}}+\epsilon_{\mathbf{k+Q}})+\Delta_{\mathbf{k}}\Delta^*_{\mathbf{k}}(G_{\mathbf{k}}+G^*_{\mathbf{k}})+\epsilon_{\mathbf{k+Q}}\Delta^*_{\mathbf{k}}U_{\mathbf{k}}-\epsilon_{\mathbf{k}}\Delta_{\mathbf{k}}U^*_{\mathbf{k}}, \\ N_U &= 1/2U_{\mathbf{k}}(\epsilon_{\mathbf{k}}-\epsilon_{\mathbf{k+Q}})^2-\Delta_{\mathbf{k}}(\Delta_{\mathbf{k}}U^*_{\mathbf{k}}-\Delta^*_{\mathbf{k}}U_{\mathbf{k}})-\epsilon_{\mathbf{k}}\Delta_{\mathbf{k}}G^*_{\mathbf{k}}+\epsilon_{\mathbf{k+Q}}\Delta_{\mathbf{k}}G_{\mathbf{k}}. \end{aligned} \tag{14}$$

The system of equations (11)–(13) was solved numerically. As expected, the parameter $U_{\mathbf{k}}$ is negligibly small. The computed phase diagram of the δ dependence of the critical temperatures for $\Delta_0(T_C)$ and $G_0(T^*)$ at $\mathbf{Q}=(\frac{11}{12}\pi, \frac{11}{12}\pi)$ is close to the corresponding diagrams proposed in experimental works (see, for example, Ref. 11). In Fig. 1 three different doping cases are presented as an example of the temperature dependences found for the amplitudes of the order parameters $\Delta_0(T_C)$ and $G_0(T)$: α_1, α_2, and α_3, where the parameter α is given by the ratio $\alpha(\delta)=(\delta-\delta_{\min})/(\delta_{\rm opt}-\delta_{\min})$. Here $\delta_{\min}$ is the minimum value of the doping corresponding to the appearance of a superconducting state. In all cases, for $\delta<\delta_{\rm opt}=0.315$ (i.e., the existence of a CDW) the temperature dependence of the superconducting order parameter differs considerably from the BCS case. In the case of a strongly overdoped regime the ratio $4\Delta_0/k_BT_C=4.2$; for $\delta_{\rm opt}$ it equals 4.5; it then increases, as seen in Fig. 1, and reaches values of the order of 10 for $\delta>\delta_{\min}$ (i.e., in the strongly underdoped region). This kind of variation of $4\Delta_0/k_BT_C$ has already been noted in a number of experimental works.[12] The computed temperature

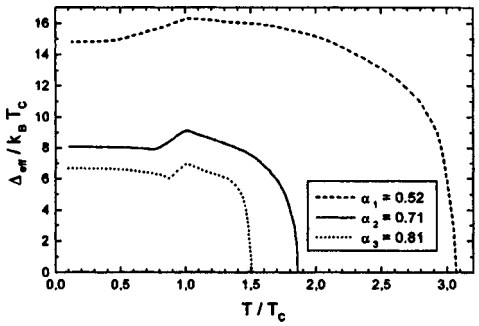

FIG. 2. Predicted examples of nonmonotonic temperature variations of the effective gap Δ_{eff} between peaks of the density of states of the energy spectrum.

dependences of the pseudogap G_0 exhibit nonmonotonic behavior as temperature decreases; this has not been noticed previously. It would be interesting to check this prediction of the theory experimentally. Thus, if the effective gap parameter $\Delta_{\text{eff}}(T)$, determined as the energy interval between peaks in the density of states, is measured in scanning tunneling spectroscopy experiments (see, for example, Ref. 12), then on account of the nonmonotonic behavior of $G_0(T)$ anomalies should be observed in the plot for $\Delta_{\text{eff}}(T)$: 1) In type α_1 samples $\Delta_{\text{eff}}(T)$ will decrease (!) as $T \to 0$; 2) for $\alpha \approx \alpha_3$ a local minimum should be observed in the plot of $\Delta_{\text{eff}}(T)$. Examples of such plots calculated on the basis of expressions (9) and (10) are presented in Fig. 2. In our opinion the indicated anomalies can be seen from the experimental data.[12,13] These results, however, require a more detailed experimental check on samples with different doping indices.

This work was supported in part by the State Science and Technology Program ''Superconductivity'' (Project No. 98014).

[a)]e-mail: Mikhail.Eremin@ksu.ru

[1] H. Ding, M. R. Norman, J. C. Campuzano *et al.*, Phys. Rev. B **54**, R9678 (1996).
[2] J. M. Harris, Z.-X. Shen, P. J. White *et al.*, Phys. Rev. B **54**, 15665 (1996); G. V. M. Williams, J. L. Tallon, E. M. Haines *et al.*, Phys. Rev. Lett. **78**, 721 (1997).
[3] Yu. V. Kopaev, in *The Problem of High-Temperature Superconductivity* [in Russian], edited by V. L. Ginzburg and D. A. Kirzhnits, Nauka, Moscow, 1977.
[4] C. A. Balseiro and L. M. Falicov, Phys. Rev. B **20**, 4457 (1979).
[5] S. V. Varlamov, M. V. Eremin, and I. M. Eremin, JETP Lett. **66**, 569 (1997).
[6] M. V. Eremin, S. G. Solov'yanov, and S. V. Varlamov, Zh. Éksp. Teor. Fiz. **112,** 1763 (1997) [JETP **85**, 963 (1997)].
[7] Z.-X. Shen and D. S. Dessau, Phys. Rep. **253**, 1 (1995).
[8] I. Eremin, M. Eremin, S. Varlamov *et al.*, Phys. Rev. B **56**, 11305 (1997).
[9] N. M. Plakida, R. Hayn, and J. L. Richard, Phys. Rev. B **51**, 16599 (1995).
[10] S. M. Hayden, G. Aeppli, T. G. Perring *et al.*, Phys. Rev. B **54**, R6905 (1996).
[11] G. V. M. Williams, J. L. Tallon, and J. W. Loram, Phys. Rev. B **57**, 14702 (1998); G. V. M. Williams, J. L. Tallon, R. Michalak, and R. Dupree, Phys. Rev. B **54**, 1 (1996).
[12] Ch. Renner, B. Revaz, J.-Y. Genoud *et al.*, Phys. Rev. Lett. **80**, 149 (1998); N. Miyakawa, P. Guptasarma, J. Zasadzinski *et al.*, Phys. Rev. Lett. **80**, 157 (1998); Y. Sezaki, T. Ekino, and H. Fujii, in *Abstracts of the Conference on Strongly Correlated Electron Systems*, Paris, France, July 15–18, 1998; T. Ekino, Y. Sezaki, and H. Fujii, Physica B, in press.
[13] A. G. Loeser, Z.-X. Shen, M. C. Schabel *et al.*, Phys. Rev. **56,** 14185 (1997).

Translated by M. E. Alferieff

Lagrangian instanton for the Kraichnan model

E. Balkovsky

Department of Physics of Complex Systems, Weizmann Institute of Science, Rehovot 76100, Israel

V. Lebedev

Department of Physics of Complex Systems, Weizmann Institute of Science, Rehovot 76100, Israel; Landau Institute for Theoretical Physics, Russian Academy of Sciences, 117940 Moscow, Russia

(Submitted 8 September 1998)
Pis'ma Zh. Éksp. Teor. Fiz. **68**, No. 7, 588–593 (10 October 1998)

We consider high-order correlation functions of the passive scalar in the Kraichnan model. Using the instanton formalism, we find the scaling exponents ζ_n of the structure functions S_n for $n \gg 1$ under the additional condition $d\zeta_2 \gg 1$ (where d is the dimensionality of space). At $n < n_c$ (where $n_c = d\zeta_2/[2(2-\zeta_2)]$) the exponents are $\zeta_n = (\zeta_2/4)(2n - n^2/n_c)$, while at $n > n_c$ they are n-independent: $\zeta_n = \zeta_2 n_c/4$. We also estimate the n-dependent factors in S_n. © *1998 American Institute of Physics.* [S0021-3640(98)01319-X]

PACS numbers: 47.27.Ak

Anomalous scaling is probably the central problem of the theory of turbulence. In 1941 Kolmogorov formulated his famous theory[1] wherein scaling behavior of different correlation functions of velocity in a turbulent flow was predicted. Experimentally one observes deviations from the scaling exponents proposed by Kolmogorov. It is recognized that the deviations are related to rare strong fluctuations which make the main contribution to the correlation functions.[2] This phenomenon, called intermittency, is the most striking peculiarity of developed turbulence.

One of the classic objects in the theory of turbulence is so-called passive scalar advected by a fluid; the role of the scalar can be played by temperature or by the density of pollutants. Correlation functions of the scalar in a turbulent flow possess a scaling behavior which in the frame of the theory analogous to that of Kolmogorov was established by Obukhov and Corrsin.[3] Intermittency enforces deviations from the Obukhov exponents that appear to be even stronger than the deviations from the Kolmogorov exponents for the correlation functions of the velocity.[4]

A consistent theory of turbulence describing anomalous scaling has not been constructed yet because of difficulties associated with the strong coupling inherent to developed turbulence. This is a motivation for attempts to examine the intermittency phenomenon in the framework of different simplified models. The most popular model used for this purpose is the Kraichnan model of the passive scalar advection,[5] where the advecting velocity is believed to be short-correlated in time. It allows one to examine the statistics

 © 1998 American Institute of Physics

of the scalar in more detail. The scalar in the Kraichnan model exhibits strong intermittency even if such is absent in the advecting velocity. The fact was proved both theoretically[6–8] and numerically.[9] In the theoretical works the equation for the n-point correlation function F_n was solved assuming that different parameters, such as ζ_2, $2-\zeta_2$, or d^{-1}, are small. The order of the correlation functions that can be examined in such a way is bound from above. There have been several attempts to find the scaling of the correlation functions for larger n. In the work by Kraichnan[10] a closure was assumed, enabling him to find ζ_n for any n. An alternative scheme was proposed in Ref. 11. An attempt to solve the problem at large n was made in Ref. 12.

In the present work we develop a consistent formalism based on the path-integral representation of the dynamical correlation functions of classical fields.[13] The basic idea, which was set forth in Ref. 14, involves the possibility of using the saddle-point approximation in the path integral at large n. The saddle-point conditions are integro-differential equations describing an object that, by analogy with the quantum field theory, we call instanton. The instantonic method had already been successfully used in some contexts.[15,16] The formalism presented in this paper enables one to find correlation functions of the passive scalar for arbitrary $n \gg 1$, provided $d\zeta_2 \gg 1$.

Advection of a passive scalar θ by a velocity field v is described by the equation

$$\partial_t \theta + \mathbf{v}\cdot\nabla\theta - \kappa\nabla^2\theta = \phi, \tag{1}$$

where κ is the diffusion coefficient and ϕ is the source of the scalar. In a turbulent flow v and ϕ are random functions of time and space coordinates. Then passive scalar correlation functions are determined by the statistics of v and ϕ. Usually, one treats simultaneous correlation functions $F_n = \langle \theta(\mathrm{r}_1) \ldots \theta(\mathrm{r}_n)\rangle$, since large-scale velocity fluctuations destroy temporal correlations.

It is convenient to examine the anomalous scaling in terms of the structure functions

$$S_n(\mathbf{r}) = \langle |\theta(\mathbf{r}/2) - \theta(-\mathbf{r}/2)|^n \rangle. \tag{2}$$

One expects that in the convective interval of scales the structure functions reveal a scaling behavior $S_n(r) \propto r^{\zeta_n}$. The exponents ζ_n are of great interest since they reflect the intermittency. In the frame of the Obukhov theory[3] $\zeta_n = (n/2)\zeta_2$. Thus the differences $(n/2)\zeta_2 - \zeta_n$ give the anomalous scaling exponents.

In the Kraichnan model v and ϕ are independent random functions δ-correlated in time and described by Gaussian statistics. Therefore, the statistical properties of the fields are entirely characterized by their pair correlation functions. For the pumping one has $\langle \phi(t_1,\mathbf{r}_1)\phi(t_2,\mathbf{r}_2)\rangle = \delta(t_1-t_2)\chi(r_{12})$, where $\chi(x)$ is a smooth function decaying on a scale L. The constant $\chi(0) \equiv P_2$ determines the pumping rate of θ^2. For the velocity field one has

$$\langle v_\alpha(t_1,\mathbf{r}_1) v_\beta(t_2,\mathbf{r}_2)\rangle = \delta(t_1-t_2)\{\mathcal{V}_0\delta_{\alpha\beta} - \mathcal{K}_{\alpha\beta}(\mathbf{r}_1-\mathbf{r}_2)\}.$$

The quantity $\mathcal{V}_0$ is an $\mathbf{r}$-independent constant which represents the contribution of large-scale velocity fluctuations. Since a homogeneous advection does not influence S_n, one should keep in the correlation function also a small $\mathbf{r}$-dependent correction $\mathcal{K}$, which is assumed to possess some scaling properties:

$$\mathcal{K}_{\alpha\beta}(\mathrm{r}) = \frac{D}{d} r^{-\gamma}\left[r^2 \delta_{\alpha\beta} + \frac{2-\gamma}{d-1}(r^2\delta_{\alpha\beta} - r_\alpha r_\beta)\right], \tag{3}$$

where D is a constant characterizing the strength of the velocity fluctuations. One assumes that fluctuations of the velocity are strong enough to ensure a large value of the Peclet number, that is $L^{2-\gamma} \gg r_d^{2-\gamma} \sim \kappa/D$. Then there exists a convective interval of scales $r_d \ll r \ll L$. We will be interested in the scaling properties of correlation functions of θ only in this interval, assuming L/r to be the largest parameter in the theory.

Within the Kraichnan model one can derive a closed equation for any correlation function F_n (Refs. 5,8,17). The equation for F_2 can be solved.[5] In the convective interval $S_2(r) = 2[F_2(0) - F_2(r)] \propto r^\gamma$, which implies that $\zeta_2 = \gamma$. However, for $n > 2$ the equations for F_n are too complicated to be solved exactly. In Refs. 7 and 8 the equations were analyzed in the limits $(2-\gamma) \ll 1$ and $d\gamma \gg 1$. The analysis led to the answer

$$\zeta_n = \frac{n\gamma}{2} - \frac{2-\gamma}{2(d+2)} n(n-2). \tag{4}$$

The first term in the right-hand side of Eq. (4) represents the normal scaling, and the second term is just the anomalous scaling exponent. The calculations leading to (4) are correct if the anomalous contribution is much smaller than the normal one. To overcome the restriction we proposed a procedure which will be described in detail elsewhere.[18] Below we sketch our scheme.

The diffusivity κ does not enter the expressions for the structure functions in the convective interval.[2] However, it is not possible to put simply $\kappa = 0$, since the diffusion provides an important regularization. Suppose that two infinitely close fluid particles do not disperse without diffusion, and the average value of θ^2 is infinite, as is seen from Eq. (6). Nevertheless, we put $\kappa = 0$, approximating the structure functions as averages of the powers of the smoothed difference

$$\vartheta = \int dx\, \beta(\mathbf{x})\, \theta(0,\mathbf{x}), \quad \beta = \delta_\Lambda\left(\mathbf{x} - \frac{r}{2}\right) - \delta_\Lambda\left(\mathbf{x} + \frac{r}{2}\right), \tag{5}$$

where $\delta_\Lambda(\mathbf{x})$ is a function which rapidly tends to zero at $r > \Lambda^{-1} \gg r_d$ and is normalized by the condition $\int dx\, \delta_\Lambda(\mathbf{x}) = 1$. In the absence of diffusion, the regularization is provided by the finite support of δ_Λ.

In the diffusionless case Eq. (1) can be solved in terms of Lagrangian trajectories s:

$$\theta(0,\mathrm{r}) = \int_{-\infty}^{0} dt'\, \phi[t', \mathbf{s}(t',\mathbf{r})], \quad \partial_t \mathbf{s} = \mathbf{v}(t,\mathbf{s}). \tag{6}$$

The times here are negative due to causality and r is supposed to be the terminating point of the trajectory $\mathbf{s}(t,\mathbf{r})$: $\mathbf{s}(t=0,\mathbf{r}) = \mathbf{r}$. Then we can obtain

$$\langle |\vartheta|^n \rangle = \int \frac{dy\, d\vartheta}{2\pi} \langle \exp(-\mathcal{F} - iy\vartheta + n\, \ln|\vartheta|) \rangle_v, \tag{7}$$

$$\mathcal{F} = \frac{y^2}{2} \int dt\, dr_1\, dr_2\, \chi(R_{12}) \beta(\mathbf{r}_1) \beta(\mathbf{r}_2), \tag{8}$$

where $R_{12}=|s(t,\mathbf{r}_1)-s(t,\mathbf{r}_2)|$. The brackets in the right-hand side of Eq. (7) denote averaging over the statistics of $\mathbf{v}$, while the statistics of ϕ has already been taken into account there.

Note that $\mathcal{F}$ defined by Eq. (8) depends only on the absolute values $R_{12}(t)$ of Lagrangian differences. Therefore, instead of averaging over the statistics of v one may find an answer by averaging over statistics of R_{12}, which can be established starting from the relation

$$\gamma^{-1}\partial_t R_{12}^{\gamma}=\zeta_{12}\equiv R_{12}^{\gamma-2}R_{12\alpha}(v_{1\alpha}-v_{2\alpha}), \tag{9}$$

which follows from Eq. (6). Using the statistical properties of ζ and employing the conventional procedure,[13] we find the effective action

$$i\mathcal{I}=i\int_{-\infty}^{0}dt\int dr_1\,dr_2\,m_{12}(\gamma^{-1}\partial_t R_{12}^{\gamma}+D)-\frac{D}{d}\int_{-\infty}^{0}dt\int dr_1\,dr_2\,dr_3\,dr_4\,Q_{12,34}m_{12}m_{34} \tag{10}$$

describing the statistics of R_{12}. Here $m_{12}\equiv m(t,\mathbf{r}_1,\mathbf{r}_2)$ is the auxiliary field conjugate to R_{12}. The explicit expression for the function Q is rather cumbersome. We will need it only in the leading order in $1/d$:

$$Q_{12,34}=\frac{1}{4}R_{12}^{\gamma-2}R_{34}^{\gamma-2}(R_{23}^{2-\gamma}+R_{14}^{2-\gamma}-R_{13}^{2-\gamma}-R_{24}^{2-\gamma})(R_{23}^{2}+R_{14}^{2}-R_{13}^{2}-R_{24}^{2}). \tag{11}$$

Now, we can rewrite (7) as a path integral

$$\langle|\vartheta|^n\rangle=\int\frac{dy\,d\vartheta}{2\pi}\mathcal{D}R\,\mathcal{D}m\exp(i\mathcal{I}-\mathcal{F}-iy\vartheta+n\,\ln|\vartheta|). \tag{12}$$

The definition of R leads to the triangle inequalities

$$R_{12}+R_{23}>R_{13}, \tag{13}$$

to be satisfied for any three points. Actually, the inequalities are constraints that should be imposed on the field R_{12} when integrating in Eq. (12).

We calculate the integral (12) in the saddle-point approximation, assuming the number n to be large enough. Here we will present only results of the calculations to be described in Ref. 18.

At $n<n_c$, where

$$n_c=d\gamma/(2(2-\gamma)), \tag{14}$$

we obtain

$$S_n\sim\left(\frac{n}{\gamma}\frac{P_2C_1}{D}L^{\gamma}\right)^{n/2}\left(\frac{r}{L}\right)^{\zeta_n}, \tag{15}$$

$$\zeta_n=n\gamma/2-(2-\gamma)n^2/(2d). \tag{16}$$

The quantity C_1 in expression (15) is a constant of order unity, whose value depends on the shape of χ (that is on the details of the pumping) and is consequently nonuniversal. Note that the $\mathbf{r}$-independent factor in (15) is determined by the single-point root-mean-square value of the passive scalar $\theta_{\mathrm{rms}}^2\sim P_2L^{\gamma}/(D\gamma)$. Comparing expression (16) with

(4), we see that they coincide under the conditions $n \gg 1$ and $d \gg 1$ that were implied in our derivation. Surprisingly, the n dependence of ζ_n given by Eq. (4) is correct not only in the limit $n \ll n_c$ but up to $n = n_c$, which is the boundary value for (15) and (16). In the case $n > n_c$ the scaling exponents ζ_n appear to be n-independent and equal to the value $\zeta_c = d\gamma^2/(8(2-\gamma))$. The n-dependent numerical factors can be found in two limits: $n - n_c \ll n_c$ and $n \gg n_c$. At $n \gg n_c$ the structure functions are

$$S_n \sim \left(\frac{n}{\gamma} \frac{P_2 C_2}{D} L^{\gamma} \right)^{n/2} \left(\frac{r}{L} \right)^{\zeta_c}. \tag{17}$$

The quantity C_2 in Eq. (17) is again a nonuniversal constant of order unity.

The vicinity of the critical value $n = n_c$ requires a separate consideration. The expression for the structure functions can be written as

$$S_n \sim \left(\frac{(n-n_c)^2}{\gamma n_c} \frac{P_2 C_{\pm}}{D} L^{\gamma} \right)^{n_c/2} \left(\frac{r}{L} \right)^{\zeta_n}, \tag{18}$$

which implies the condition $|n - n_c| \ll n_c$. The factors $C_{\pm}$ are nonuniversal constants of order unity which are different for the cases $n < n_c$ and $n > n_c$. The exponents ζ_n in expression (18) are determined by Eq. (16) at $n < n_c$ and $\zeta_n = \zeta_c$ at $n > n_c$. The main peculiarity that appears in expression (18) is its critical dependence $\propto |n - n_c|^{n_c}$, which is saturated at very small $n_c - n$. The condition that determines the validity of Eq. (18) is $\gamma \ln L/r \gg n_c/|n - n_c|$.

Let us discuss our results. We have found the n dependence of the structure function exponents ζ_n which grow with increasing n up to $n = n_c$ and then cease to vary. Our results contradict to the schemes proposed in Refs. 10 and 11. The value ζ_c is different and smaller than the constant obtained in Ref. 12, which can be regarded as an estimated upper bound. Eq. (16), valid at $n < n_c$, exactly corresponds to the log-normal statistics.[19] The log-normal answer can be obtained if one assumes that for a large fluctuation, giving the main contribution to S_n, the pumping is inessential and that the fluctuation is smooth on the scale r. Then, we find from Eq. (1) that the passive scalar difference satisfies the equation $\partial_t \ln(\Delta\theta) = -\mathbf{v}\cdot\mathbf{r}/r^2$, where we replaced $\nabla\theta$ by $\Delta\theta/r$. From here, as a consequence of the central limit theorem, we immediately get the log-normal statistics for $\Delta\theta$. The saturation at $n > n_c$ can be explained by the presence of quasi-discontinuous structures in the field θ making the main contribution to the high-order correlation functions of θ. Note also a similar nonanalytic behavior of ζ_n for Burgers' turbulence,[2] which is explained by presence of shocks in the velocity field. Although formally our scheme is applicable only in the limit $d\gamma \gg 1$, this simple physical picture allows one to hope that the main features of our results persist for arbitrary values of the parameters. This hope is supported by Ref. 20, where a saturation of ζ_n was observed in numerical simulations of the Kraichnan model at $d = 3$.

We are grateful to G. Falkovich for valuable remarks, and to M. Chertkov, R. Kraichnan, D. Khmelnitskii, and M. Vergassola for helpful discussions. E. B. acknowledges support by a Joseph Meyerhoff scholarship and a grant from the Israel Science Foundation. V. L. acknowledges support from the Minerva Center for Nonlinear Physics at the Weizmann Institute and from the ENS-Landau Institute Twinning Programme.

[1] A. N. Kolmogorov, C. R. Acad. Sci. URSS **30**, 301 (1941).
[2] U. Frisch, *Turbulence: the Legacy of A. N. Kolmogorov*, Cambridge University Press, New York, 1995.
[3] A. M. Obukhov, C. R. Acad. Sci. URSS, Geogr. Geophys. **13**, 58 (1949); S. Corrsin, J. Appl. Phys. **22**, 469 (1951).
[4] R. Antonia, E. Hopfinger, Y. Gagne, and F. Anselmet, Phys. Rev. A **30**, 2704 (1984).
[5] R. H. Kraichnan, Phys. Fluids **11**, 945 (1968).
[6] B. Shraiman and E. Siggia, C. R. Acad. Sci. **321**, Ser. II, 279 (1995); Phys. Rev. Lett. **77**, 2463 (1996).
[7] K. Gawedzki and A. Kupiainen, Phys. Rev. Lett. **75**, 3608 (1995); D. Bernard, K. Gawedzki, and A. Kupiainen, Phys. Rev. E **54**, 2564 (1996); J. Stat. Phys. **90** (1998) [*sic*].
[8] M. Chertkov, G. Falkovich, I. Kolokolov, and V. Lebedev, Phys. Rev. E **52**, 4924 (1995); M. Chertkov and G. Falkovich, Phys. Rev. Lett. **76**, 2706 (1995).
[9] R. H. Kraichnan, V. Yakhot, and S. Chen, Phys. Rev. Lett. **75**, 240 (1995); U. Frisch, A. Mazzino, and M. Vergassola, Phys. Rev. Lett. **80**, 5532 (1998).
[10] R. H. Kraichnan, Phys. Rev. Lett. **52**, 1016 (1994).
[11] V. Yakhot, Phys. Rev. E **55**, 329 (1997).
[12] M. Chertkov, Phys. Rev. E **55**, 2722 (1997).
[13] P. C. Martin, E. Siggia, and H. Rose, Phys. Rev. A **8**, 423 (1973); C. de Dominicis, J. Phys. (Paris), Colloq. **37**, C1-247 (1976); H. Janssen, Z. Phys. B **23**, 377 (1976).
[14] G. Falkovich, I. Kolokolov, V. Lebedev, and A. Migdal, Phys. Rev. E **54**, 4896 (1996).
[15] V. Gurarie and A. Migdal, Phys. Rev. E **54**, 4908 (1996); E. Balkovsky, G. Falkovich, I. Kolokolov, and V. Lebedev, Phys. Rev. Lett. **78**, 1452 (1997); E. Balkovsky and G. Falkovich, Phys. Rev. E **57**, 1231 (1998).
[16] G. Falkovich and V. Lebedev, Phys. Rev. Lett. **79**, 4159 (1997).
[17] B. Shraiman and E. Siggia, Phys. Rev. E **49**, 2912 (1994).
[18] E. Balkovsky and V. Lebedev, Phys. Rev E, to be published.
[19] A. N. Kolmogorov, J. Fluid Mech. **12**, 82 (1962).
[20] U. Frisch, A. Mazzino, and M. Vergassola, *Proceedings of the European Geophysical Society Meeting*, 1998.

Published in English in the original Russian journal. Edited by Steve Torstveit.

Space–time dynamics of nanoparticles of a magnetofluid in a laser beam

S. R. Nersisyan and N. V. Tabiryan
Institute of Applied Physics, Armenian National Academy of Sciences, 375014 Erevan, Armenia

(Submitted 12 August 1998)
Pis'ma Zh. Éksp. Teor. Fiz. **68**, No. 7, 594–598 (10 October 1998)

Laser-induced space–time dynamics of nanoparticles of a magnetofluid was observed. Visualization was effectuated and the redistribution of the particles was measured. These showed a strong decrease in the particle density on and around the periphery of the laser beam axis. A number of proofs showing that the thermal diffusion of nanoparticles plays the key role in determining the dynamics of the particle redistribution are presented. High-quality pictures taken of the self-modulation of the laser beam serve as a new and powerful method for investigating transport phenomena and the nonlinear interaction of light with colloids. © *1998 American Institute of Physics.*
[S0021-3640(98)01419-4]

PACS numbers: 61.46.+w, 75.50.Mm, 82.70.Dd

Interesting effects due to the interaction of laser radiation with absorbing solutions and colloids have been discussed in some previous works. Among systems of wide fundamental and applied interest for science and technology, we call attention to liquid crystals doped with fullerene,[1] organic dyes,[2,3] polymers[4,5] and aerosol nanoparticles[6] and colloids of magnetic particles.[7–9]

In the present letter we report results for the laser-induced space–time dynamics of the redistribution of nanoparticles of a magnetofluid. This phenomenon could be universal for absorbing mixtures which provide internal feedback that determines the concentration profile and temperature of a colloid in a laser beam.

The essence of the experiment is very simple and consists in the following. Focused laser radiation is incident normally on a thin magnetofluid layer of thickness $L = 50\ \mu$m. The outgoing radiation is detected and investigated in the far zone. A single-mode He–Ne laser with maximum power up to 40 mW and wavelength $\lambda = 632.8$ nm was used. The beam radius $w = 0.6$ mm (HWe^{-2}M). The magnetofluid cell consists of a colloidal mixture of magnetite (Fe_3O_4) powder in kerosene, whose volume fraction is 6%, and the average particle size is of the order of 10 nm. The absorption coefficient σ_0, which we measured for low radiation powers $P \sim 10\ \mu$W, was $\sigma_0 = 550\ \text{cm}^{-1}$.

As the power of the incident radiation increased, a system of concentric rings formed in the far zone. The parameters of this pattern — the number of rings and their divergence — characterize quite accurately the laser-induced change in the refractive

 © 1998 American Institute of Physics

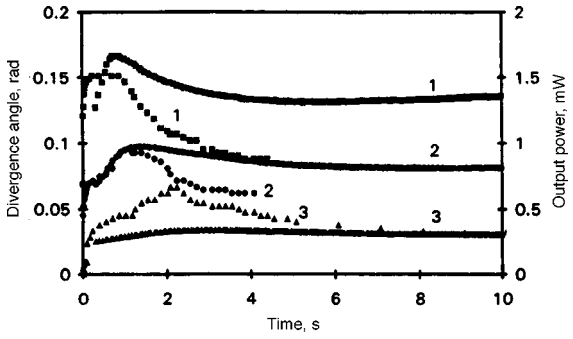

FIG. 1. Dynamics of the divergence (left side) and total power (right side) of the exit beam for different values of the incident beam power: *1* — 22.5 mW; *2* — 12 mW; *3* — 4.2 mW.

index and therefore the light-induced modulations of the material parameters of the medium. This method has been used successively for many years to investigate the interaction of laser radiation with different nonlinear media.[10,11]

We note the unique ring-formation dynamics observed in our experiment when the laser radiation is switched on suddenly. Specifically, at fixed power incident radiation power the parameters of the ring structure (number of rings and their divergence) in the far zone at first reach a certain maximum value, after which the structure contracts to a smaller divergence and a smaller number of rings. Such complex behavior has been observed in liquid crystals under very definite geometric conditions of their interaction with laser radiation;[11–13] it is a consequence of the nonlinear propagation of *elliptically* polarized light in a *highly anisotropic* and strongly *inhomogeneous* medium.

It is important to note that we are dealing here with complex behavior in an *isotropic* and *homogeneous* medium, as a magnetofluid interacting with a *linearly* polarized light beam. Therefore there arises also the question of the mechanism leading to the modulation of the refractive index of the medium, giving rise to the above-indicated scenarios of the dynamics of the ring structure in a magnetofluid.

The answers to these problems can be found in the basic features of the phenomena determined in the course of the experiment. Figure 1 shows the dynamics of the angle of divergence and the total power of the outgoing beam when the laser radiation is switched on suddenly. One can see that at fixed incident beam power both quantities first increase and then decrease in time. The changes in the transmittance and divergence become stronger as the incident radiation power increases. It was verified that uniform heating of the magnetofluid cell does not produce any substantial effects.

The characteristic features obtained can be interpreted by taking into consideration the fact that we are dealing with thermal diffusion (Soret effect), induced by strong, spatially localized, heating of the magnetofluid layer in a laser beam. Specifically, the outflow of absorbing nanoparticles from the central part of the beam (from the region with high temperature gradients) in the direction of the colder periphery is apparently the only reason for nonlinear absorption — an increase in the transparency of the material with increasing radiation power. The increase in transparency, however, results in a decrease of absorption, which in turn results in a decrease of the temperature gradients.

Therefore the particles float back into the central part of the beam and absorption once again increases. To confirm the scenario described above, we performed a series of experiments and formulated a number of theoretical proofs.

The laser illuminated spot on the magnetofluid layer was visualized directly under an optical microscope. Figure 2 displays the pictures obtained at the moment of maximum transmittance of the magnetofluid layer and at the moment when a lower transmittance is established. As one can see from Fig. 2a, at the moment of peak transmittance two regions with high transparency appear on a section of the magnetofluid layer. One region — on the beam axis — can be attributed to thermal diffusion of absorbing particles out of the hotter, entrance boundary in the direction of the cooler, exit boundary of the magnetofluid cell. It can be shown that such a redistribution of absorbing particles increases the transparency of the magnetofluid cell.

The origin of the other region — the circular region of high transparency (Fig. 2a) — is due to the transverse temperature gradient, which for a Gaussian beam with intensity $I=I_0\exp(-r^2/w^2)$ reaches a maximum at a distance $r=w/2^{1/2}$ from the beam axis.

Figure 2b shows a picture of the magnetofluid layer after a lower transmittance is stabilized. This demonstrates the partial return of the particles into the region inside the beam.

The theoretical description of the phenomenon is based on solving a system of diffusion and heat-conduction equations taking account of the dependence of the absorption coefficient on the concentration of absorbing particles:

$$\partial c/\partial t = D\Delta c + D_T c(1-c)\Delta T, \tag{1a}$$

$$\partial T/\partial t - \chi\Delta T = \sigma I/\rho c_p\,. \tag{1b}$$

In Eq. (1) the constant D (cm^2/s) characterizes ordinary diffusion; the parameter D_T(cm^2/s) is the thermal diffusion coefficient; c is the concentration of the absorbing particles in the medium; χ (cm^2/s) is the thermal conductivity; ρc_p ($\mathrm{J/cm^3\cdot K}$) is the specific heat of the material; σ (cm^{-1}) is the absorption coefficient; I ($\mathrm{W/cm}^2$) is the intensity of the laser radiation; and, α determines the absorption coefficient of magnetite.

A qualitative analysis of this system of equations shows the possibility of the above-described complex nonlinear dynamics and determines the condition for its appearance that relates the radiation intensity with the absorption coefficient, beam radius, and cell thickness. In the case of weak absorption, $\sigma L \ll 1$, $\sigma w \ll 1$ this condition has the comparatively simple form

$$\sigma_0 I \geqslant \frac{\rho c_p \chi^2}{4D_T}\left(\frac{1}{w^2}+\frac{1}{L^2}\right). \tag{2}$$

According to Eq. (2), there exists a threshold intensity where the character of the particle redistribution becomes complex, as was observed in the experiments. Moreover, according to Eq. (2), at fixed radiation power there exists a critical cell thickness above which the dynamics of the process becomes complex:

$$L \geqslant L_c = w/\sqrt{(4D_T\sigma_0 P/\pi\rho c_p\chi^2)-1}\,. \tag{3}$$

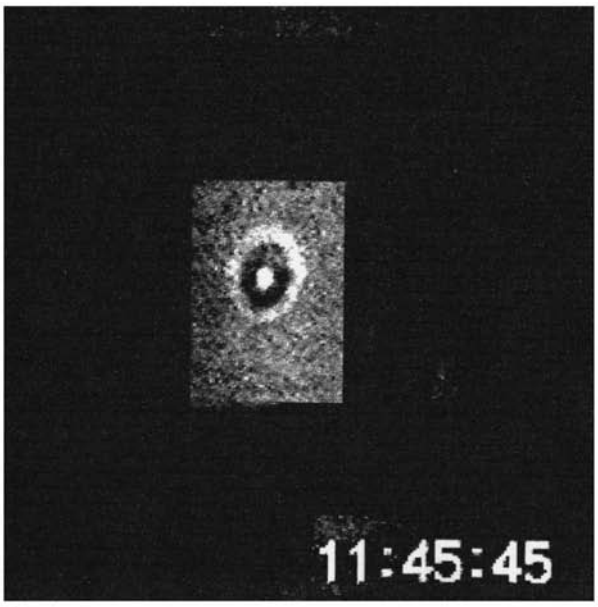

a

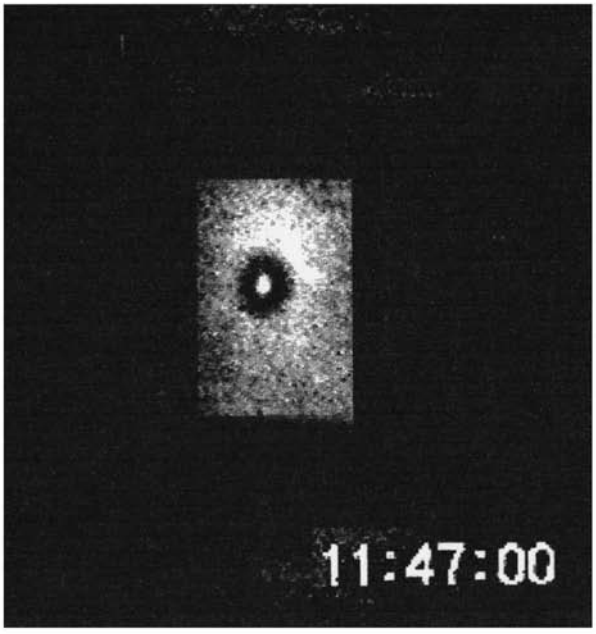

b

FIG. 2. Picture of the region in the magnetofluid layer illuminated with a focused laser beam as seen under a microscope: a) picture taken at the moment of peak transmittance; b) picture taken after stabilization of transmission.

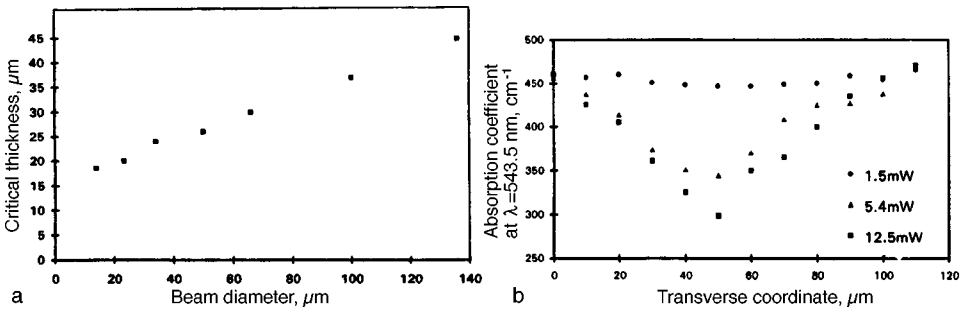

FIG. 3. a) Experimentally obtained dependence of the critical thickness L_c on beam diameter. b) Profile of the absorption coefficient in the stable state, measured by scanning a weak probe beam across the spot of the strong pump beam.

We checked this prediction in experiments with magnetofluid layers of different thickness. The radius of the beam waist was also varied. Figure 3a shows the experimentally obtained dependence of the critical thickness L_c on the beam diameter $2w$ with fixed incident beam power $P=8.5$ mW. This dependence was found to be linear, in accordance with the theoretical prediction.

The expression (3) makes it possible to determine the thermal diffusion constant of the magnetofluid by measuring the slope of the curve of L_c versus w (see Fig. 3a). Taking for the material parameters of the magnetofluid the typical values for liquids $\rho c_p \sim 1$ J/cm$^3\cdot$K and $\chi\sim 10^{-3}$ cm^2/s and the experimental values for σ_0 ($\sigma_0=550$ cm^{-1}) and $P=8.5$ mW, we obtain $D_T\sim 10^{-7}$ cm$^2\cdot$s/K. This result is very reasonable compared with the typical values of the thermal diffusion constants for similar colloids. However, it should be noted that Eqs. (2) and (3) have only a qualitative value in the process that we are discussing.

A key experiment proving our main hypothesis of laser-induced redistribution of absorbing particles consisted in measuring the spatially localized transmittance of the magnetofluid layer. For this, a weak (~ 10 μW) and narrow ($w\sim 20$ μm) green He–Ne laser ($\lambda=543.5$ nm) probe beam was scanned across the region where the magnetofluid was illuminated with a strong red pump laser beam ($\lambda=632.8$ nm). The green laser beam was chosen for ease of adjustment and to decrease the noise due to reflection and scattering of the strong red beam. A lens focused both beams onto the magnetofluid cell. The measurements were performed in a stationary state, i.e., after the transient process stabilized. The green beam was prebroadened so as to obtain a narrower focal waist. Under a microscope it was verified and established that the diameter of the red beam is 90 μm while the diameter of the green beam was 20 μm. The position of the probe beam during scanning across the pump beam was monitored under the microscope. The absorption-coefficient profile obtained in this way in the stationary state is presented in Fig. 3b for several values of the pump beam power. One can see that the curve is quite smooth for low powers, while for higher powers the absorption coefficient in the central region of the pump beam decreases sharply.

It is interesting to note that the particle concentration on the beam axis can decrease by more than a factor of 2 as a result of the Soret effect. The increase in temperature in the experiment reached 30°. Therefore the concentration modulation ($\partial n/\partial c\sim 1$), rather

than the temperature modulation ($\partial n/\partial T \sim 10^{-4}$ K^{-1}), made the main contribution to the change in the refractive index. This circumstance is not very obvious for such a strong absorbing medium.

In summary, the present letter reported the direct observation and investigation of the dynamics of space–time redistribution of nanoparticles induced by a laser beam in a magnetofluid. Feedback giving rise to the complex dynamics of the interaction of light with a strongly absorbing colloidal liquid on account of the Soret effect was observed. The results obtained make it possible to estimate the thermal diffusion constant for the magnetofluid. In the future, we shall concentrate our attention on the new possibilities that the interaction of light with colloidal liquids containing absorbing nanoparticles could give for fundamental research and applications of such research in optical technology.

[1] I. C. Khoo, Opt. Lett. **20**, 2137 (1995).
[2] Janossy, Phys. Rev. E **49**, 2957 (1994).
[3] D. Voloshschenko *et al.*, Jpn. J. Appl. Phys. **34**, 566 (1995).
[4] G. Golemme *et al.*, Opt. Lett. **22**, 1226 (1997).
[5] S. R. Sutherland *et al.*, Appl. Phys. Lett. **64**, 1074 (1994).
[6] M. Kreuzer *et al.*, Appl. Phys. Lett. **62**, 1712 (1993).
[7] T. Du, S. Yuan, and W. Luo, Appl. Phys. Lett. **65**, 1844 (1994).
[8] T. Du and W. Luo, Mod. Phys. Lett. B **9**, 1643 (1995).
[9] J. C. Bacri *et al.*, Phys. Rev. Lett. **74**, 5032 (1995).
[10] F. B. Dabby *et al.*, Appl. Phys. Lett. **16**, 362 (1970).
[11] N. V. Tabiryan, B. Ya. Zel'dovich, and A. V. Sukhov, *The Orientational Optical Nonlinearity of Liquid Crystals* (Special Issue of Mol. Cryst. Liquid Cryst., **136**, No. 1, 1986).
[12] V. Carbone *et al.*, Phys. Rev. E **47**, 3741 (1993).
[13] E. Santamato *et al.*, Phys. Rev. Lett. **64**, 1377 (1990).

Translated by M. E. Alferieff